INFORMATION TO USERS

This manuscript has been reproduced from the microfilm master. UMI films the text directly from the original or copy submitted. Thus, some thesis and dissertation copies are in typewriter face, while others may be from any type of computer printer.

The quality of this reproduction is dependent upon the quality of the copy submitted. Broken or indistinct print, colored or poor quality illustrations and photographs, print bleedthrough, substandard margins, and improper alignment can adversely affect reproduction.

In the unlikely event that the author did not send UMI a complete manuscript and there are missing pages, these will be noted. Also, if unauthorized copyright material had to be removed, a note will indicate the deletion.

Oversize materials (e.g., maps, drawings, charts) are reproduced by sectioning the original, beginning at the upper left-hand corner and continuing from left to right in equal sections with small overlaps. Each original is also photographed in one exposure and is included in reduced form at the back of the book.

Photographs included in the original manuscript have been reproduced xerographically in this copy. Higher quality 6" x 9" black and white photographic prints are available for any photographs or illustrations appearing in this copy for an additional charge. Contact UMI directly to order.

UMI

A Bell & Howell Information Company
300 North Zeeb Road, Ann Arbor MI 48106-1346 USA
313/761-4700 800/521-0600

MULTIAXIAL CYCLIC TESTING OF SATURATED OTTAWA SAND

by

Maung Maung Gyi

A Thesis Submitted to the Faculty of the

DEPARTMENT OF CIVIL ENGINEERING
AND ENGINEERING MECHANICS

In Partial Fulfillment of the Requirement
For the Degree of

MASTER OF SCIENCE
WITH A MAJOR IN CIVIL ENGINEERING

In the Graduate College

THE UNIVERSITY OF ARIZONA

1996

STATEMENT BY AUTHOR

This thesis has been submitted in partial fulfillment of requirements for an advance degree at The University of Arizona and is deposited in the University Library to be made available to the borrower under the rules of Library.

Brief quotation from this thesis are allowable without special permission, provided that accurate acknowledgment of source is made. Requests for permission of extended quotation from or reproduction of this manuscript in whole or part may be granted by the head of the major department or Dean of the Graduate College when in his or her judgment the proposed use of the material is in the interest of the scholarship. In all other instances, however, permission must be obtained from the author.

Signed: _____

APPROVAL BY THE THESIS DIRECTOR

This thesis has been approved on the dates shown below:

_____ 6-4-96

Chandrakant S. Desai — Date

Regent's Professor of Civil Engineering

ACKNOWLEDGMENTS

I wish to express my gratitude to my thesis advisor, Regents' Professor Chandrakant Desai, for his teaching, guidance, encouragement, and support during the course of research. Without the support and guidance of Dr. Desai this thesis cannot be finished.

I would like to thank the members of my committee, Dr. D. Contractor and Dr. P. Kiousis for their advice and criticism, which helped to improve my work. I owe a special debt to Professor D. Contractor for his kind support during the course of my study.

Special thank are due my friends and colleagues Mr. A. Alanazy, Mr. I. Park, Mr. T. Dishongh, Dr. J. Toth, Mr. C. Shao and Dr. D. Rigby, for many useful discussions and help during the course of research.

The author express his appreciation to the staff and technicians of the Department of Civil Engineering and Engineering Mechanics, particularly Ms. Barbara and Mr. Peter Boyle, Mr. Gene Townsend and Mr. Tom Demma.

Finally, I would like to especially thank my wife Hla Hla Htay for her patience, my son Aung Thiha for his cheerful attitude and my parents for their encouragement and assistance during my studies.

TABLE OF CONTENTS

LIST OF FIGURES

Page

LIST OF FIGURES ...CONTINUED

LIST OF FIGURES...CONTINUED

LIST OF FIGURES------CONTINUED

LIST OF FIGURES------CONTINUED

LIST OF FIGURES------CONTINUED

LIST OF FIGURES-----CONTINUED

LIST OF TABLES

ABSTRACT

Static and dynamic behavior of the dry and saturated Ottawa sand are studied in the constitutive modeling laboratory, by using cubical multiaxial device with servo-controlled loading system and high speed automatic data acquisition system.

In this investigation, the multiaxial cubical device with servo-controlled loading system and high speed automatic data acquisition system is used to apply independently the three-dimensional loading and measure corrosponding strains and stress. The conventional tests such as the direct shear and cylindrical triaxial cannot apply indenpendly three-dimensional states of stress to a soil sample. Therefore, the conventional equipment allows testing of samples only along a limited number of stress paths. The cubical triaxial device, on the other hand, is capable of applying the general three-dimensional state of stress.

The previous cubical device is mechanically controlled, and therefore some form of servo-controlled system and high-speed data acquisition system was required to perform the cyclic test, which require severals simultaneous readings of pore pressures and displacements.

So, the cubical multiaxial device is modified to include the servo-controlled pressure system and automatic data acquisiton sysem. To understand the cyclic behavior and post cyclic behavior, comprehensive laboratoy tests have been performed on the dry and saturated Ottawa sand, covering a number of relative densities and confinements.

Some of the these tests will be used for the formulation of the disturbed state concept (DSC) model in the future.

Chapter 1

INTRODUCTION

1.1 General

The main objective of this thesis is to study the dry and saturated behavior of Ottawa sand by using servo-controlled loading and automatic data acquisition systems. The conventional testing in which cylindrical specimens are tested, two of the three principal stresses are equal. The third principal stress, being different from the other two, provides the principal stress difference. Such axisymmetric loading is not common in practice. Therefore, the conventional equipments allow testing of samples only along a limited number of stress paths. Hence, the material parameters obtained from such limited tests may not be valid under all states of stress. The truly triaxial device on the other hand, is capable of applying a general three-dimensional stress paths. Therefore, the constitutive behavior of materials can be studied under all significant of states of stress.

Many of the earlier cubical devices were mechanically controlled, and therefore testing was limited to simple stress path and was not convinent. Therefore, some form of servo-controlled system is required to perform the cyclic tests which required faster loading and unloading, and to follow generalized stress paths.

In addition, the high speed data acquisition system is required to take several simultaneous readings of pressures and displacements during the tests. Therefore, a servo-controlled cubical multiaxial device with a hight speed data acquisition system is required.

Liquefaction of saturated sands during earthquakes has often been a major cause of damage to buildings and earth embankments. Much of the damage occurring during the 1964 earthquakes in Niigata, Japan and Anchorage, Alaska was caused by the liquefaction and consequent failure of sandy foundation soils or by liquefaction-induced landslides. Severe settlement and lateral displacement of foundation caused by soil liquefaction also occurred in the Chilean earthquake of 1960. Recent earthquakes and resulting catastrophic events have focused much attention on the behavior of saturated sands where undrained condition conditions prevailed. These events, more than anything else, probably did more to simulate geotechnical engineering studies of earthquake-induced liquefaction than any other factor. In addition, the record of major landslides, lateral movements of the bridge suppports and failure of the waterfront structures reported in recent years as a result of this phenomenon have led to increasing efforts in development of procedures for evaluating the cyclic liquefaction or cyclic mobility potential of soil deposits.

Liquefaction induced by static loading has been a familiar topic to the virtually all geotechnical engineers since the classical work of Casagrande (1936) in this area, culminating in vastly improved understanding of phenomena such as the massive Fort Peck

Dam slide in 1936, failure of river banks, and the disastrous Abervan tailings piles slide in 1964 (Seed, 1979).

The response of the a saturated sand deposit to earhquake motion is a very important and difficult problem of soil dynamics. The dynamic response, at least for the loose to medium dense sands, is dominated by the effects of progressive pore-water pressure increases that develop during an earthquake.

The resistance to deformation at any point in the sand deposits is a function of effective stress which is turn depends on the rates of generations and dissipation of pore-water pressure. The cyclic response of a saturated sand layer is a very complicated process.

Cyclic triaxial tests have been used for seismic liquefaction evaluation of saturated sands since the pioneering work of Seed and Lee (1966) on the isotropically consolidated specimens. In this approach, saturated sand samples are consolidated in the Triaxial apparatus under appropriate stress conditions and alternating shear loads of the controlled magnitudes and frequencies are applied with no drainge allowed. Measurements of the pore water pressure changes and of the deformation behavior of sample are made, so that the onset liquefaction can be detected. The main conclusions derived from the triaxial studies are that the larger the cyclic stresses, the looser the samples and lower the confining pressure, the fewer are the number of cycles of a given shear stress required to cause liquefaction.

1.2 Scope and Objectives of the Research

This research is intended to modified the existing cubical device by using the servo-controlled valves and high speed automatic data acquisition system and then study the static and cyclic behavior of Ottawa sand (silica sand). So the objectives of this research are:

- To modify the existing cubical device by using servo-controlled valves and high speed automatic data acquisition system,
- To review the existing experimental and theoretical work on cyclic behavior and liquefaction studies of saturated sand,
- To perform a series of static tests on the dry Ottawa sand of 60 % relative density with different confining pressure,
- To perform a series of cyclic tests on the 20%, 40%, 60% relative density with various confining pressures, 69, 138 and 207 kPa. In particular, the focus is on the medium dense sand (60% relative density),
- To perform the static test, immediately after liquefaction to understand the postliquefaction behavior of sand,
- To interpret the results and presents the stress- strain response of sand and liquefaction potential of sand,
- To obtain data to enable development of the Disturbed State Model, in the future .

1.3 Organization of Text

A review of the previous liquefaction studies and cyclic behavior of sand is presented in Chapter two together with effect of sample preparation and testing procedures.

Chapter three presents the description of the servo-controlled mutiaxial device with automatic data acquisition system. The detailed description the data acquasiton system including, the Das-1600 data acquisition board, PDISO-8 isolated 8 digital input and 8 relay output board and EXP-16, 16-channel multiplexer and signal condition board can be found in this chapter. This chapter also presents the servo-controlled valves, including the two-way solenoid valves, solid state relay and pressure transducer. The pore pressure measurement and drainage are resented in this chapter.

The test material, sample preparation and test procedures are provided in the Chapter four.

Chapter five presents the results of experimental investigation. The behavior of Ottawa sand under static loading and cyclic loading, postcyclic undraind behavior are also presented here.

Chapter six presents the conclusions implied from the results of this research as well as recommendations for future research.

Chapter 2

LITERATURE REVIEW

2.1 Introduction

Liquefaction is a phenomenon where frictional soil suddenly loses its strength due to the loss of effective stress. Seismic ground motion can cause soil liquefaction. Liquefaction of saturated sands during earthquakes has often been a major cause of damage to buildings and earth embankments. Many failures of earth structures, slopes, and foundations on saturated sands have been attributed in the literature to the liquefaction of sands. Classical examples of liquefaction are flow slides that have occurred in the provenience of Zealand in Holland (Geuze, 1948 and Koppejan et. al., 1948) and in the point bar of Mississippi River. The failure of Fort Peck Dam in Montana in 1938 (Casagrande, 1965) and the Lower Lan Norman Dam (Seed et al., 1971) during the 1971 San Franado Earthquake in California provides typical examples of liquefaction failures of hydraulic-filled dams. The best known cases of foundation failures due to liquefaction are those that occurred during the 1964 earthquake in Niigata, Japan (Kishida, 1965).

Much of the damage occurring during the 1964 earthquakes in Niigata, Japan and Anchorage, Alaska was caused by the liquefaction and consequent failure of sandy foundation soils or by liquefaction-induced landslides. Severe settlement and lateral

displacement of foundation caused by soil liquefaction also occurred in the Chilean earthquake of 1960. Recent earthquakes and resulting catastrophic events have focused much attention on the behavior of saturated sands where undrained condition conditions prevailed. These events, more than anything else, probably did more to simulate geotechnical engineering studies of earthquake-induced liquefaction than any other factor. In addition, the record of major landslides, lateral movements of the bridge supports and failure of the waterfront structures reported in recent years as a result of this phenomenon has led to increasing efforts in development of procedures for evaluating the cyclic liquefaction or cyclic mobility of soil deposits.

Liquefaction induced by static loading has been a familiar topic to the virtually all geotechnical engineers since the classical work of Casagrande (1936) in this area, culminating in vastly improved understading of phenomena such as the massive Fort Peck Dam slide in 1936, failure of river banks, and the disastrous Abervan tailings piles slide in 1964 (Seed, 1979).

The response of the a saturated sand deposit to earthquake motion is a very important and difficult problem in soil dynamics. The dynamic response, at least for the loose to medium dense sands, is dominated by the effects of progressive pore-water pressure increases that develop during an earthquake. The resistance to deformation at any point in the sand deposits is a function of effective stress, which is turn depends on the rates of generation and dissipation of pore-water pressure.

2.2 Previous Liquefaction Studies

A qualitative understanding of the mechanism underlying the liquefaction of saturated sands subjected to cyclic loading, such as that induced by earthquakes, has been recognized widely since first examined by Casagrande in 1936. Cyclic triaxial tests have been used for seismic liquefaction evaluation of saturated sands since the pioneering work of Seed and Lee (1966) on the isotropically consolidated specimens. The same authors later tested anisotropically consolidated specimen to simulate insitu static shear stresses. It was further developed by Lee and Seed (1967a and 1967b).

In this approach, saturated sand samples are consolidated in the Triaxial apparatus under appropriate stress conditions and alternating shear loads of the controlled magnitudes and frequencies are applied with no drainage allowed. Measurements of the pore water pressure changes and of the deformation behavior of sample are made, so that the onset liquefaction can be detected. The main conclusions derived from the triaxial studies are that the larger the cyclic stresses, the looser the samples and lower the confining pressure, the fewer are the number of cycles of a given stress required to cause liquefaction.

Laboratory tests based on approximations or simulations of the preceding stress conditions have been the principle means of studying liquefaction. Comprehensive reviews of laboratory test methods used for evaluating liquefaction potential have been

presented by Seed and Peacock (1971). The cyclic triaxial test has been uesd widely: Yen (1967), Rocker (1968), Lee and Fitton (1968), Castro (1969), Shibata (1970), Finn et. al (1971) Tanimoto and Shuga (1970, 1971), Ishhara and Yasuda (1972), Lee and Albaisa (1974), Wong, Seed and Chan (1975), Lee and Focht (1975), Lee (1976), Ishihara (1995), Vaid and Thomas (1995) and Vaid (1995).

2.3 Cyclic Shear Stresses, Liquefaction and Cyclic Mobility

The basic cause of cyclic mobility or liquefaction in saturated coheinsionless soils during earthquake is the buildup of excess hydrostatic pressure due to application of cyclic shear stresses induced by groundmotions. These stresses are generally considered to be due primarly to upward propagation of shear waves in a soil deposit, although other forms of wave motions are also expected to occur.

The cyclic triaxial test has been widely used to study the various factors controlling the liquefaction characteristics of sand. In the simplest form of such a test, samples saturated sands are initially consolidated under an ambient pressure and then subject to a uniform cyclic deviatoric stress under undrained conditions.

Figure 2.1 presents the soil elements under a cyclic stress condition (Seed, 1979). As a consequence of the applied cyclic stresses, the structure of the cohesionless soils tends to become more compact with a resulting transfer of stress to the pore water and a reduction in stress in soil grains. As a result, the soil grain structure rebonds to the extent

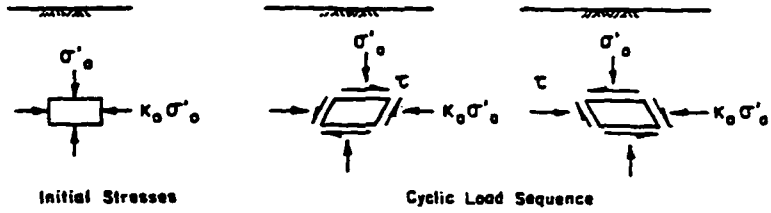

a) IDEALIZED FIELD LOADING CONDITIONS

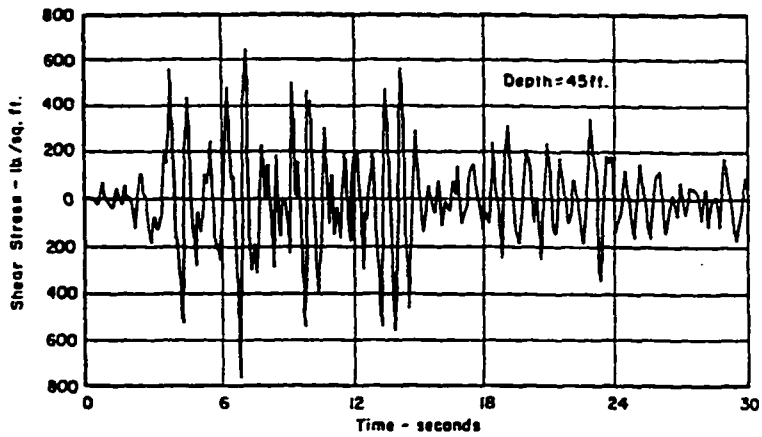

b) SHEAR STRESS VARIATION DETERMINED BY RESPONSE ANALYSIS

Figure 2.1 Idealized Field Loading Conditions (Seed, 1979)

required to keep the volume constant, and this interplay of volume reduction and soil structure rebond determines the magnitude of the increase in pore water pressure in the soil (Seed, 1979). Figure 2.2 presents the schematic diagram of mechanism of pore pressure generation during cyclic loading (Seed, 1979). As shown in the figure 2.2, the effective pressure is decrease during the cyclic loading and the pore-water pressure is increased. The increase of pore-water pressure is due to the interplay of compression due to the loading and soil sturcture rebound to keep the volume constant. The figure 2.2 shows the compression curve due to loading and rebound curve due to soil structure rebound.

As the pore-water pressure approaches a value equal to the applied confining pressure, the sand begins to undergo deformations. If the sand is loose, the pore pressure will increase suddenly to a value equal to the applied confining pressure, and the sand will rapidly begin to undergo large deformations with shear strains that may exceed 20 % or more. If the sand will undergo unlimited deformations without mobilizing significant resistance to deformation, it can be said to be ***liquefied*** (Seed, 1979). So the term of the ***liquefaction*** indicates a condition where a soil will undergo continued deformation at a constant low residual stress or with no residual resistance, due to the build up and maintenance of high pore water pressures which reduce the effective confining pressure to a very low value. The ***initial liquefaction*** indicates a condition where during the course of cyclic stress application, the excess pore-water pressure becomes equal to the applied confining pressure on completion of any full stress cycle.

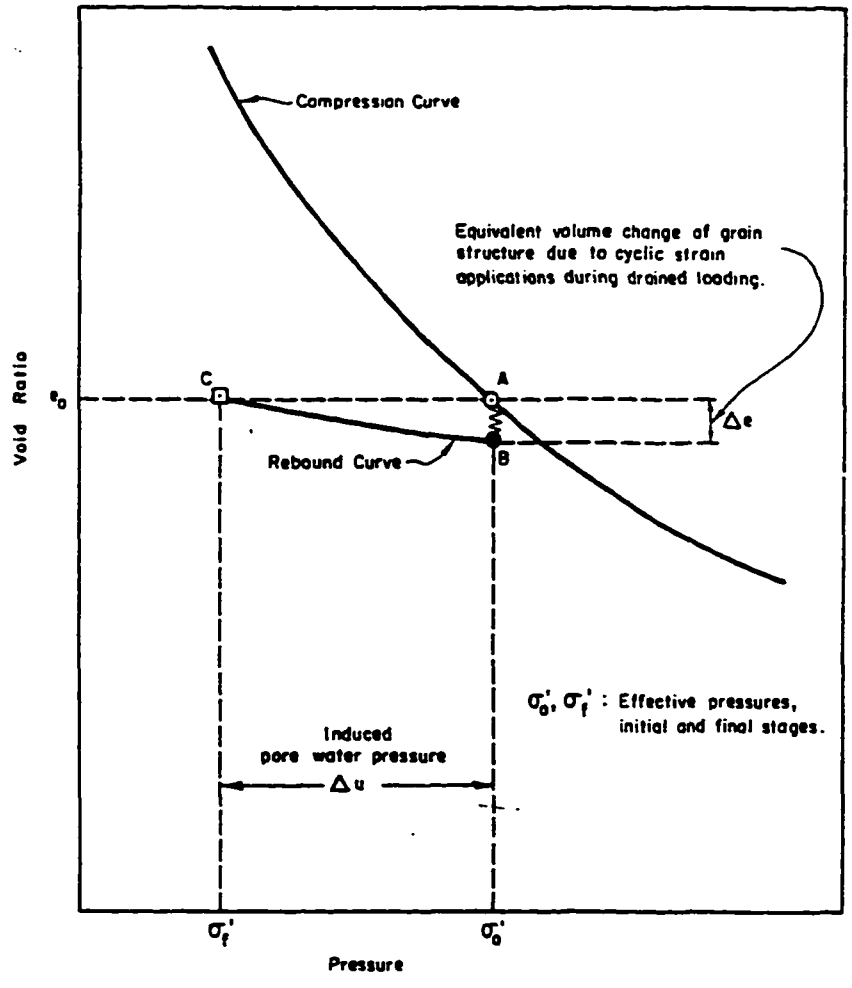

Figure 2.2 Schematic Diagram of Mechanism of Pore-pressure Generation during Cyclic Loading (Seed, 1979)

The term ***cyclic mobility*** or "development of a peak cyclic pore pressure ratio of 100% with a ***limited strain potential***" means, for any cyclic loading condition, there appears to be a cyclic strain level at which the soil will be able to withstand any number of cycles of a given stress without further increase in maximum deformation. The ***cyclic mobility*** is explained as below.

For the dense sand, it may develop a residual pore water pressure, on completion of a full stress cycles, which is equal to the confining pressure, but when the cyclic stress is applied on the next stress cycle, the soil will tend to ***dilate***, the pore pressure will drop if the soil is undrained, and the soil will ultimately develop enough resistance to withstand the applied stress. As the cyclic loading increases, the amount of deformation required to produce a stable condition may increase.

So the ***cyclic mobility*** indicates a condition in which cyclic stress applications develop a condition of initial liquefaction and subsequent cyclic stress application cause ***limited strains*** to develop, either because of the remaining resistance of the soil to deformation or because of the soil dilates, the pore pressure drops and the soil stabilizes under applied loads (Prakash, 1980).

The upward flow of water to the ground surface from an underlying layer in which pore pressure ratio of significant magnitude has been produced by the earthquake ground motions may well be the cause of the surface manifestation of liquefaction, such as sand boils, a *quick condition*, which can cause major damage to structures supported

on the near-surface soil (Ambraseys and Sarma, 1969; Seed, 1975: Yoshimi and Kuwabara, 1973).

Niigat Earthquake, Japan, (1964)

In Niigata Earthquake, Japan (1964), the peak cyclic pore pressure ratio of 100% were developed between depths of 15 ft to 40 ft during the 50 sec. duration of earthquake shaking, with a consequent development pore pressure ratios equal to 100% at depths of 10 ft., 3 ft. and 1 ft. at times of approx. 3 min, 4 min and 13 min respectively, after the ground motion had stopped (Seed, 1975). Figure 2.3 presents the pore pressure ratio vs time in the Niigata earthquake. Figure 2.4a presents the analysis of liquefaction potential of Niigata Earthquake (June16, 1964). This analysis is based on the SPT values (standard penetration test) and cyclic stress ratio at any depth in the ground.

$$N_1 = C_N \; N \qquad \text{.....(1)}$$

where, N_1 = corrected SPT value based on the overburden pressure

C_N = facor (can used value of Peck , 1970 or Gibbs and Holtz ,1957)

N = measured SPT value

The cyclcic stress ratio at any depth in the ground can be determined from the following equation.

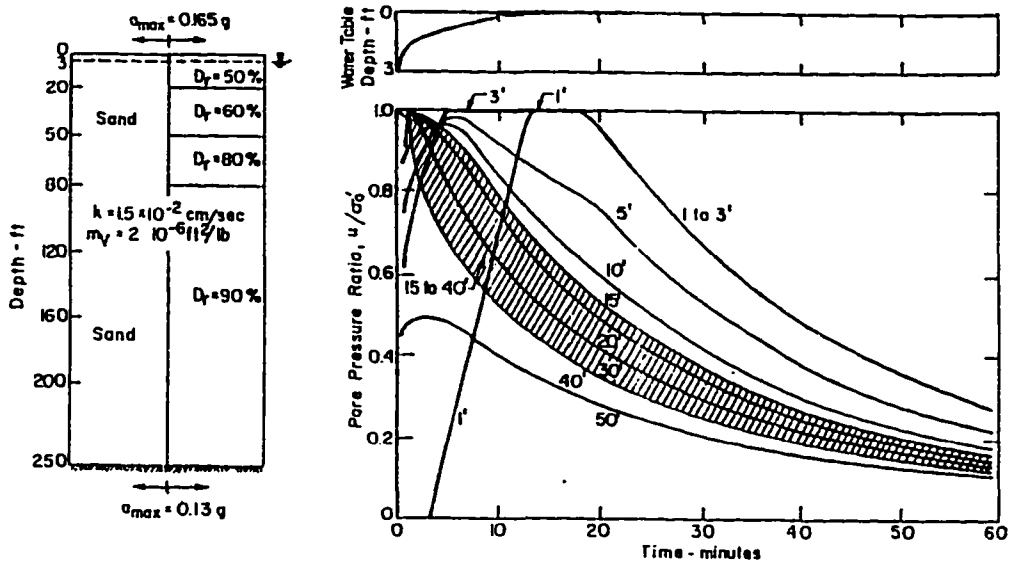

Figure 2.3 Pore Pressure vs Time in the Niigata Earthquake (Seed, 1979)

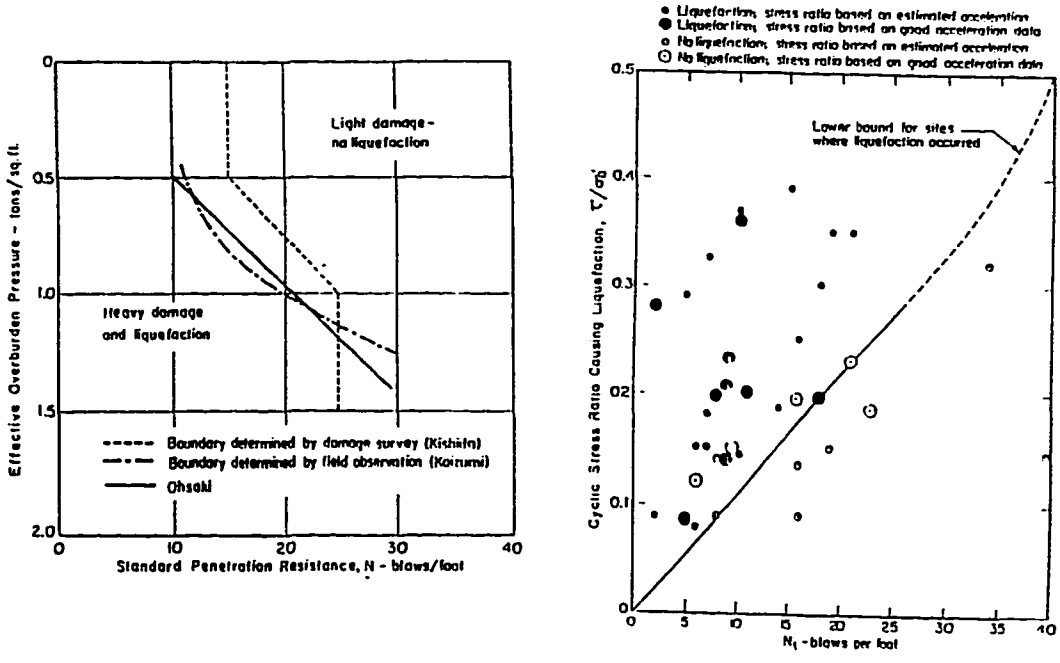

Figure 2.4a Analysis of Liquefacton Potential of Niigata Earthquake (Seed, 1979)
2.4b Correlation Chart between Corrected SPT Values and Cyclic Stress Ratio (Seed, 1979)

$$\tau_{av} / \sigma_0' = 0.65\, a_{max}\, \sigma_0\, r_d / g\sigma_0' \quad \text{.....(2)}$$

Where, τ_{av} / σ_0' = cyclic stress ratio

σ_0' = effectic overburden presssure

r_d = a stress reduction factor varying from a value of one at the ground surface to a value of 0.9 at the depth of 30 ft.

a_{max} = maximum acceleration at the ground surface

So for any given site and a given value of maximum ground acceleration, the possibility of cyclic mobility or liquefaction can readily be obtained by using the correleation chart between the corrected SPT values and cyclic stress ratio. In this chart (Figure 2.4b) the value above the line indicates the possible liquefaction. Another method is compare with the cyclic stress ratio of the equation 2 with the insitu cyclic stress ratio and if insitu cyclic stress raation is less than cyclic stress ratio, the soil will liquefy (Yokel, Dorby, Powell and Ladd, 1980).

Liquefaction Under Static Loading

Vaid and Thomas (1995) stated that, under the static loading the term liquefaction is associated with a strain softening type of undrained response, resulting in either unlimited or limited flow deformation (Figure 2.5). This type of strain softening response is termed as *contractive* by Castro (1969). The term *dilative* is used when the strain softening does not occur.

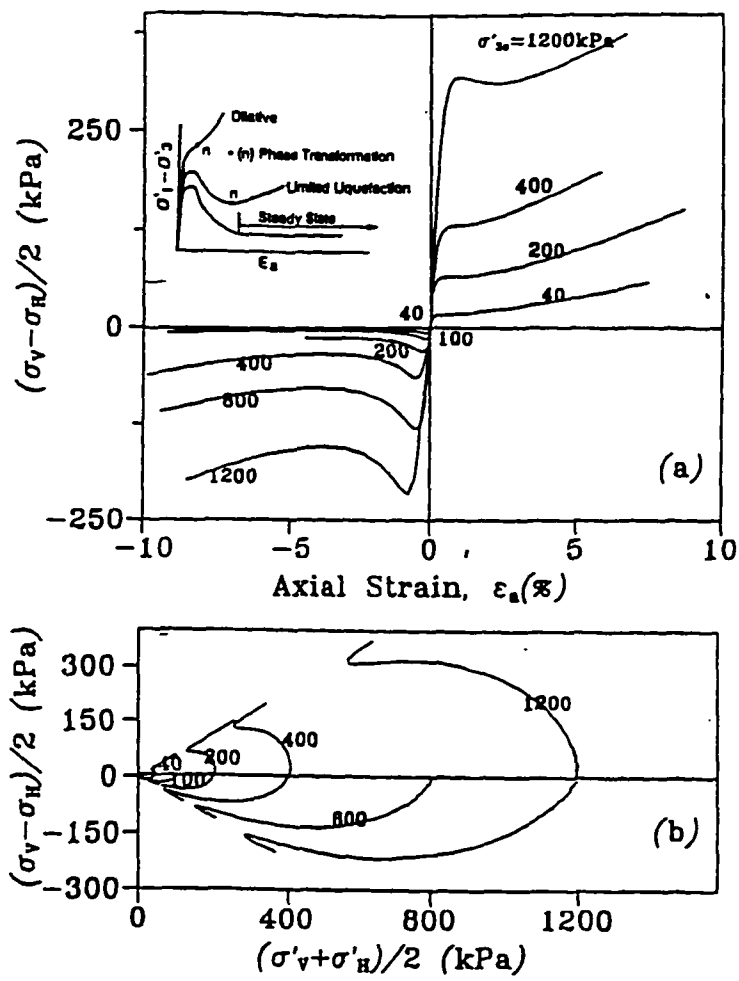

Figure 2.5 Static Undrained Behavior of Loose Fraser River Sand (Vaid and Thomas, 1995)

2.4 Behavior of Sands under Cyclic Stress Application

Results of the Cyclic Test

Several cyclic undrained triaxial tests on saturated sand have been investigated by Seed and Lee (1966) on Sacramento River sand retained between No. 50 and No.100 US sieves. The result of a typical test in loose sand (void ratio, e = 0.87) is shown in Figure 2.6. For this test, the initial all-round pressure and the initial pore water pressure 195.96 kPa (28.4 psi) and 136.32 kPa (14.2 psi), respectively. The cyclic deviator stress σ_d was applied with a frequency of 2 cycles/sec. Figure 2.6a is a plot of axial strain, change in pore-water pressure. Figure 2.6b shows that the changes in pore-water pressure become equal to the confining pressure during ninth cycle, indicating that the effective confining pressure is equal to zero. During the tenth cycle, the axial strains exceed 20 % and the soil is liquefied.

Figure 2.7 shows the typical pulsating load test on dense Sacramento River Sand. As shown in the figure, after about 13 cycles, the changes in pore-water pressure become equal to confining pressure; however, the axial strain amplitude did not exceed 10 % even after 30 cycles of load application. Figure 2.8 shows the typical record of time histories of load, axial deformation and pore-water pressure (Tokei et al., 1986).

Relationship between Stress Ratio and Numbers of Cycles

Figure 2.9 presents the stress ratio vs number of cycles to cause liquefaction for the Montery sand. This figure indicates that the stress ratio is one of the control factor of

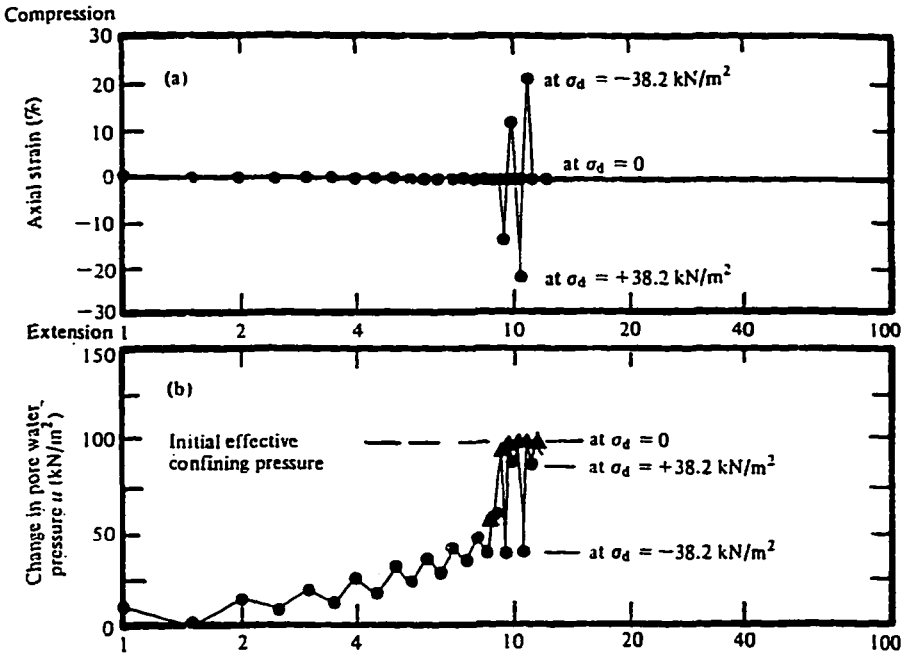

Figure 2.6 Typical Pulsating load test on loose Scramento River Sand (a) axial strain vs number of cycles and (b) observed change in pore-water pressure vs number of cycles (relative density = 38 %)

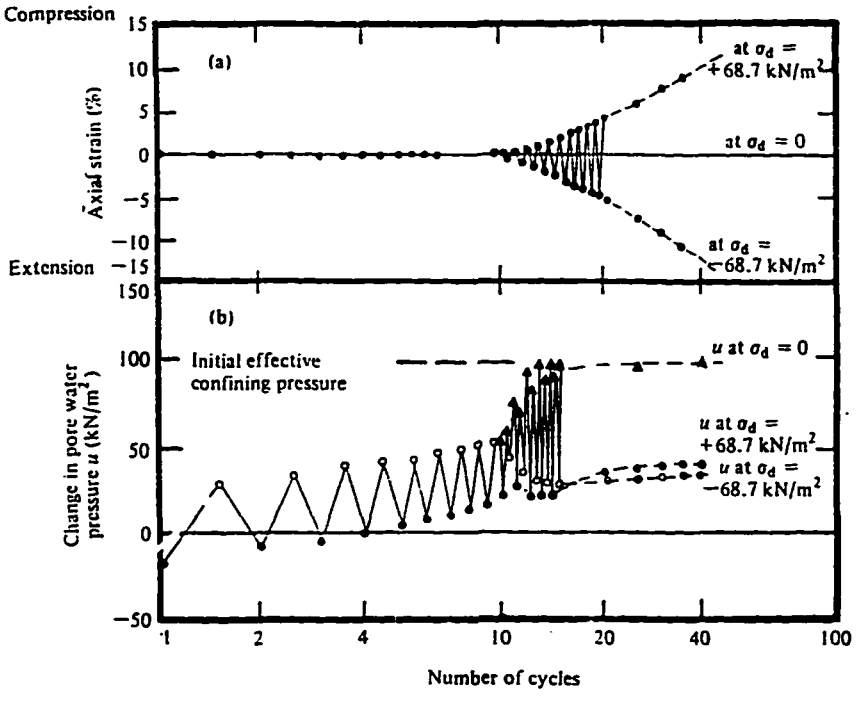

Figure 2.7 Typical Pulsating Load Test on Dense Sacremento River Sand (Seed and Lee, 1966)

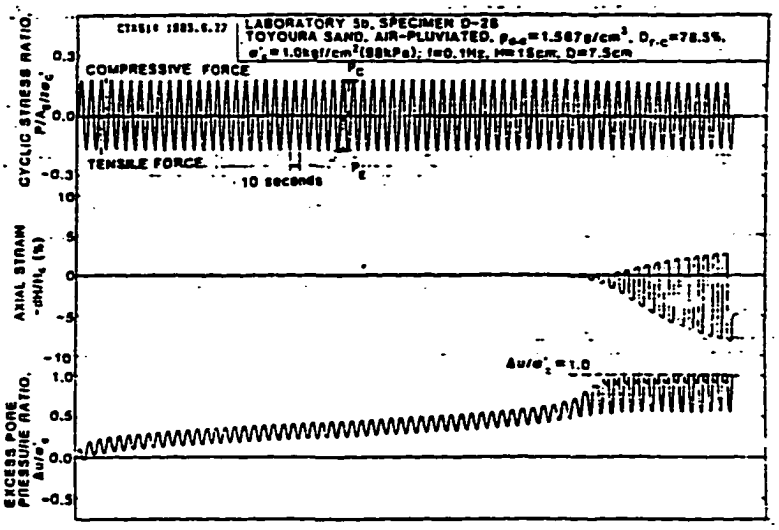

Figure 2.8 Typical Record of Load, Axial Deformation and Pore-water Pressure (Tokei et al. 1986)

the liquefaction. If you use the higher stress ratio, the number of cycles required to initial liquefaction is smaller and if you use the smaller stress ratio, the number of cycles required to initial liquefaction is higher. It is true because the stress ratio (SR) is equal to the half of the deviatoric stress devided by the effective confining pressure. If you are using the higher stress ratio means, you are using the higher deviatoric stress and because of your deviatoric stress is higher it is easier to deform the sample.

Relationship between Relative Densities and Numbers of Cycles

Figure 2.10 presents the a summary of axial strain, number of cycles for ***initial and final liquefaction*** , and the relative density for Sacramento River Sand. The figure clearly indicates that for the ***loose sand*** (Dr = 38%), the initial liquefaction reached at the 9 cycles. Then the sample deformed greatly and suddently increased to the 20% axial strain.

For the ***dense sand*** (Dr = 78 and 100 %) the sample obtain the ***initial liquefaction*** at the 8 to 11 cycles, but the axial strain increase very slowly and finally reached the axial strain 15% at 50 cycles (Dr = 78%) and 10 % at 300 cycles (Dr = 100%).

Relationship between Cyclic Deviatoric Stress and Numbers of Cycles

The relationship between the magnitude of magnitude of σ_d against the number of cycles of pulsating load applications for the liquefaction of the same loose sand is shown in Figure 2.11. According to this figure, the number of cycles of pulsating load application increases with the decrease of value of σ_d (Seed and Lee, 1966).

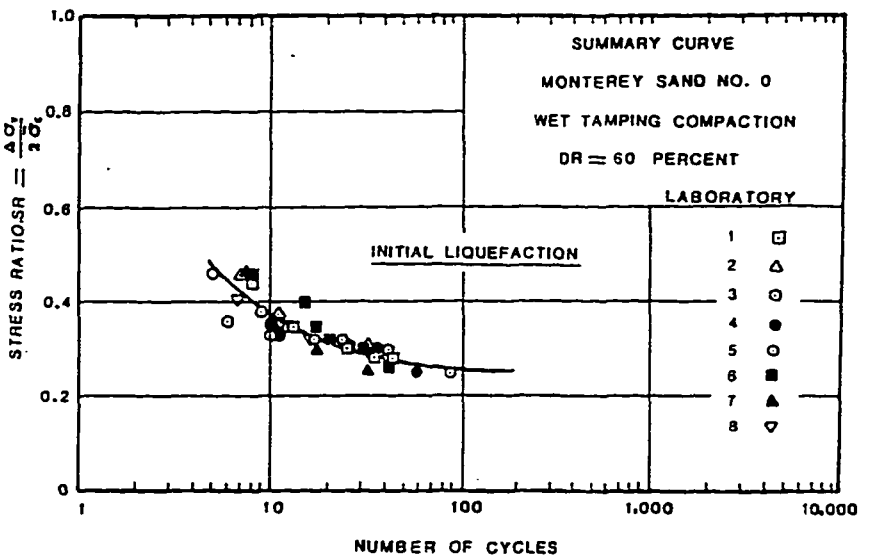

Figure 2.9 Stress Ratio Vs Number of Cycles of Monterey Sand No.0 (Silver et. al., 1976)

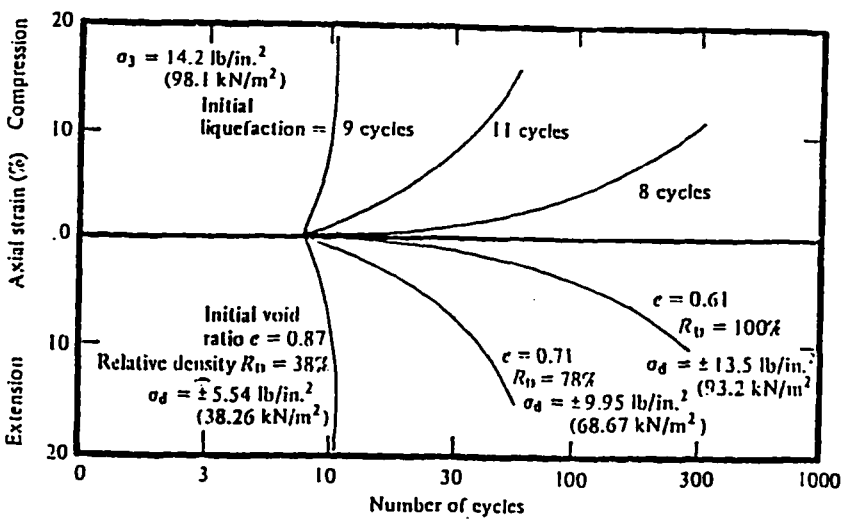

Figure 2.10 Relative Density Vs Number of Cycles of Sacramento River Sand (Seed and Lee, 1966)

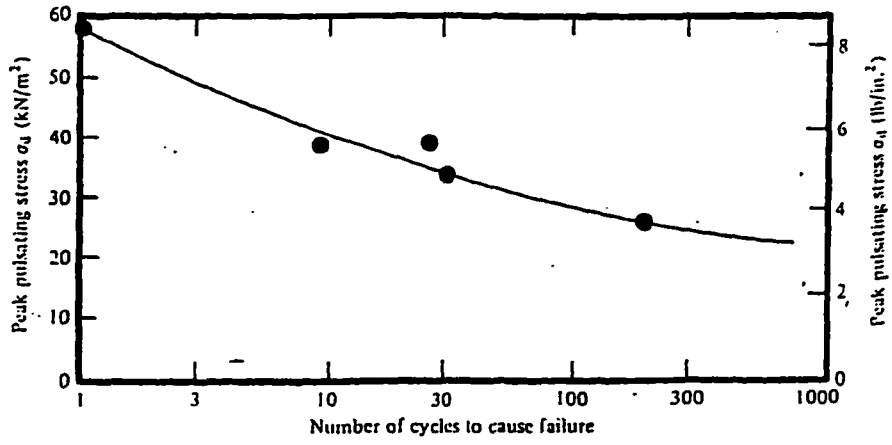

Figure 2.11 Relationship between Pulsating deviator stress and number of cycles (Seed and Lee, 1966)

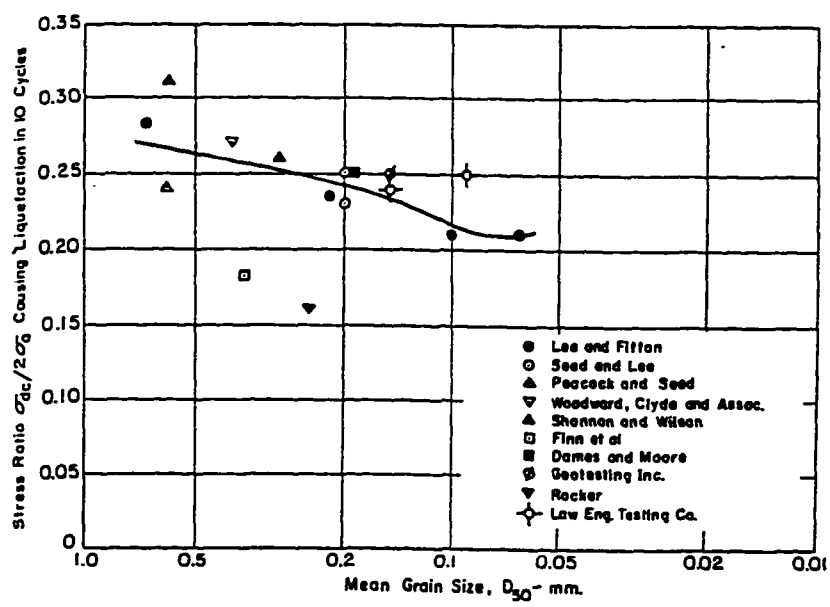

Figure 2.12 Stress condition causing liquefaction of sand in 10 cycles (Seed and Peacock, 1971)

Relationship between Mean Grain Size and Stress Ratio

The stress conditions causing liquefaction of sand in 10 cycles are shown in Figure 2.12 for different mean grain size (D_{50} in mm). The tests are performed in the various laboratories and indicates that the magnitude of the stress ratio causing liquefaction tends to decrease as mean grain size decreases from 1 mm to 0.1 mm. If the mean grain size is become smaller, the required deviatoric stress to reached the liquefaction, become smaller (Seed and Peacock, 1971).

Rate of Pore-pressure Buildup

The rate of pore-water pressure buildup in cyclic triaxial test can be found in Figure 2.13 (Seed and Martin and Lysmer, 1976). This curve is based on the cyclic loading tests and it has been found that the rate of build up of pore-water pressure generally lies within a fairly narrow range and plotted in normalized form. The tests on different sands in cyclic triaxial compression test indicate that the data falling within the band shown in the Figure 2.13.

In this curve the N_l is the number of the uniform stress cycles required to produce a condition of ***initial liquefaction*** (excess pore-water pressure = effective confining presssure) under undrained condition. Based on this curve the rate of pore pressure generation can be calculated from the following equation.

$$r_N = \left[1/2\,(1-\cos\pi\, r_u)\right]^{\alpha} \qquad \text{.....(3)}$$

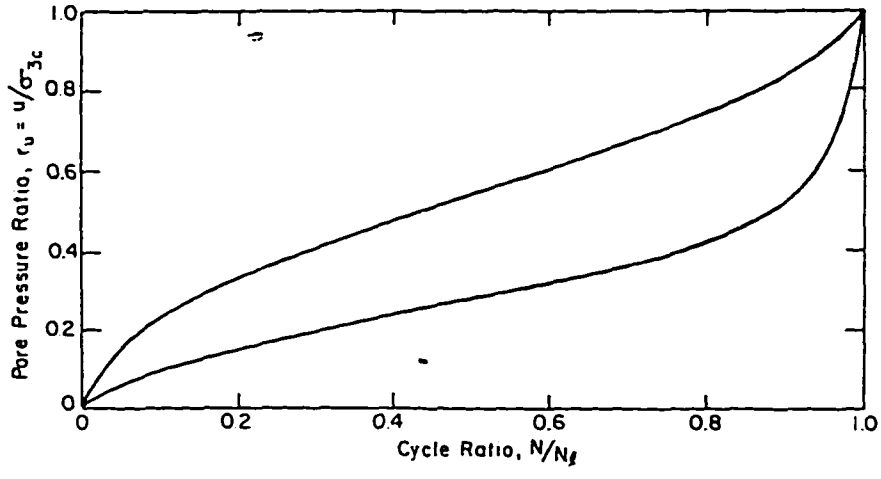

Figure 2.13 Pore-water Pressure Buildup in Cyclic Triaxial Test (Seed et. al., 1976) N=equivalent uniform Cycles, N_L= numbers of unifrom stress cycles required to produce liquefacttion, Pore Pressure Ratio = ratio of excess pore-water pressure to effective confining pressure

Where r_N = the ratio of number of applied stress cycles N to the accumulattive number of cycles required to cause liquefaction N_L

$r_N = N / N_L$

α = a function of the soil properties and test conditions and the center fo the curve is 0.7

From the above equation (2) the pore pressure ratio r_u , can be shown in terms of the cyucle ratio.

$$r_u = 0.5 + \frac{1}{\pi} arc \sin (2 r_N^{1/\alpha} - 1) \quad \text{.....(4)}$$

Cyclic Behavior of Fraser River Sand

Figure 2.14 to 2.19 show static undrained, cyclic and post cyclic behavior of Fraser River Sand (Vaid and Thomas, 1995). Figure 2.14 pesents the static undrained behavior of the Fraser sand at relative dinsity of 19, 40 and 59%. The figure indicates that **less dilative behavior** is noted in compression , with an incrasing confining stress at each density. On the extension side, the **contractive response** is found in the higher confining pressure.

Figure 2.15 presents the static undrained loading-unloading behavior of the Fraser River Sand at Dr = 19%. The sand shows the dilative in the compression but contractive, of the liquefaction type in extension. The test indicates that, on unolading the specimen liquefy and the excess pore-water pressure equal to the effective confingin pressure. The Vaid and Thomas (1995) noted this behavior as liquefaciton induced by a static load/unload cycle.

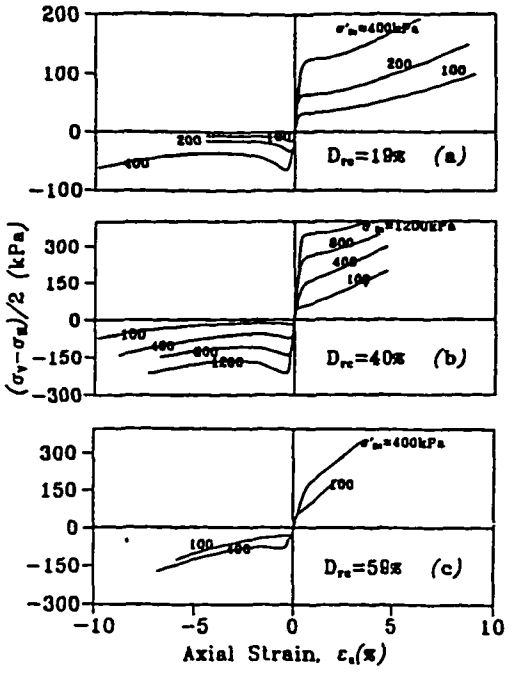

Figure 2.14 Static Undrained Behavior of Fraser River Sand at Several Relative Densities (Vaid and Thomas, 1995)

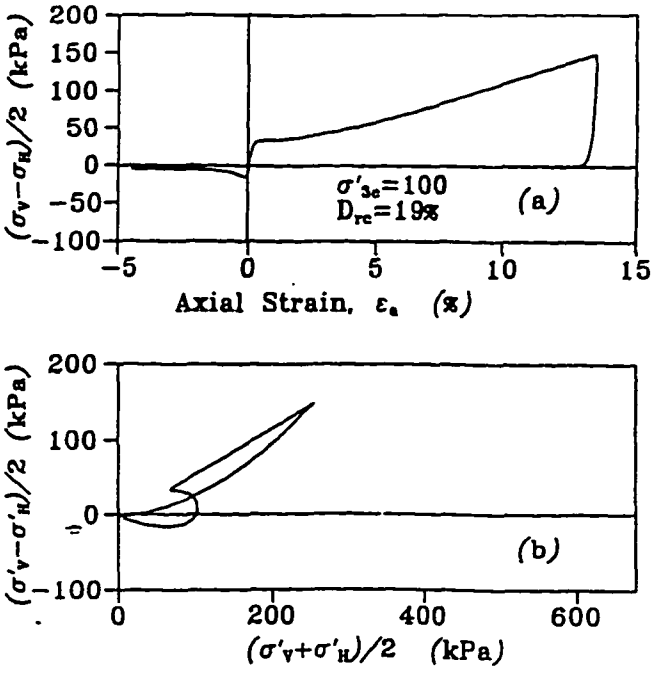

Figure 2.15 Undrained Static Load/Unload behavior of Fraser River Sand (Vaid and Thomas, 1995)

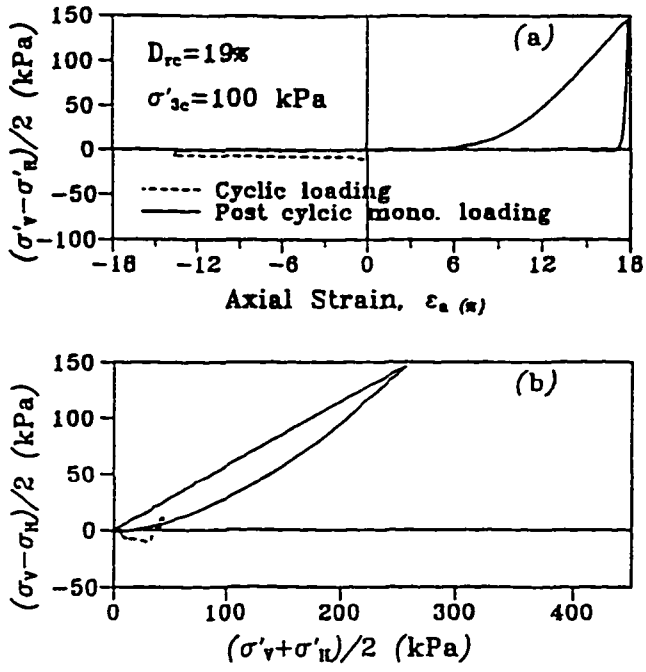

Figure 2.16 Zero Effective Stress State Following Liquefaction by Cyclic Loading (Vaid and Thomas, 1995)

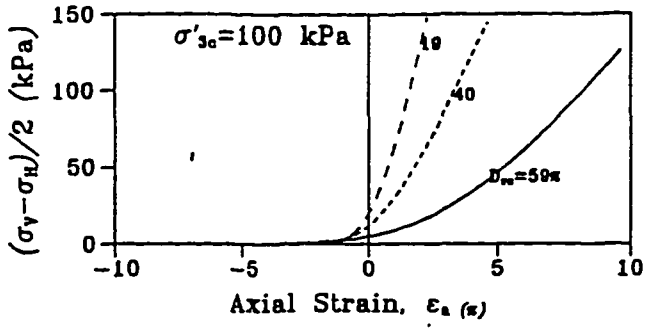

Figure 2.17 Relative Densities Effect on Postliquefaction Response (Vaid and Thomas, 1995)

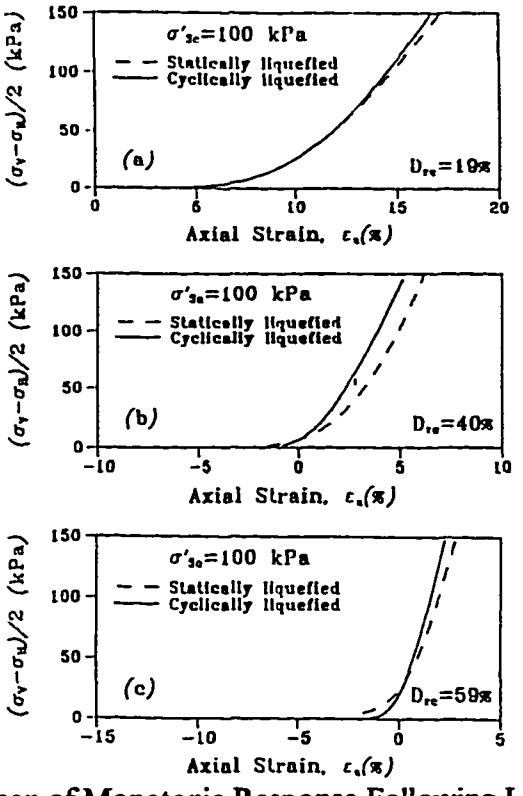

Figure 2.18 Comparison of Monotonic Response Following Liquefaction by Cyclic and Static Load/Unload Test of Fraser River Sand (Vaid and Thomas, 1995)

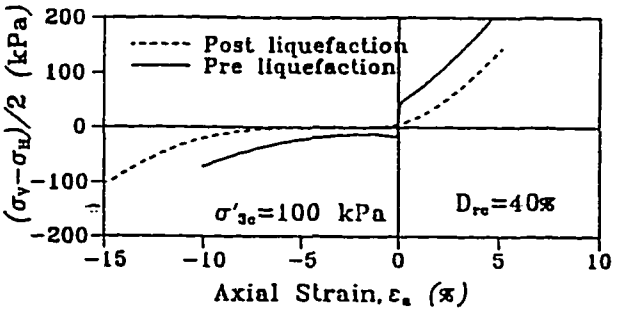

Figure 2.19 Comparison of Static and Postliquefaction Response of Fraser River Sand (Vaid and Thomas, 1995)

Figure 2.16 shows the response during the last loading cycles along with the postcyclic monotonic response of Fraser River Sand at Dr = 19% (Vaid and Thomas, 1995). They reported that during postliquefaction undrained compression loading, the sand deformed at virtually zero stiffness over a large range of axial strain and then the stiffness increases with an increase in strain. Vaid and Thomas (1995) reported that this stress-strain response in which the modulus increases with an increase in the axial strain is opposite to the usual response of soil in which the modulus drcreases with an increase in strain. This unsual stress-strain response of the liquefied soil results from the fact that upon shearing in soil dilates all the way causing the effective stress to increase.

The Figure 2.17 shows the postliquefaction monotonic response at three ralative densities and indicates that the stiffness decreases with an increase in relative density. The last part of the curves show that the curve become linear.

The comparison of the postliquefaction behavior induced by a static load/unload cycle with the cyclic loading can be found in Figure 2.18. The responses are essentially similar (Vaid and Thomas, 1995). Figure 2.19 presents the comparison of the preliquifaction and postliquefaction stress-strain response (Vaid and Thomas, 1995) and reported that the stiffness of the sand decreases with an increase in the strain until the phase transformation state (PT), but the stiffness increases continuously with strain during postliquefaction monotonic loading.

Cyclic Behavior of Ottawa Sand

Figure 2.20 presents results of the triaxial test on medium dense Ottawa sand (Finn, Bransby and Pickering, 1970). The figure shows the excess pore-water pressure, axial strain and deviator stress. The type of laoding is the type b loading shown on the top of the figure.

Figure 2.21 shows the liquefaction resistance of Ottawa sand in simple shear and triaxial compression (Finn et. al., 1970). The two lines in the figure indicate for the Dr = 37 and 70%. Liquefaction resistance of Ottawa sand at different confining pressure is shown in Figure 2.22. Figure 2.23 presents the resistance to liquefaction of Ottawa sand in triaxial apparatus with 2 kg/cm ^{2} confining pressure .

2.5 Influence of Various Parameters on Soil Liquefaction Potential

There are anumbers of factors controlling on the soil liquefaction potential, and main factors among them are;

(1) Grain Characteristics

(2) Relative density, D_r,

(3) Confining pressure, σ_0,

(4) Peak pulsating stress, σ_d,

(5) Wave form,

(6) Frequency,

(7) Soil type,

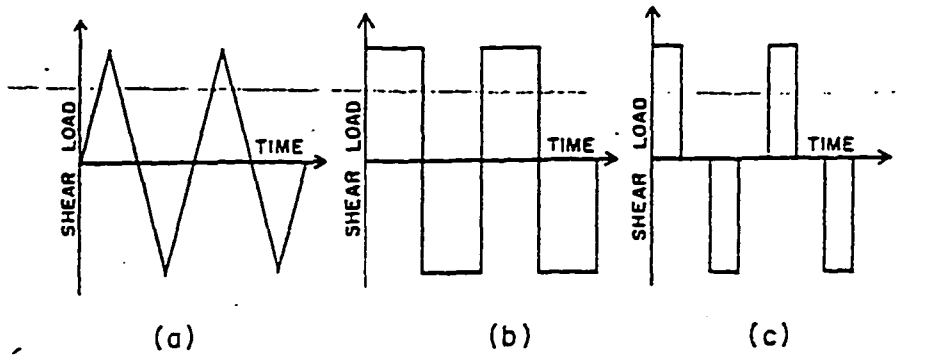

ALTERNATIVE WAVEFORMS OF SHEAR LOADING

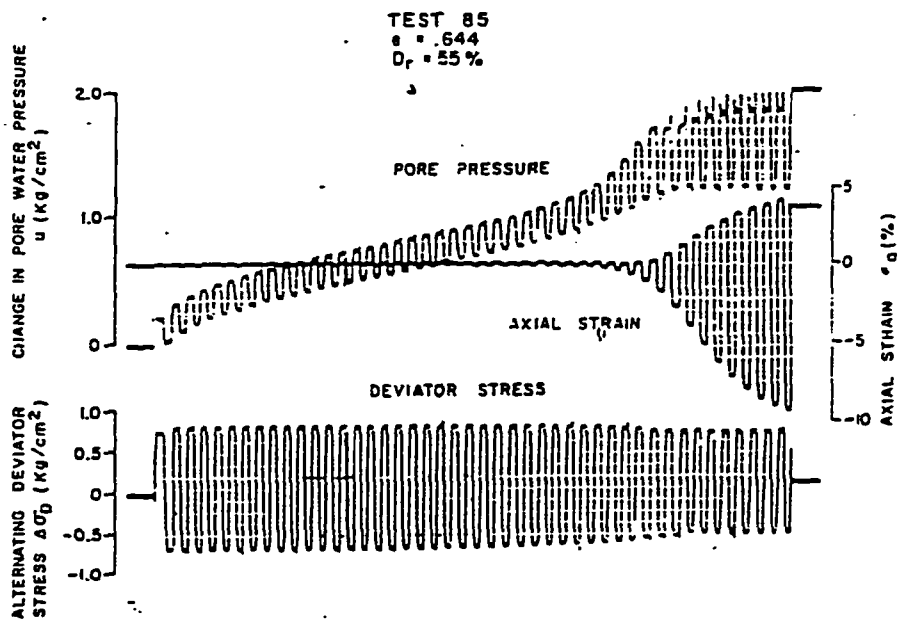

Figure 2.20 Results of Triaxial Test on Medium Dense Ottawa Sand (Finn et al., 1970)

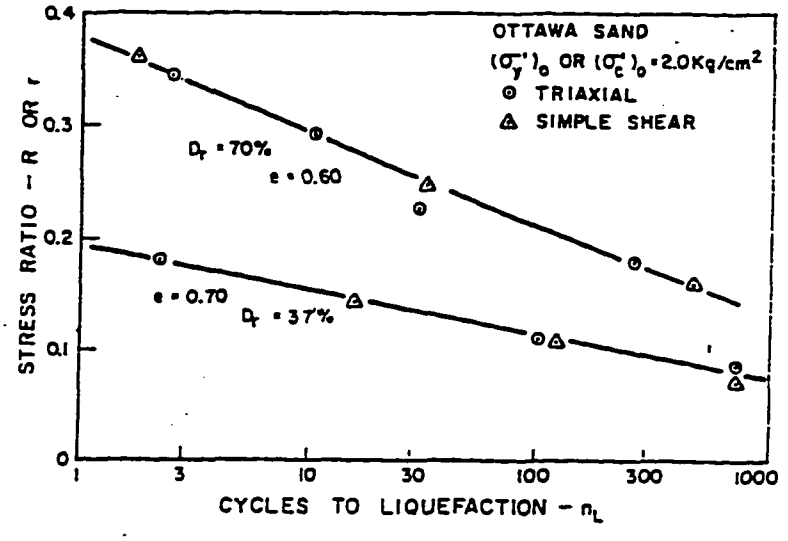

Figure 2.21 Liquefaction Resistance of Ottawa Sand in Simple Shear and Triaxial compression (Finn et. al., 1970).

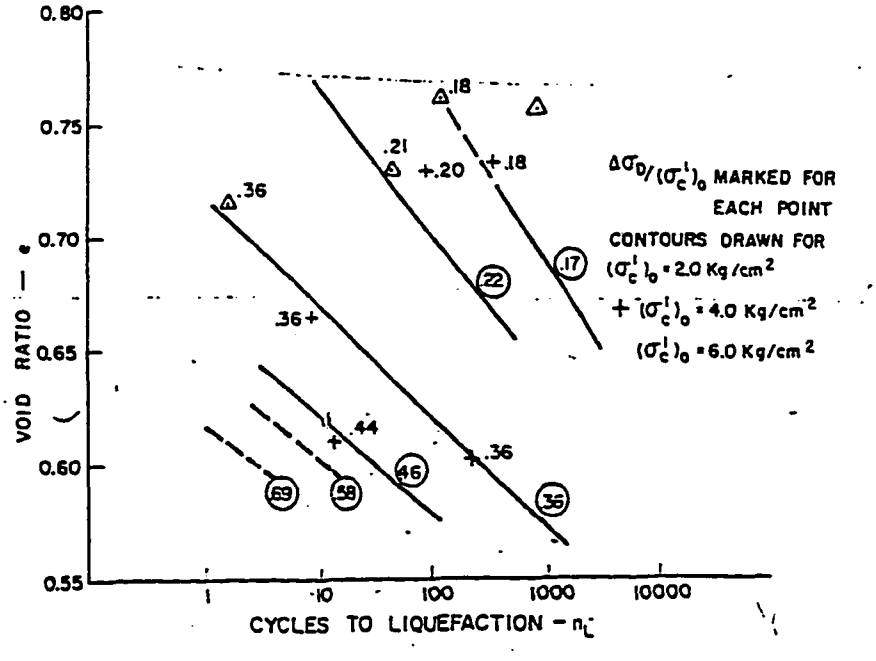

Figure 2.22 Liquefaction of Ottawa Sand at Differnt Confining Pressure (Finn et. al., 1970)

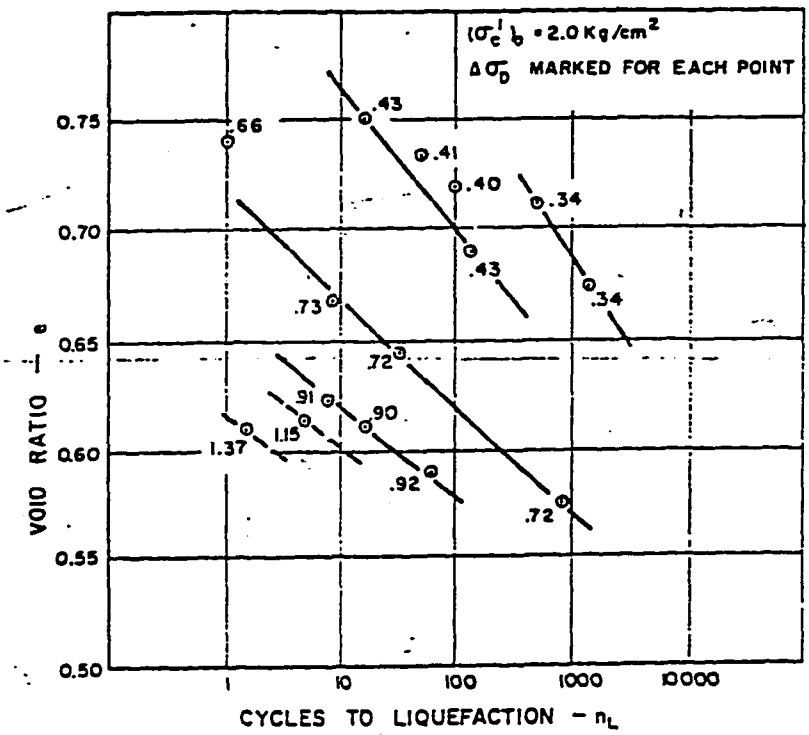

Figure 2.23 Resistance to Liquefaction of Ottawa Sand in Triaxial apparatus with 2 kg/cm^2 Confining Pressure

(8) Initial stress, and

(9) Sample preparation.

(1) Grain Characteristics

The marked variation in cyclic stress ratios causing a peak cyclic pore pressure ratios (the ratio of excess pore-water pressure to the effective confining pressure) of 100% in a given number of cycles for different sands prepared in the same manner and to the same relative density provide ample evidence that cyclic loading characteristics are influenced considerably by the **properties of the grains**.

Annaki (1975) tested four sands having very similar grain size distribution curves (the pattern of the grain size distribution curve is similar) and compacted them by the same procedure to the same relative density, only to find that the stress ratios causing a peak cyclic pore pressure ratio (the ratio of excess pore-water pressure to the effective confining pressure) of 100% varied from the mean by as much as 20 %. Castro and Polous (1977) presented the data showing similar large variation. Fine and uniform sands are believed to be more prone to liquefaction than coarse sands. Uniformly graded sands are more susceptible to liquefaction than well-graded sands.

(2) Effect of Relative Density

Since the earliest studies of soil behavior under cyclic loading conditions, it has been recognized that the cyclic stresses required to develop peak cyclic pore pressure ratios of 100 % or a given amount of strain is influenced by the relative density of soil.

Figure 2.24 shows the effect of relative density of a soil liquefaction. The top part

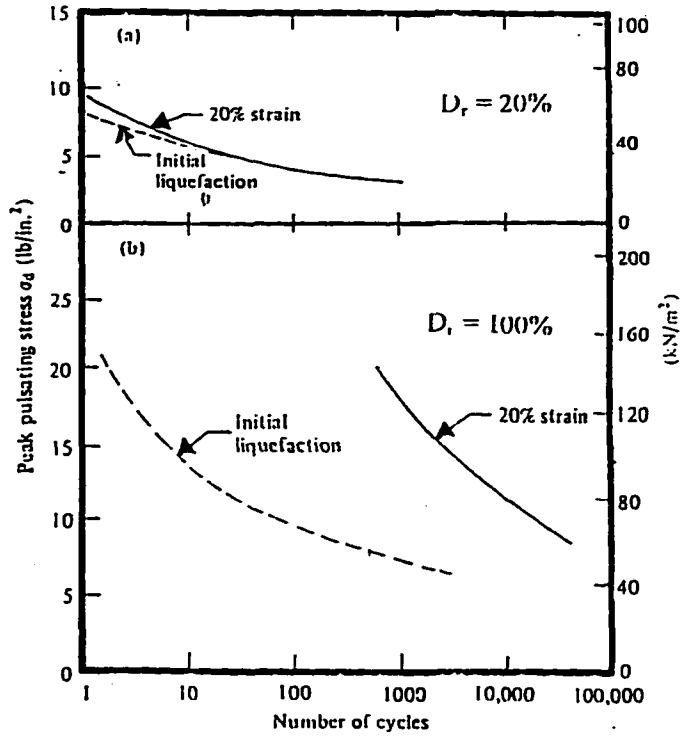

Figure 2.24 Effect of Relative Density on Soil Liquefactoin (Lee and Seed, 1967)

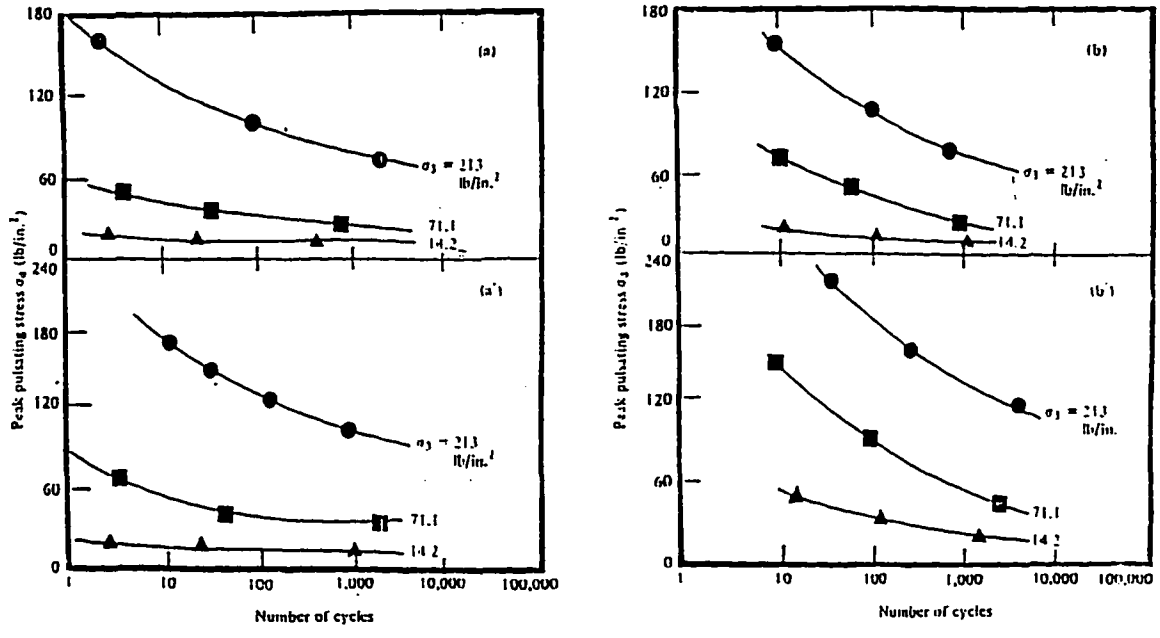

Figure 2.25 Effect of Confining Pressure on Liquefaction for Sacramento River Sand, Dr=100%,e=0.61 (a) Initila Liquefaction (b) 20% Strain (Lee and Seed, 1967)

of the figure indicates that the initial liquefaction and failure develop simultaneously in the loose ($D_r = 20\%$) but the numbers of cycles increase between the initial liquefaction and failure in the dense sand ($D_r = 100\%$) (lower figure).

(3) Effect of Confining Pressure

The effect of confining pressure on liquefaction is shown in Figure 2.25. The lower the confining pressure acting on a sand, the lower the number of cycles required to induced liquefaction failure.

(4) Effect of Peak Pulsating Stress (Cyclic stress)

The higher the cyclic stress to which the sand is subjected, the smaller is the number of stress cycles required to induce liquefaction or failure. Figure 2.26 shows the variation of the peak pulsating stress with the confining pressure for initial liquefaction and 20% strain (Lee and Seed, 1967).

(5) Effect of Wave Form

The difference between the cyclic strength determined for triangular wave loading was not significantly different form that evaluated for sinusoidal wave loading (Ho and Wong, 1989). Figure 2.27 shows the effect of wave form on Monterey No.0 sand at frequency of 0.25 Hz. According to the Silver et. al (1976), the severe square wave forms and sinusoidal wave forms gave cyclic strength values differing by about 10%. They noted that, the more abrupt the change in wave form and the longer the maximum load is

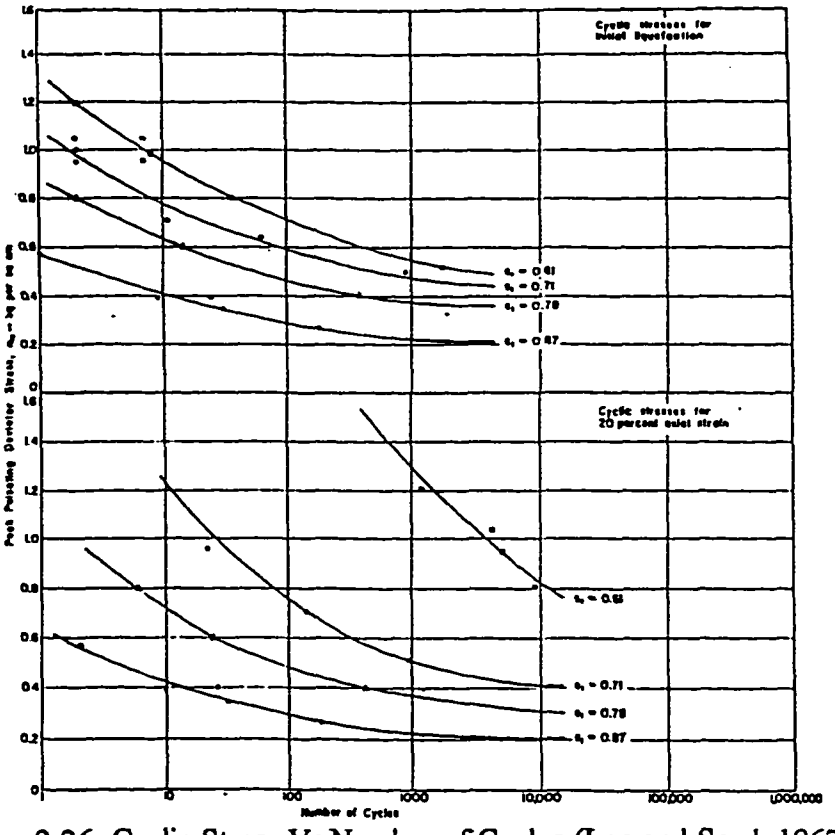

Figure 2.26 Cyclic Stress Vs Number of Cycles (Lee and Seed, 1967)

Figure 2.26 Cyclic Stress Vs Number of Cycles (Lee and Seed, 1967)

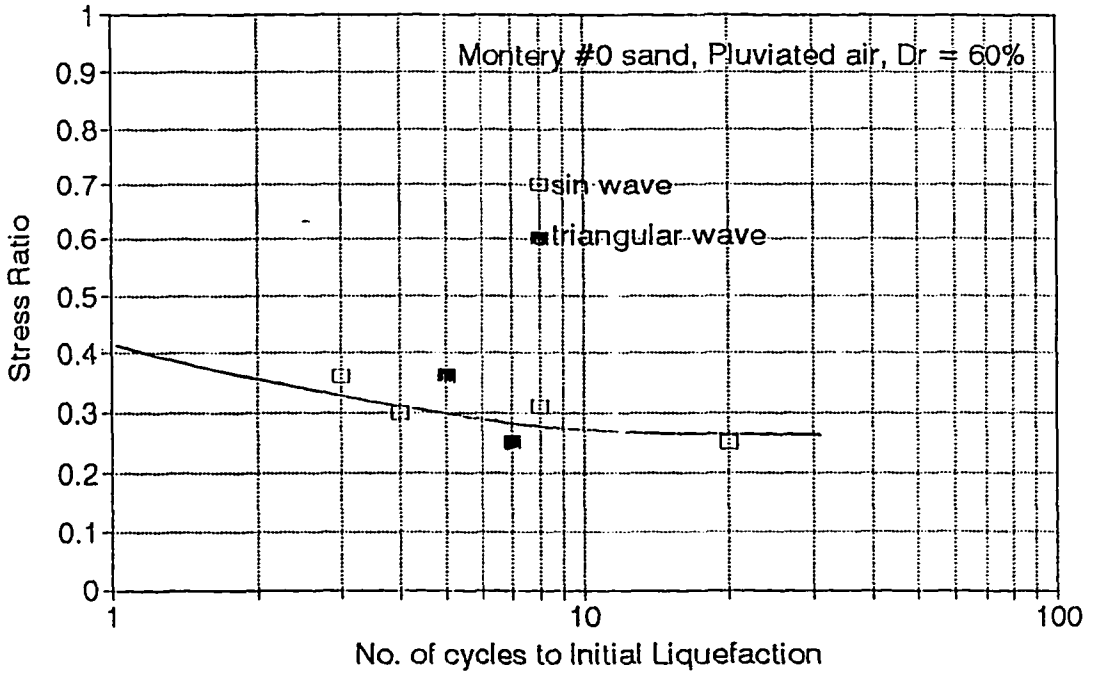

Figure 2.27 Effect of Wave Form on Montery No.0 sand at Frequency of 0.25 Hz (Ho and Wong (1989)

applied to the sample, the lower the measured cyclic strength of the soil, it is recommended to use the sine wave Figure 2.28 (Silver et al, 1976).

(6) Effect of Frequency

It has been experimentally observed that the cyclic strength of sand is almost independent of the frequency of cyclic load (Townsend, 1977). Figure 2.29 indicates that the frequency of cyclic load does not affect the cyclic strength of sand (Ho and Wong, 1989).

(7) Soil type

A soil can develop liquefaction only if the stresses acting on the soil are substantially higher than those corresponding to the steady state of deformation for given void ratio (Casagraande, 1975; Castro, 1969;Castro, 1975; Poulos, 1971). Figure 2.30 shows the steady state deformation. If the actual stress and void ratio of the sand plots above and to the right of its steady-state line, e.g., point C, liquefaction can develop, i.e., during undrained deformation of a fully saturated sand the pore pressure will increase so that the effective stress will decrease (moving to the left at constant void ratio in Fig. 2.30) until it reaches the steady-state line at point A where the sand will deform constinuously at constant shear resistance.

The steady state line is a function of soil type (Castro, 1969 and 1977). Figure 2.31a present s the steady state lines for several sands. Figure 2.31b shows the grain size curves for the sands shwon in Figure 2.31a. Table 1 shows the characteristics of the sands shown in Figure 2.31a and b.

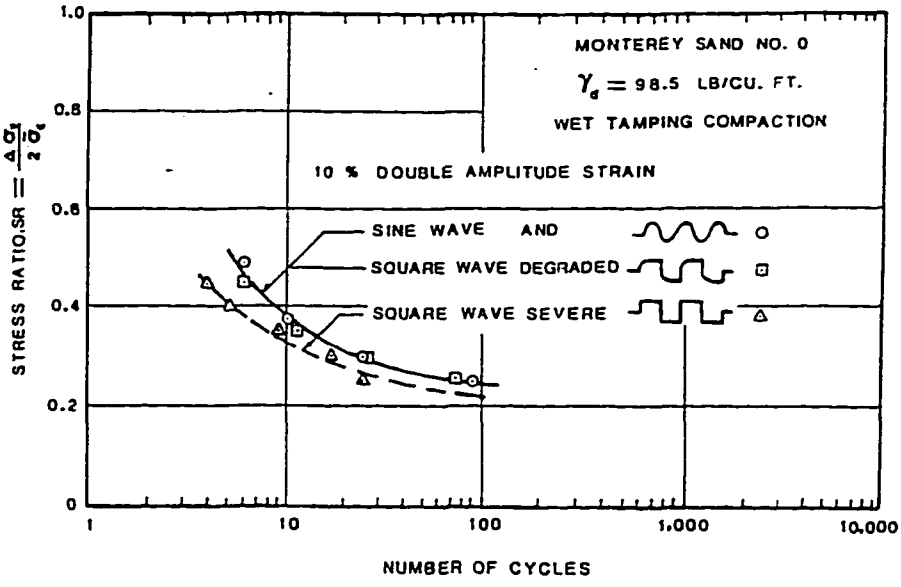

Figure 2.28 Effect of Wave Shape on Cyclic Triaxial Strength (Silver et. al., 1976)

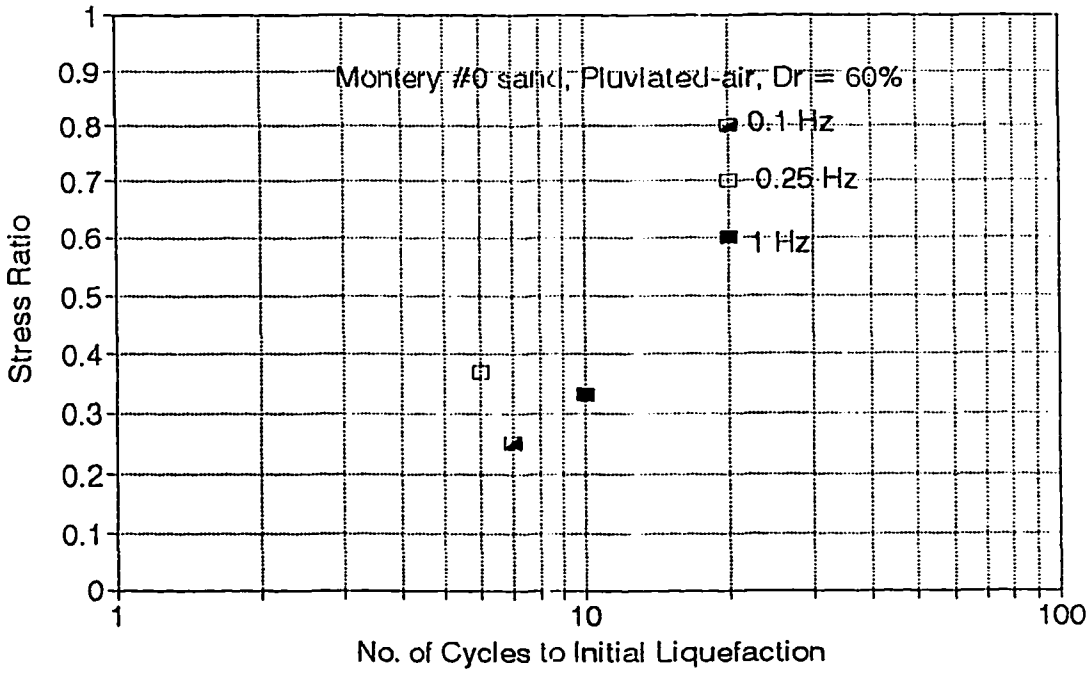

Figure 2.29 Effect of Frequency on Monterey No.0 sand with triangular wave (Ho and Wong, 1989)

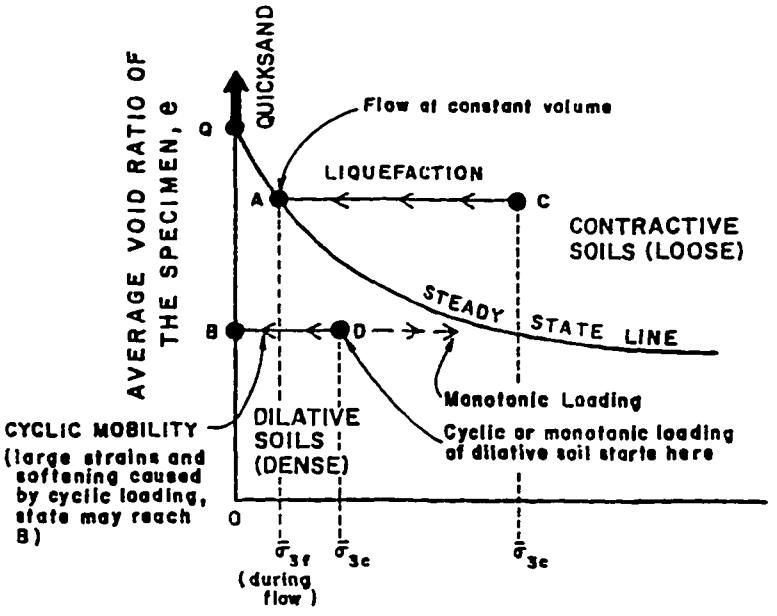

Figure 2.30 Undrained Tests on Saturated Sand Shown on State Diagram (Castro, 1969)

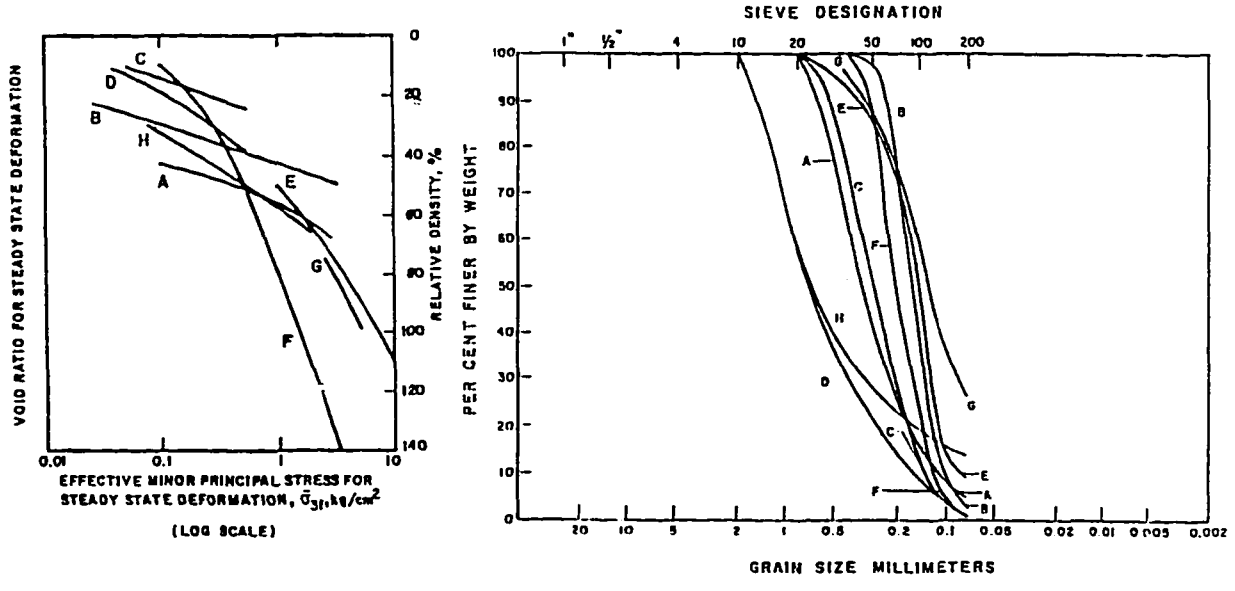

Figure 2.31a State Diagram with Steady State Lines for Various Sand (Castro, 1969)

2.31b Grain Size Curves for Sands Shown in Figure 2.31a (Castro, 1969)

Table 2.1 Characteristic of Sands Shown in Figure 2.31

Sand Designation	Grain Size Distribution D_{60} mm	C_u	% Finer Than 0.074 mm %	Grain Shape	Specific Gravity	Maximum Density pcf (5)	Minimum Density pcf (5)	Method of Specimen Preparation	Remarks
A	0.40	3.1	5	Subangular to Angular	2.72	110	84	(2)	Contains shell fragments
B	0.17	1.8	0	Subrounded	2.65	110	90	(2)	
C	0.33	2.3	1	Angular	2.87	108	90	(2)	
D	0.90	5.6	0	Subangular	2.71	114	96	(2)	
E	0.17	2.1	8	Angular	2.87	101	79	(2)	Slightly micaceous
F	0.23	2.0	0	Angular	2.50	73	56	(2)	Contains platey-shaped grains
G	0.15	-	26	Angular	2.79	-	-	Undisturbed	
H	0.85	17	13	Subangular	2.71	124	98	(2)	
L	0.74	2.5	0	Subrounded	2.66	121	104.8	(3)	
M	0.20	-	44	Angular	2.77	122 (1)	-	(4)	Micaceous, PI = 11
P	0.33	4.7	11	Subrounded to Subangular	2.66	122	98.3	(3)	
Q	1.6	32	12	Subrounded to Subangular	2.84	145	121.2	(3)	
R	0.60	2.1	0	Subrounded to Subangular	2.69	116	96.5	(3)	

(1) ASTM D1557 Compaction Test
(2) Tamping, moist soil, in layers
(3) Vibration, dry soil, in layers
(4) Kneading, moist soil, in layers
(5) To convert pcf to specific gravity, divide by 62.5

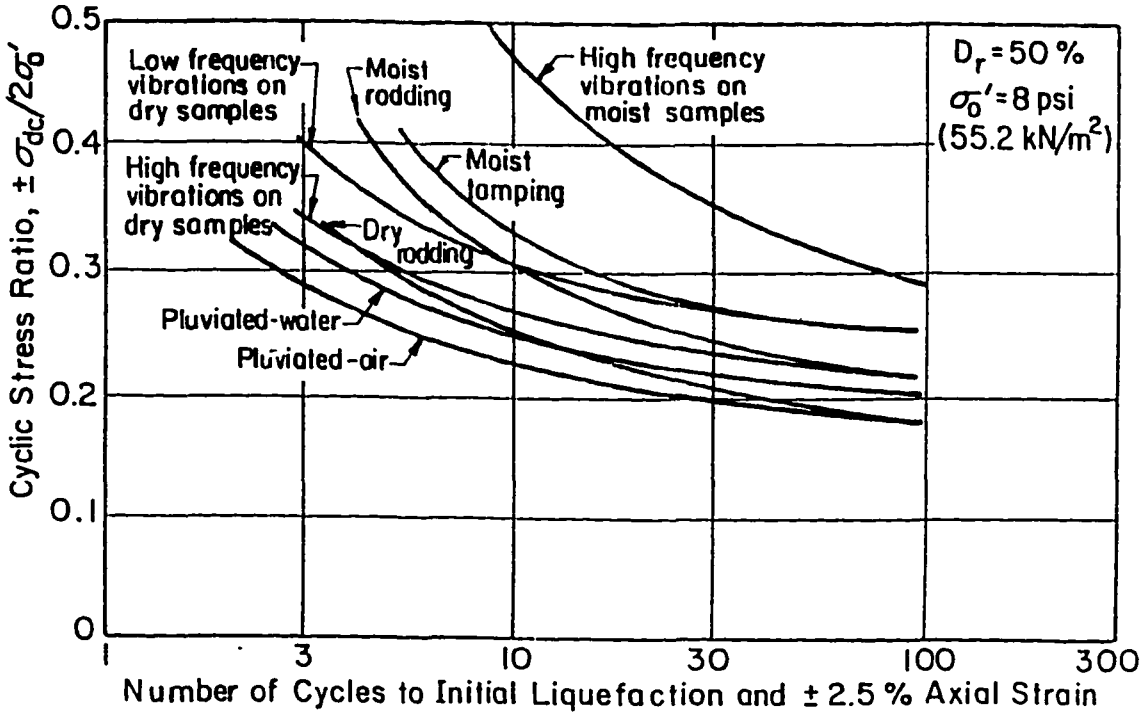

Figure 2.32 Effect of Sample Preparation Method on Liquefaction Potential (Mulilis, Chan and Seed, 1975)

(8) Effect of initial stress

A sand will reach the steady state only if the shear stresses are high enough to induce liquefaction failure. How far and how fast the sand can flow under steady-state conditions will depend on the magnitude of the difference between the applied shear stresses and the strength that remain after liquefaction.

Higher initial shear stresses increase the probability of liquefaction of contractive saturated sand, because higher initial shear stress mean that a smaller increment in stress will cause liquefaction (Castro, 1977). The initial shear stresses are measured by the principal stress ratios at the end of consolidation (effective major principal stress/effective minor principal stress).

(9)Effect of Sample Preparation

Ladd (1974, 1977) has provided a clear evidence that the characteristics of saturated sand under cyclic loading are significantly influenced by the method of sample preparation and soil structure. Typical results showing the magnitude of this effect is shown in Figure 2.32. It is clear that, depending on the method of sample preparation, the stress ratio required to cause a peak cyclic pressure ratio (the ratio of excess pore-water pressure to the effective confining pressure) of 100% in a given number of stress cycles for samples of the same sand having the same density may vary as much as 200%. Figure 2.33 presents the effect of compaction on stress-strain and volume change curves

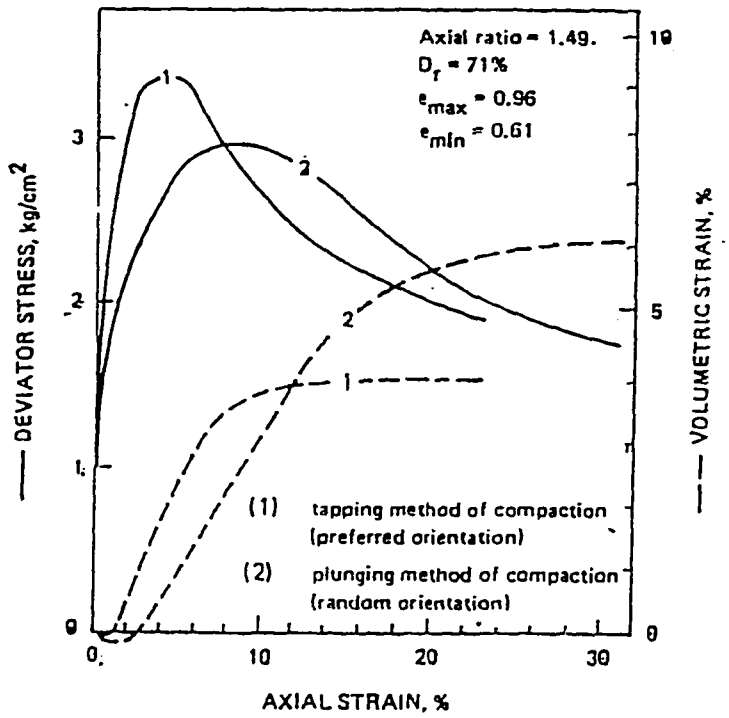

Figure 2.33 Effect of Sample Preparation on Stress-Strain and Volume Change Curve (Ladd, 1977)

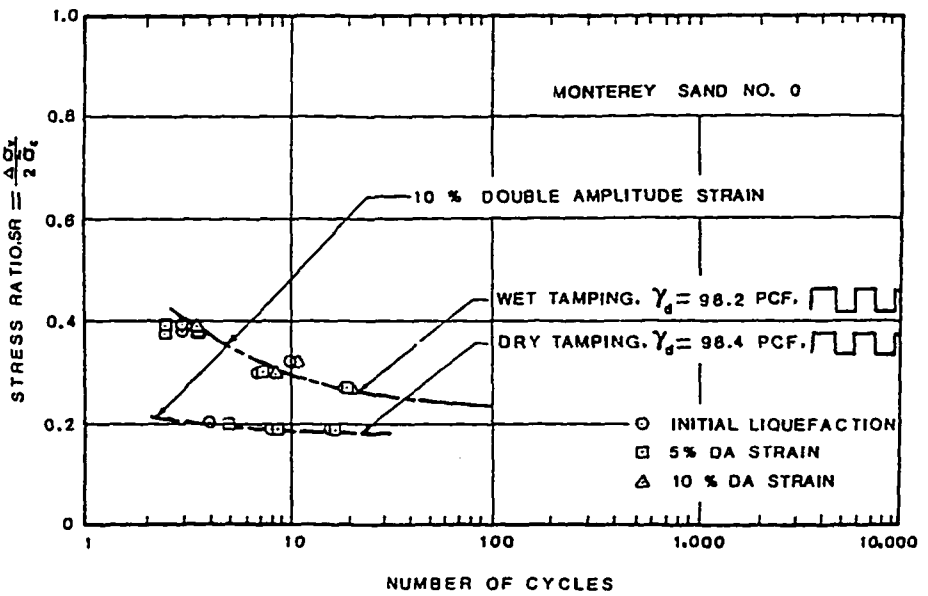

Figure 2.34 Effect of Sample Preparation on Liquefacton Potential (Silver et. al., 1976)

(Ladd, 1977). Figure 2.34 supports the view of Ladd (1977) and Mulilis, Chan and Seed (1975) by Silver et. al. (1976).

Chapter 3

DESCRIPTION OF THE SERVO-CONTROLLED CUBICAL DEVICE WITH AUTOMATIC DATA ACQUISITION SYSTEM

3.1 Cubical Device

Figure 3.1 presents the cubical device developed by the Sture and Desai (1989) in which its structural and operational features have been described.

The hollow reaction frame cube, which is cut from a solid block of 2014T-6 Aluminum, measures 19.1 cm(7.5 inches) exterior and 11.4 cm (4.5 inches) interior, per side. The frame carries the walls of the device with eight 0.95 cm (3/8 inches) steel bolts threaded into each side. A maximum hydrostatic compression pressure of 1724 kPa (250 psi) is designed on the capacity of the aluminum threads that accept these wall bolts. The frame contains 12 small threaded holes for sample vacuum lines, pore pressure measurement and drainage. The interior of the frame is designed to accept a10.2 cm (4 inch) cube sample that is held in place by 6 flexible silicone membranes. The flanges of the silicone membranes rest in the shallow recess on each frame side.

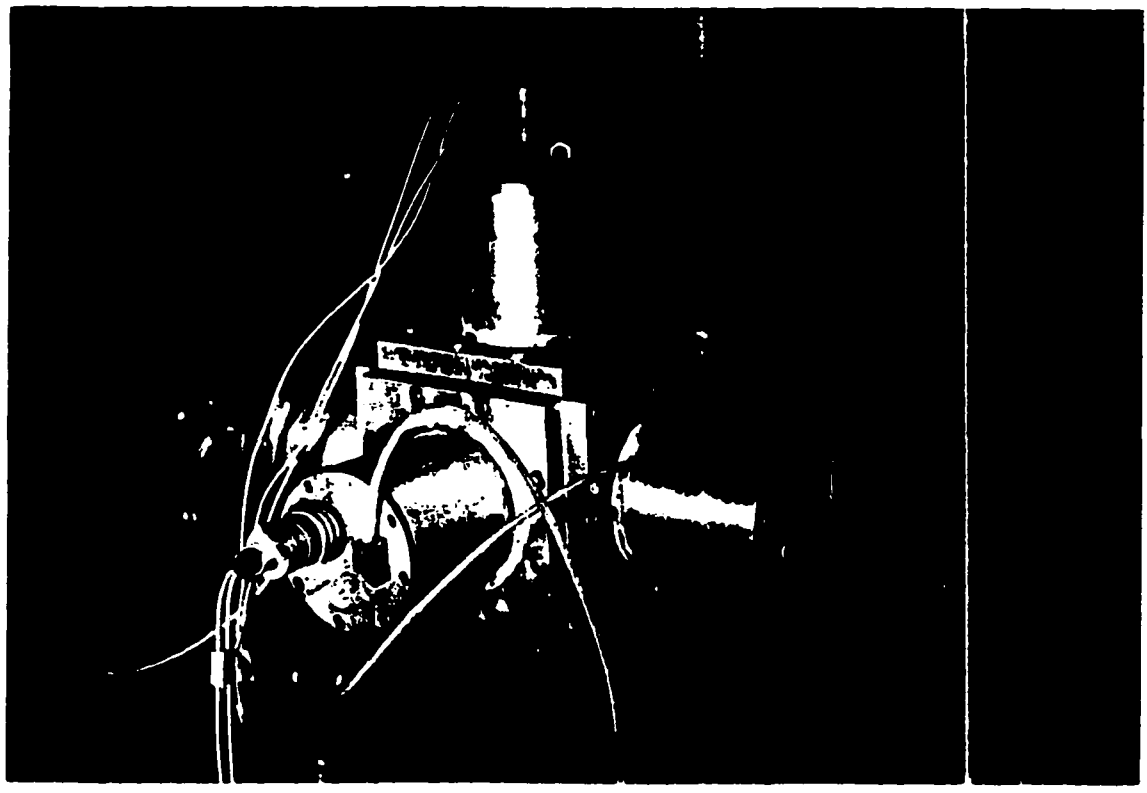

Figure 3.1 Photograph of Cubical Device

3.2Data Acquisition System

Figure 3.2 shows the schematic diagram of the hardware interfacing of the data acquisiton system. Figure 3.3 shows the schematic diagram of the hardware interfacing of the data acquisition system. The automated data acquisiton system consisted of the following major components:

- DAS-1600 high speed analog and digital I/O board (Manufacturer produces two types of DAS-1600 series board, and the board we were using is DAS-1601 board)
- PDISO-8 Isolated 8 digital input and 8 relay output Board
- EXP-16 16-Channel Multiplexer and Signal Condition Board

Figure 3.4 presents the PC-486 with the DAS-1600 board (at the bottom) and PDISO-8 board (on top). In this system there were more than 16 channels of measurements, analog input expansion sub-multiplexer (Model EXP-16, MetraByte Corporation) was used, together with STA-16 Screw Terminal Accessory Board. Figure 3.5 shows the STA-16 and STA-8 AO (STA-16 is closed to computer) which are connected to the DAS-1600 board (DAS-1600 board is installed at the bottom part of the computer) and PDISO-8 board. The STA-8 AO, EXP-16 and 5V power supply and digital pore-water pressure meter are shown in Figure 3.6.

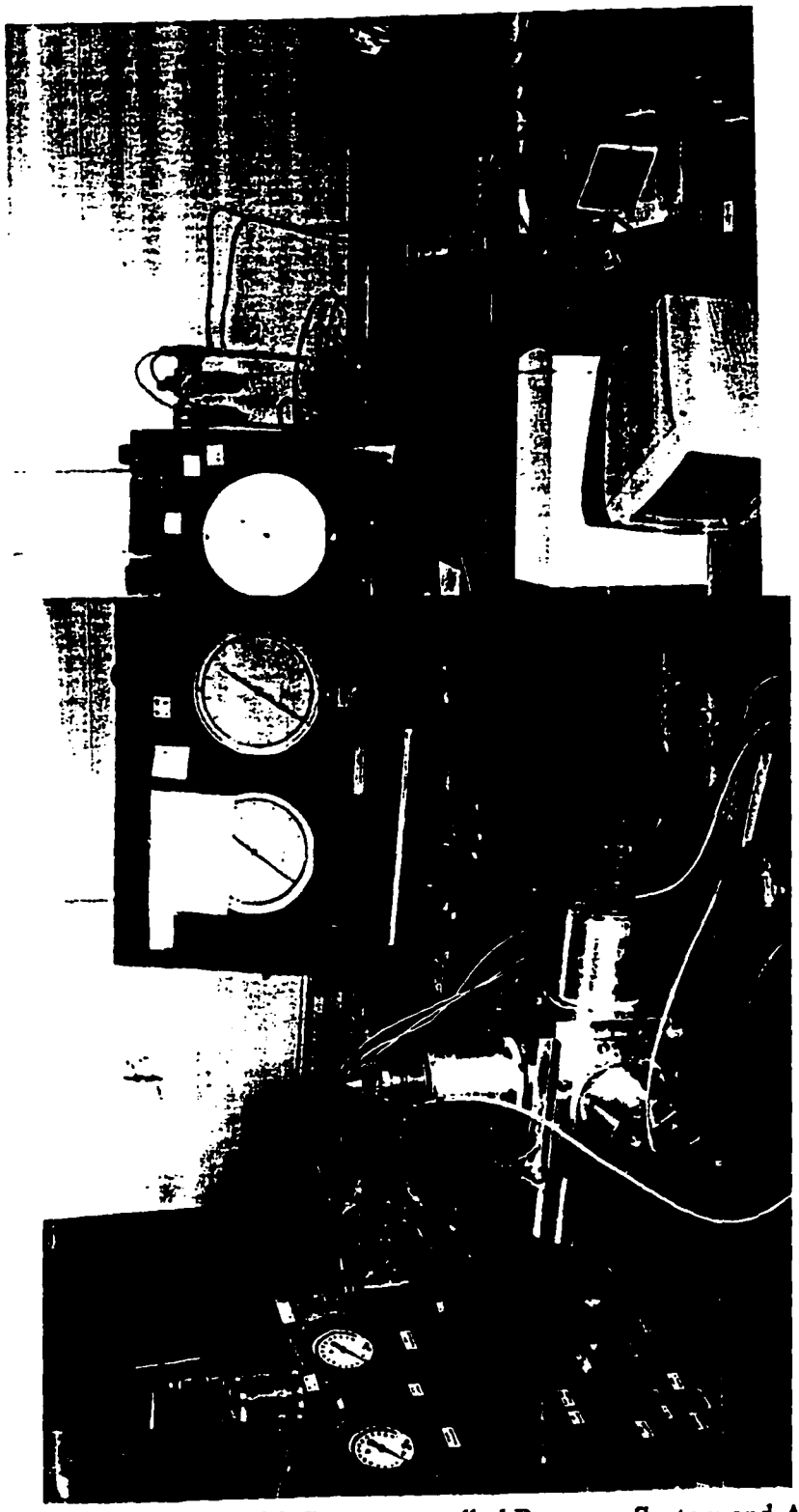

Figure 3.2 Cubical Device with Servo-controlled Pressure System and Automatic Data Acquisition System

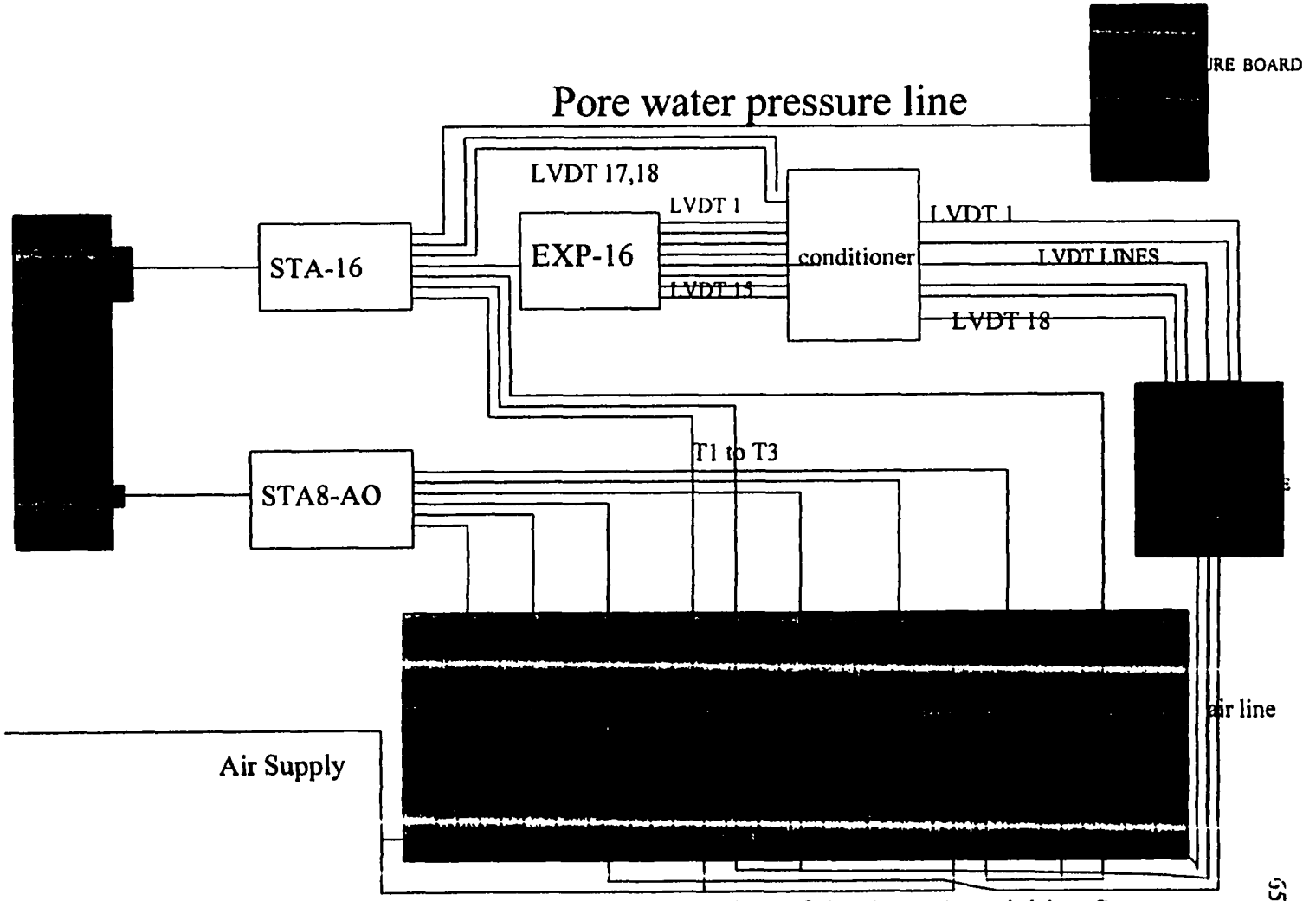

Figure 3.3 Hardware Configuration of the Data Acquisition System

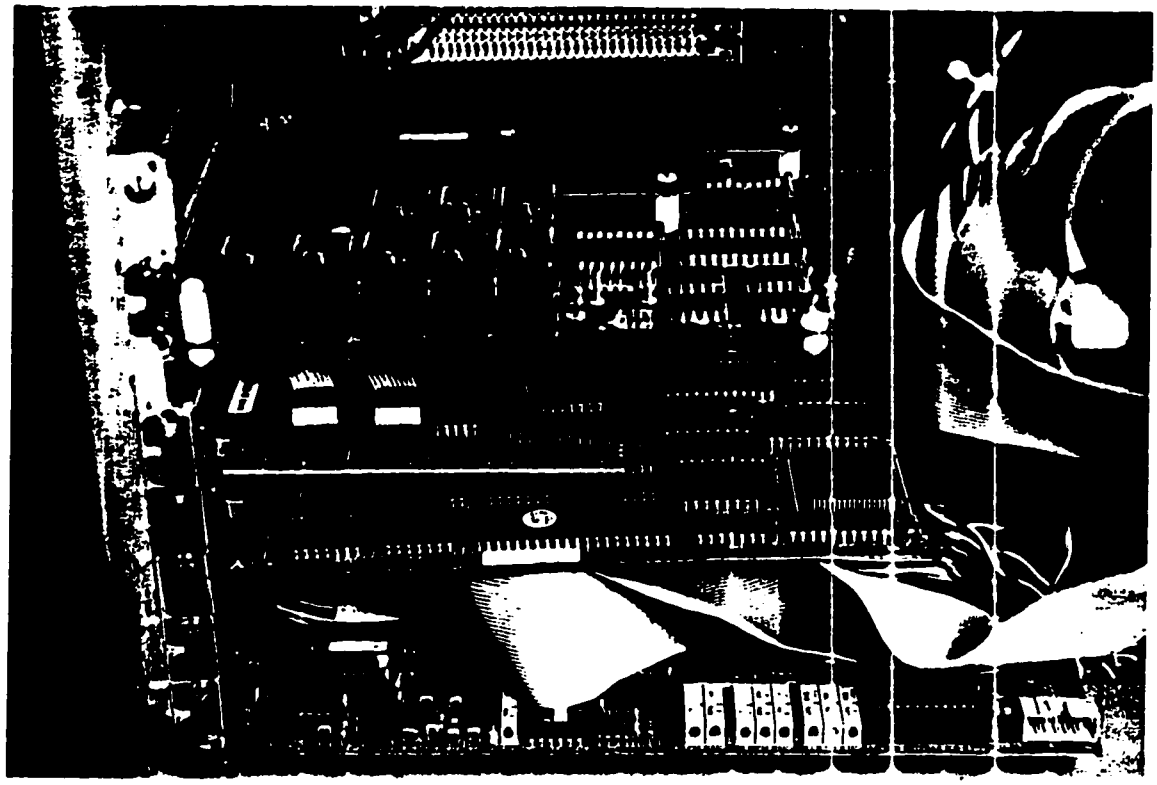

Figure 3.4 DAS-1600 board (bottom) and PDISO-8 board (top) slotted into the PC-486 Mother Board

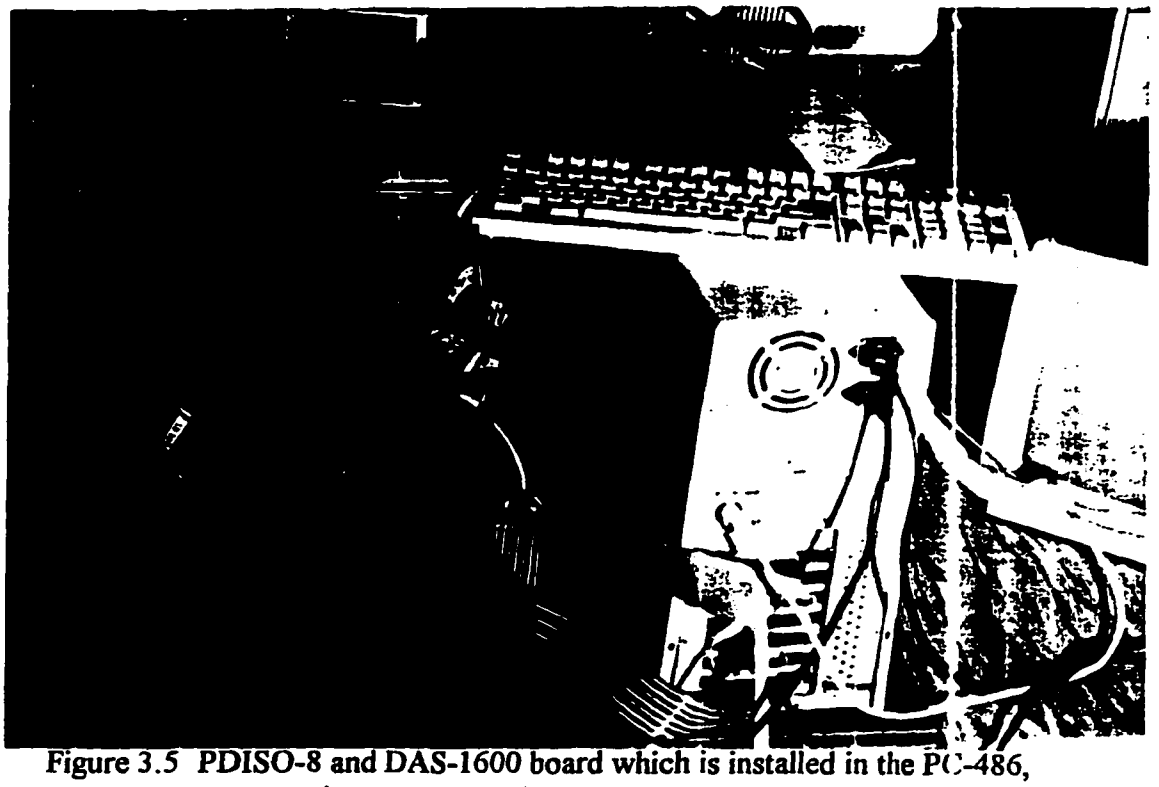

Figure 3.5 PDISO-8 and DAS-1600 board which is installed in the PC-486, connected to STA-16 and STA-8 AO

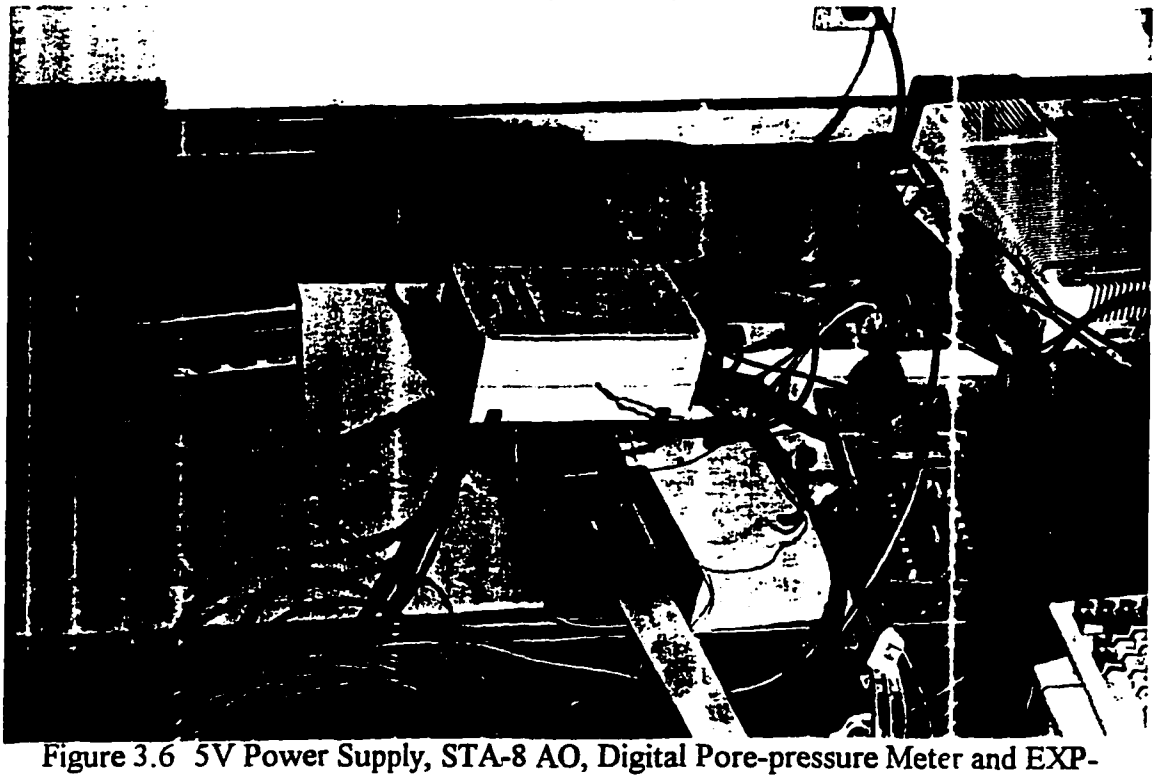

Figure 3.6 5V Power Supply, STA-8 AO, Digital Pore-pressure Meter and EXP-16 (From Left to Right)

3.2.1 DAS-1600 high speed analog and digital I/O board

Figure 3.7 presents the block diagram of the Das-1600 board. The Das-1600 board is a high speed analog and digital I/O board for the IBM PC/XT/AT and compatibles from the Keithley aMetraByte Company, Taunton, MA. The board occupies a single expansion slot in the computer (Figure 3.5, connected with the cable with red and white strip). This board is constructed with an integral ground plane to minimize noise and crosstalk even at high sample rate, see User Manual (Gyi and Desai, 1996). The important features of the DAS-1600 board is described in the following paragraphs; to know details for the DAS-1600 board and the detailed descriptions can be found in the User Manual (1996) and Function Call Driver provided by the manufacturer.

Single-ended and differential inputs

The DAS-1600 board used in this study is a high-gain board and is a switch-configurable for 16 single-ended or eight differential analog input channels (Figure 3.7, shown at top right, S5). ***Single-ended inputs*** means referred to a ***command ground*** and the ***differential inputs*** measure the ***difference between two signals***. Generally, one wants to use ***differential inputs*** for ***low-level signals*** (low voltage measurement) whose noise components is a significant part of the signals or for signals that have non-ground common mode. The ***single-ended inputs*** can be used for high-level signals (high voltage) whose noise component is not significant. Since the voltage range of LVDTs is +10 to -10V and the voltage range of pressure transducer is 0 to 5 V, the single-ended inputs are used for the test. Figure 3.8 shows the example of wiring a single-ended input

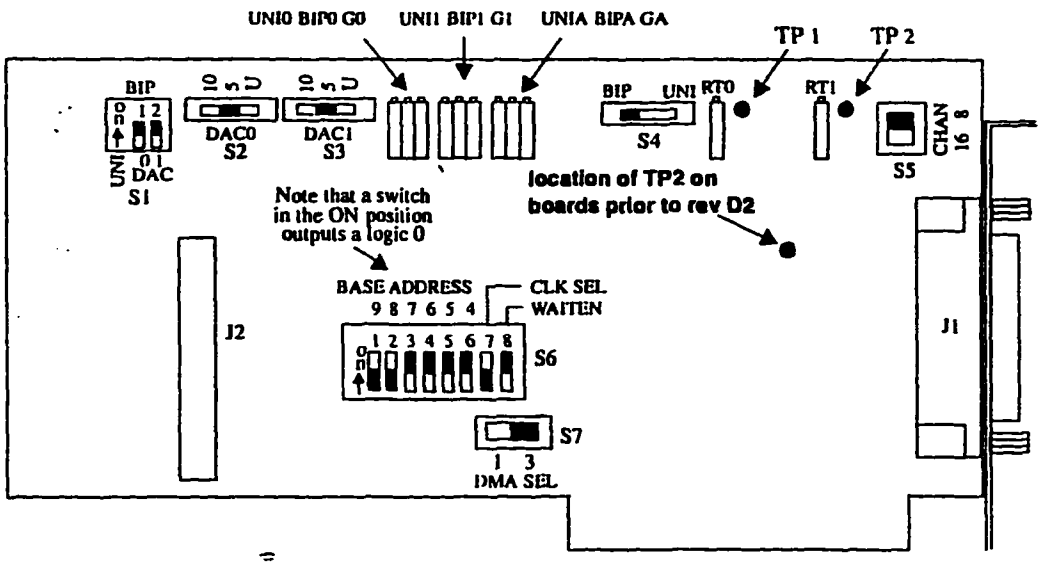

Figure 3.7 Block Diagram of DAS-1600

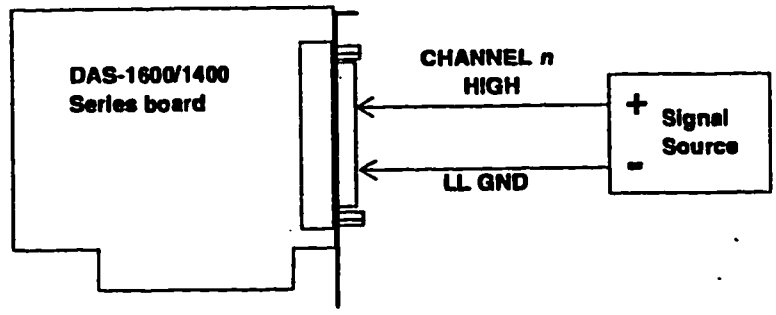

Figure 3.8 Connections for Wiring a Single Source to a DAS-1600 Board Configured for Single-Ended Inputs

If a single-end input is used, the A/D configuration should be given as single-ended inputs, in the configuration file (DAS1600.CFG). Table 3.1 presents the default configuration file setting. Table 3.2 shows the detailed connection of channels with EXP-16 and STA-16.

Bipolar or Unipolar Input

The analog inputs are switch-configurable for either unipolar (0-10V) or bipolar (+10 to -10V) signals (Figure 3.7, shown as S1). Since all the signals from the LVDTs are +10 to -10V, the switch is put in a bipolar location.

The input range can be controlled by the computer program.

Gain

Analog input channels are individually programmed for gain. The DAS-1600 have programmable gain of 1, 10, 100 and 500. The gain 1 is used because the signals from the LVDTs are already in the +10 to -10 V range. If you want to measure a signal in the range of +1.0 to -1.0V is used, employ a gain of 10 to amplify the signal to +10 to -10 V range.

Sampling Rate

Analog inputs can be sampled at a maximum of 100 ksamples (100000)/sec with 12-bit resolution (Table 3.3).

Table 3.1 Default Configuration File Setting

Options	Default settings
Board number	0
Board name	DAS1602
Address	&H300
Clock timebase	10 MHz
Wait state	No
A/D mode	Bipolar
A/D configuration	Differential
DAC0 mode	Bipolar
DAC1 mode	Bipolar
DAC0 ref	-5.0 (C0A00000)
DAC1 ref	-5.0 (C0A00000)
DMA channel	3
Interrupt level	7
Port A	Input
Port B	Input
Port CL	Input
Port CH	Input
Number of EXP-16s	0
Number of EXP-GPs	0
Number of SSHs	0

Table 3.2 Detailed Connection of The Channels with EXP-16 and STA-16

Channel Name used in the Program	Type of Channel	Connected to
0	LVDT 1	EXP-16 channel 0
1	LVDT 2	EXP-16 Channel 1
2	LVDT 3	EXP-16 Channel 2
3	LVDT 4	EXP-16 channel 3
4	LVDT 5	EXP-16 Channel 4
5	Pore water Pressure Transducer	EXP-16 Channel 5
6	LVDT 7	EXP-16 Channel 6
7	LVDT 8	EXP-16 Channel 7
8	LVDT 9	EXP-16 Channel 8
9	LVDT 10	EXP-16 Channel 9
10	LVDT 11	EXP-16 Channel 10
11	LVDT 12	EXP-16 Channel 11
12	LVDT 13	EXP-16 Channel 12
13	LVDT 14	EXP-16 Channel 13
14	LVDT 15	EXP-16 Channel 14
15	LVDT 16	EXP-16 Channel 15
16	LVDT 17	STA-16 Channel 2
17	LVDT 18	STA-16 Channel 3
18	Transducer X	STA-16 Channel 4
19	Transducer Y	STA-16 Channel 5
20	Transducer Z	STA-16 Channel 6
21	LVDT 6	STA-16 Channel 8

Table 3.3 DAS-1601 Gains, Ranges and Rates for Bipolar and Unipolar Selection

Gain	Unipolar Range	Bipolar Range	Maximum Throughput Rate
1	0.0 to +10.0 V	−10.0 to +10.0 V	100 ksamples/s
10	0.0 to +1.0 V	−1.0 to +1.0 V	100 ksamples/s
100	0.0 to +100 mV	−100 to +100 mV	70 ksamples/s
500	0.0 to +20 mV	−20 to +20 mV	30 ksamples/s

Analog-to-Digital Conversion

Analog to digital conversion (A/D) can be started in one of the three ways :

(1) software command,

(2) internal programmable interval timer (onboard pacer clock), and

(3) external trigger (external pacer clock)

Data Transfers Modes

Data transfers can be performed in one of the three ways: (1) polling a status register and reading data when ready, (2) generation of hardware interrupt and an interrupt service routine or (3) using DMA (Direct Memory Access) mode.

Single Mode

In a single-mode operation, a data acquisition board acquires a single sample from a single channel.

Synchronous Mode

In this mode, data acquisiton board acquires one or more samples from one or more channels. This mode cannot be used with the EXP-16 multiplexer.

Interrupt Mode

This mode can used for one or more samples from one or more channels, and when the data is available for transfer, the data can be transferred .

DMA Mode

DMA is a method of bypassing the CPU to transfer data directly between I/O device and computer memory. This mode cannot use the EXP-16 multiplexer.

In this study the interrupt mode is used for data transfer because of measuring signals from the multi-channles by using EXP-16 multiplexer.

Interval Timer (Hardware, internal source clock)

A three-channel programmable interval timer (Intel 82C54) provides timing for A/D conversions or generations of output pulses at any rate from 1 pulse/hr to 100 kHz. The 82C54 counter/timer can also be used to measure frequency, period, and pulse width. The DAS-1600 board uses two of the counter channels as a frequency divider for an internal 10 Mhz crystal-controlled oscillator. The internal pacer clock is derived from the onboard 82C54 counter/timer and a switch-configurable,crystal controlled 1MHz or 10MHz timebase. The maximum allowable rate is 100 ksamples (100000)/sec. The minimum conversions per hour is 0.838 for the 1MHz time base, and 8.38 for the 10MHz time base.

The external clock source must be an externally applied, TTL-compatible, rising-edge signal attached to the IPO/TRIG 0/PCKL pin (25) of the main I/O connector. An

external pacer clock source is useful if you want to pace at rate not available with the 82C54 counter/timer. In this study the 10 Mhz clock time base is used, and is also shown in the configuration file (DAS1600.CFG).

D/A output channel (Digital to Analog Channel)

The DAS-1600 also have two multiplying 12-bit D/A (digital to analog) output channels (Figure 3.7, labelled as S2 and S3). The D/A converters have switch-selectable output ranges of 0 to +5V, 0to +10V, +5 to -5V and + 10 to -10V full scale. The D/A converters may use an external DC or AC reference to achieve different output ranges.

I/O connection

The analog I/O connections are made via a 37-pin "D" connector at the rear of the host connector.

Function Call Driver

The board can be controlled by the program using High-Level Function Call Driver. In this study the program is written in Pascal Language.

Configuration File

The configuration file need to be installed before using the program. The file can be installed by the the program CONFIG.EXE provided by the manufacturer. The configuration file is read by the board's driver upon initialization.

3.2.2 PDISO-8 Isolated 8 digital input and 8 relay output Board

The PDISO-8 is a 8-channel isolated input/output interface board designed for control and sensing application. Figure 3.9 shows the system block diagram. The interface board is easily installed in any IBM PC/XT/AT or compatiable computer. The PDISO-8 provides 8 electromagnetical relay outputs and 8 isolated inputs. The board is used for switching the selenoid valves. The power required to operate the PDISO-8 is 5V which is received from the power supply box (Figure 3.6, left). Two wires come from the power supply box (5V and ground) is connected to the STA-8 AO Screw terminal Accessory. Figure 3.4 shows the PDISO-8 board installed at the top of the mother board, PC-486.

8 electro-mechanically relay outputs

This outputs (contact closures) address as a single output I/O byte. 5 of the relay provide Form C contact arrangement (change-over) (OP0 to OP4 in Figure 3.9) and the remaining 3 relays are Form A (normally open) (OP5 to OP7 in Figure 3.9). Contacts are silver with gold overlay and are rated at 3A @ 120V A.C. or 28V D.C., resistive load.

8 Isolated input

8 individual optically isolated inputs that can be read as a single I/O port byte. Inputs are not polarity sensitive and can be derived from D.C. or A.C. control voltages in the range of 5 - 24 V.

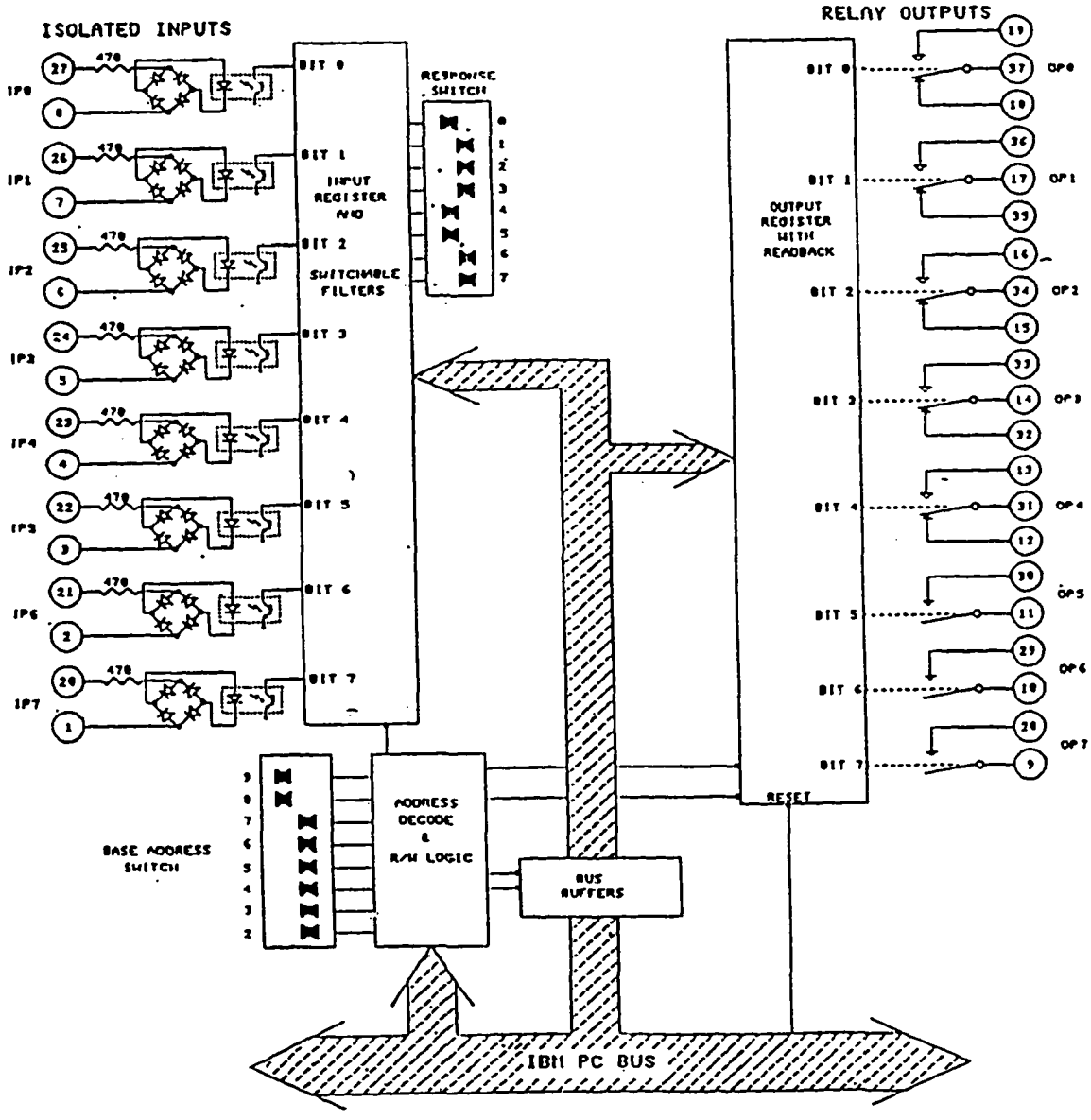

Figure 3.9 Block Diagram of PDISO-8

Registers (I/O Address)

The PDISO-8 occupies four consecutive addresses in the PC I/O address space, of which the two addresses are used, one for output/readback and one for input. The base I/O address is selected during the installation procedure and will automatically fall in a 4-bit boundary by using 8 position dip switch (Figure 3.10). The I/O registers of the PDISO-8 are located as follows.

I/O MAP

I/O ADDRESS (HEX)	FUNCTION
Base +0	relay output (read/write)
Base +1	isolated input (read)

Energize and Denergize

Data is written to all the eight relays as a single byte. Each bit within the byte controls a single relay so that a high bit (=1) energizes a particular relay and a low bit (=0) turns it off.

Programming

The PDISO-8 can be controlled by the simple command written in the program. First put the base I/O address and then give the high bit for the energize and low bit for the denergize.

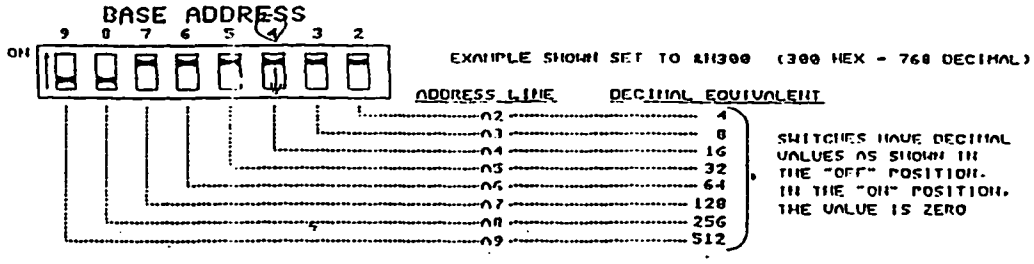

Figure 3.10 Base Address Switch Setting

Connections

Figure 3.11 presents a rear view fo the 37 pin D male connector on the back of PDISO-8. Figure 3.12 shows the detailed layout of connection between solid state relay and PDISO-8.

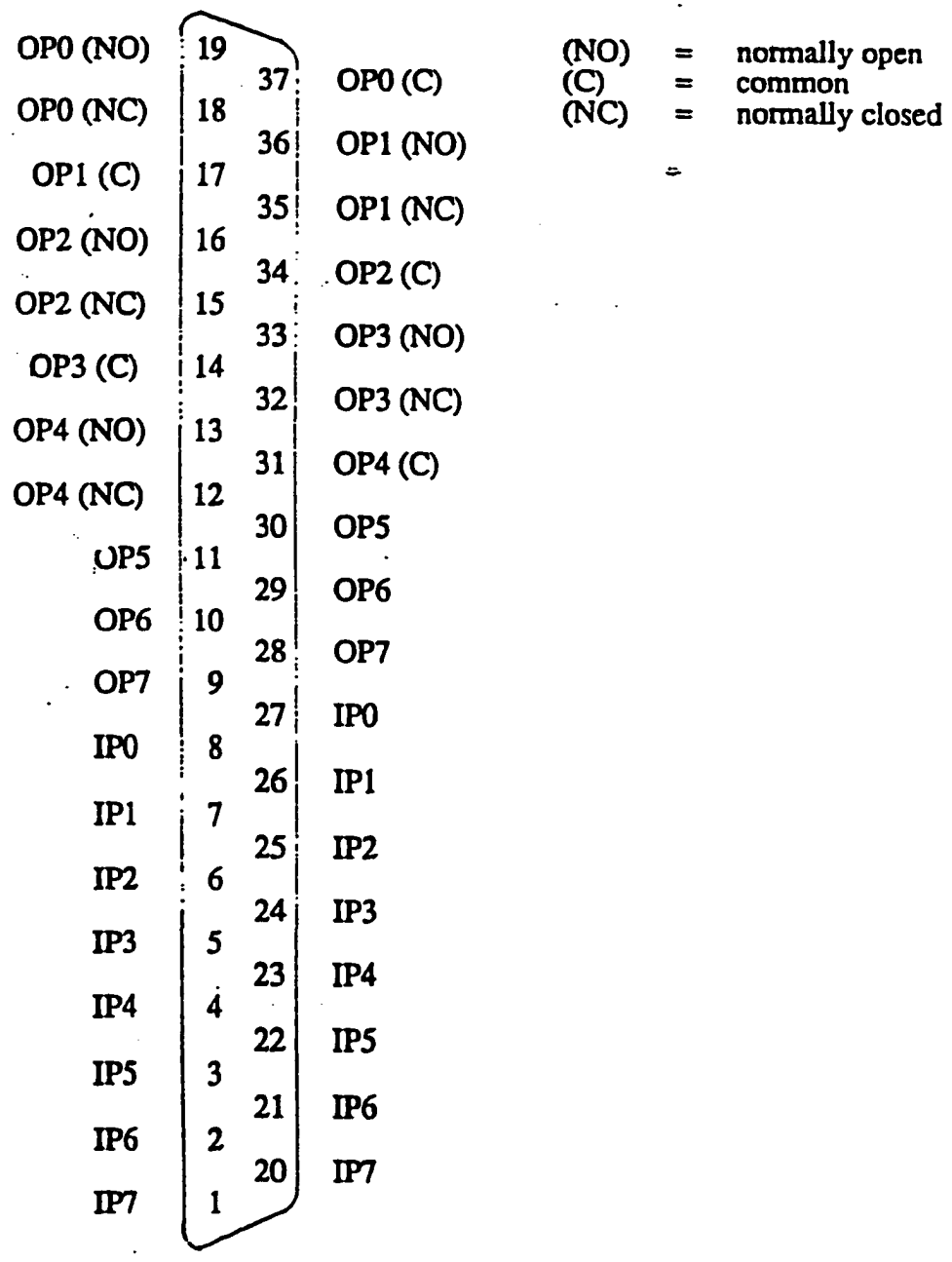

Figrue 3.11 A rear View of the 37 pin D male connector on the back of the PDISO-8

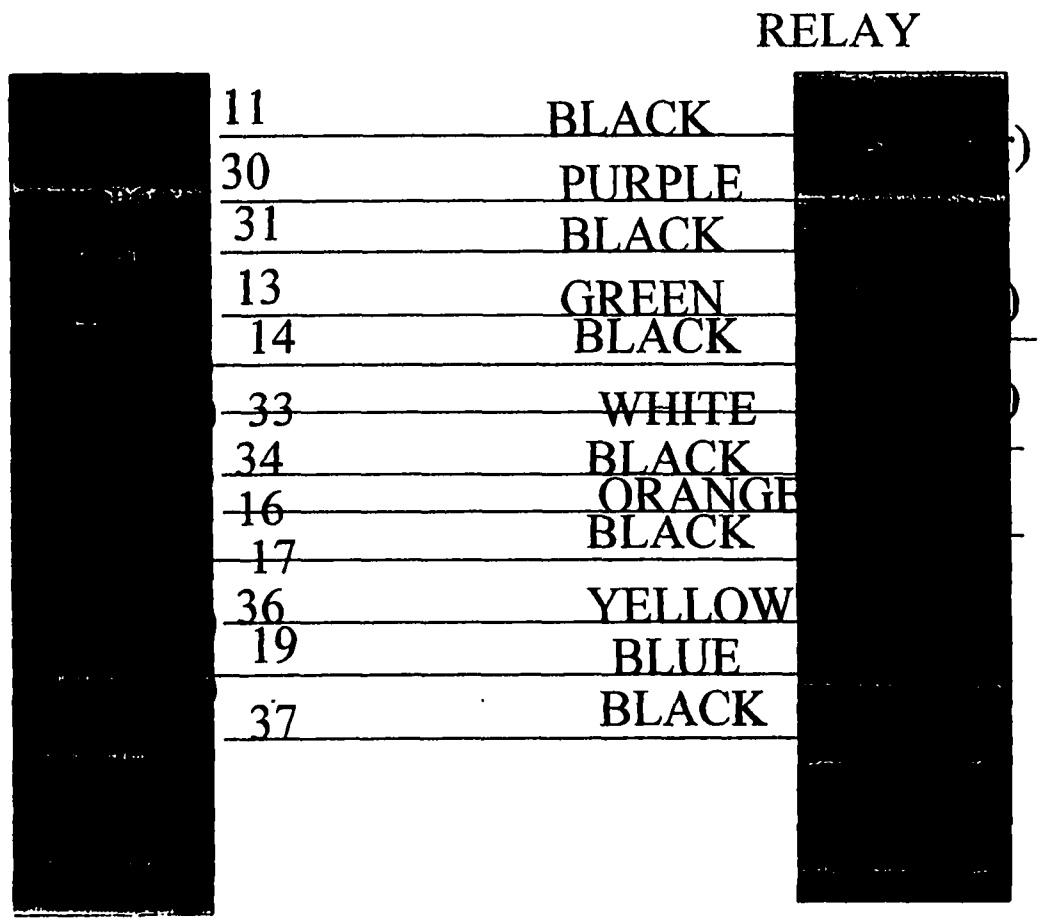

Figure 3.12 Detailed layout of the connection between Relay

3.2.3 EXP-16 16 channel Multiplexer and Signal Conditioning Board

This is a universal exapnsion multiplexer/amplifier from the Keithley MetraByte for use with the DAS-1600 data acqusiton board. Signal amplification, filtering and conditioning are also included in thi board. Figure 3.13 shows the EXP-16 board and Figure 3.14 presents the component layout of the EXP-16.

Analog & output Jumper Setting

The EXP-16 contains eight jumper-selectable outputs. This number allows up to eight EXP-16s to be connected to an DAS -1600 board without need for special cables. The user can choose to use any one of these channels by jumping Connector J4 (shown in Figure 3.14, top left) into the desired data output channel.

Gain Setting

The EXP-16 gain switch configures the entire board for the selected gain (Figure 3.15). The high-grade instrumentation amplifier provides user switch-selectable gains of 0.5, 1, 2, 10, 100, 200 and 1,000 are included. The gain of 0.5 is used in this study, because the voltage of the LVDTs are +10 to -10V in range. So, EXP-16 can produce +5 to -5V, which is the analog output voltage of the EXP-16.

Connections

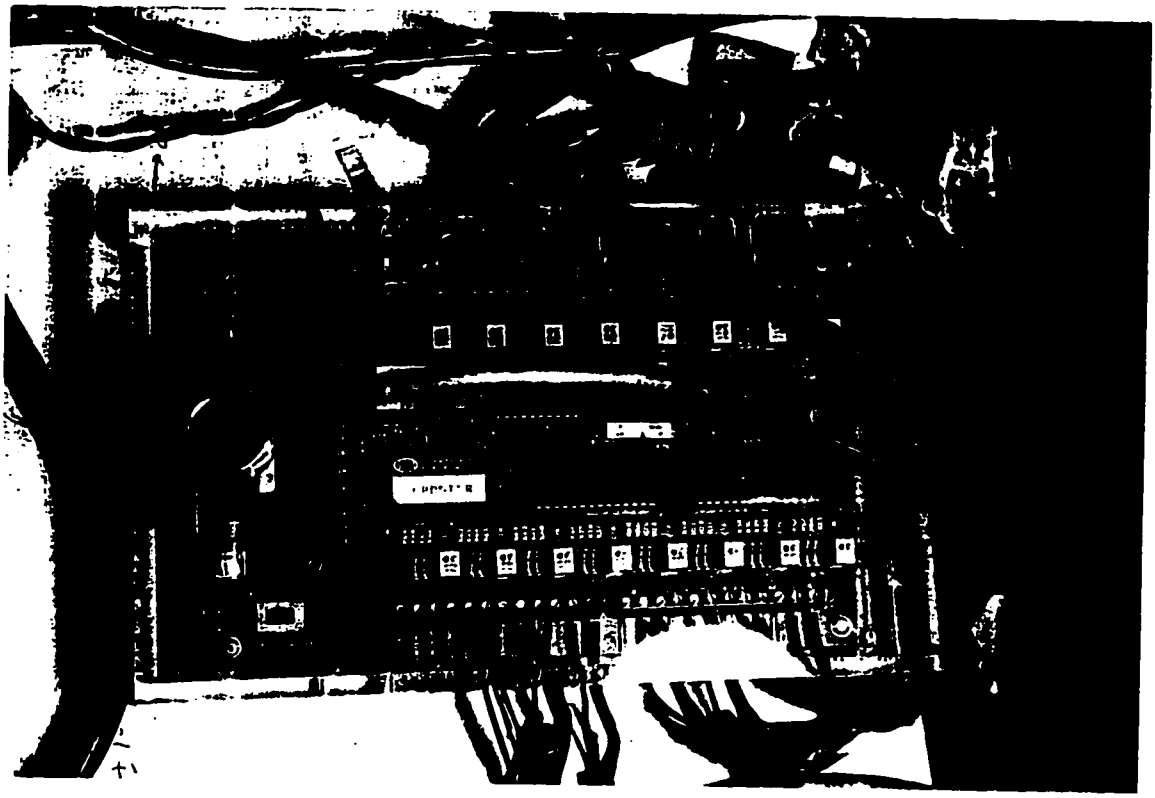

Figrure 3.13 EXP-16

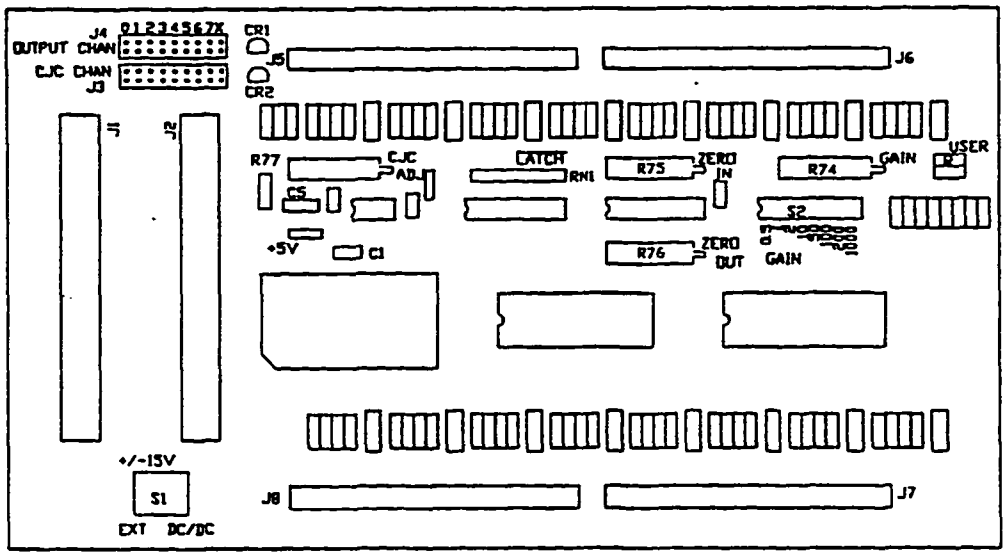

Figure 3.14 Component Layout of EXP-16

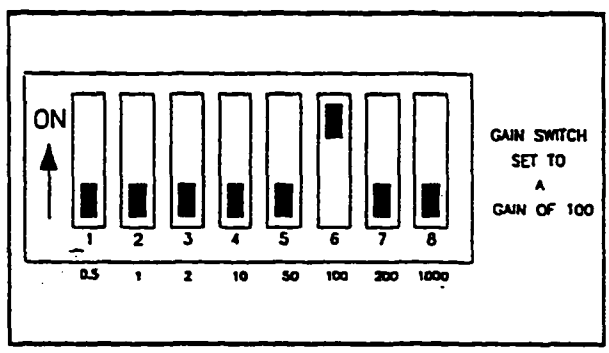

Figure 3.15 Gain Switch of EXP-16

The EXP-16 is directly connected to the STA-16 AO Universal Screw Terminal Accessory and then STA-16 A0 connected to the DAS-1600 board. Figure 3.16 shows the attaching multiple expansion accessories (EXP-16) with STA-16.

All connections to the host data-acquisiton system use one of two standard, 37 pin, D, male connectors, while all connections to the analog inputs use screw terminals.

3.2.4 STA-16 Universal Screw Terminal Accessory

The STA-16 (Figure 3.17) Screw Terminal Accessory is used for the connection to data acquisition board. Figure 3.3 shows the location of the STA-U Screw Terminal. The accessory is connect directly to the DAS-1600 board with the C-1800 cable through the J1 connection. Anothre C-1800 cable is connected to the EXP-16 along the J2 connection (Figure 3.17), which shows the STA-16 terminal names. The STA-16 is used to provide acess to all signals on the acquisition board.

The STA-16 includes two 37-pin male D-type connector tied together (Figure 3.16 to 3.18). All 37 lines are brought out to screw terminal connections. As shown in the Figure 3.16 and 3.19, the STA-16 is put between the EXP-16 and DAS-1600 board. The STA-16 is used in conjuction with an EXP-16 to provide connection to the signals not available on the EXP-16 because the EXP-16 can handle 16 channels, and there are more than 16 channels .

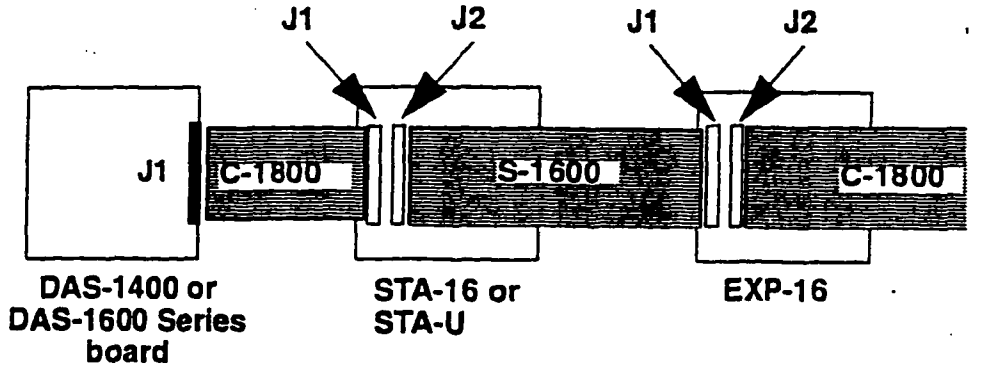

Figure 3.16 Attaching Multiple Expansion Accessories (EXP-16) with STA-16

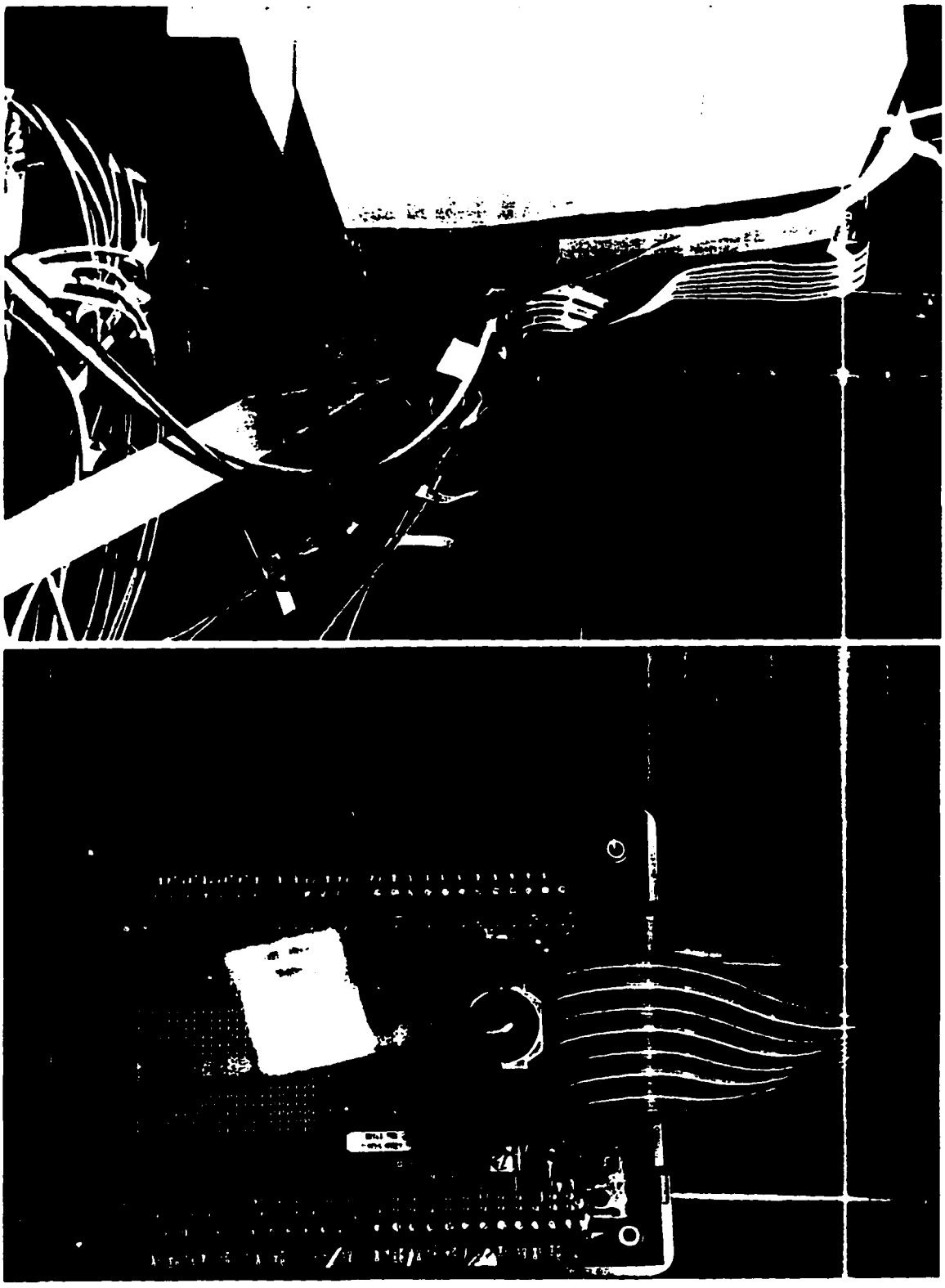

Figure 3.17 STA-16

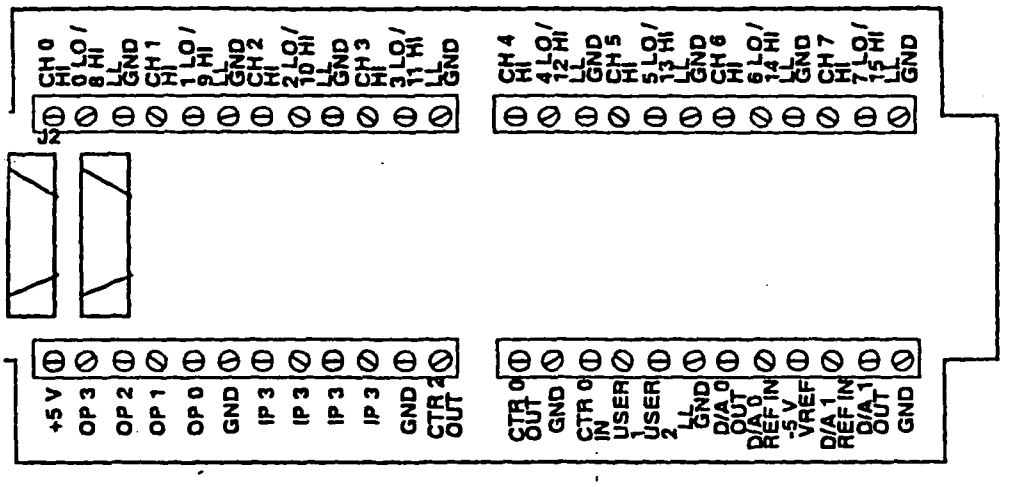

Figure 3.18 STA-16 Terminal Names

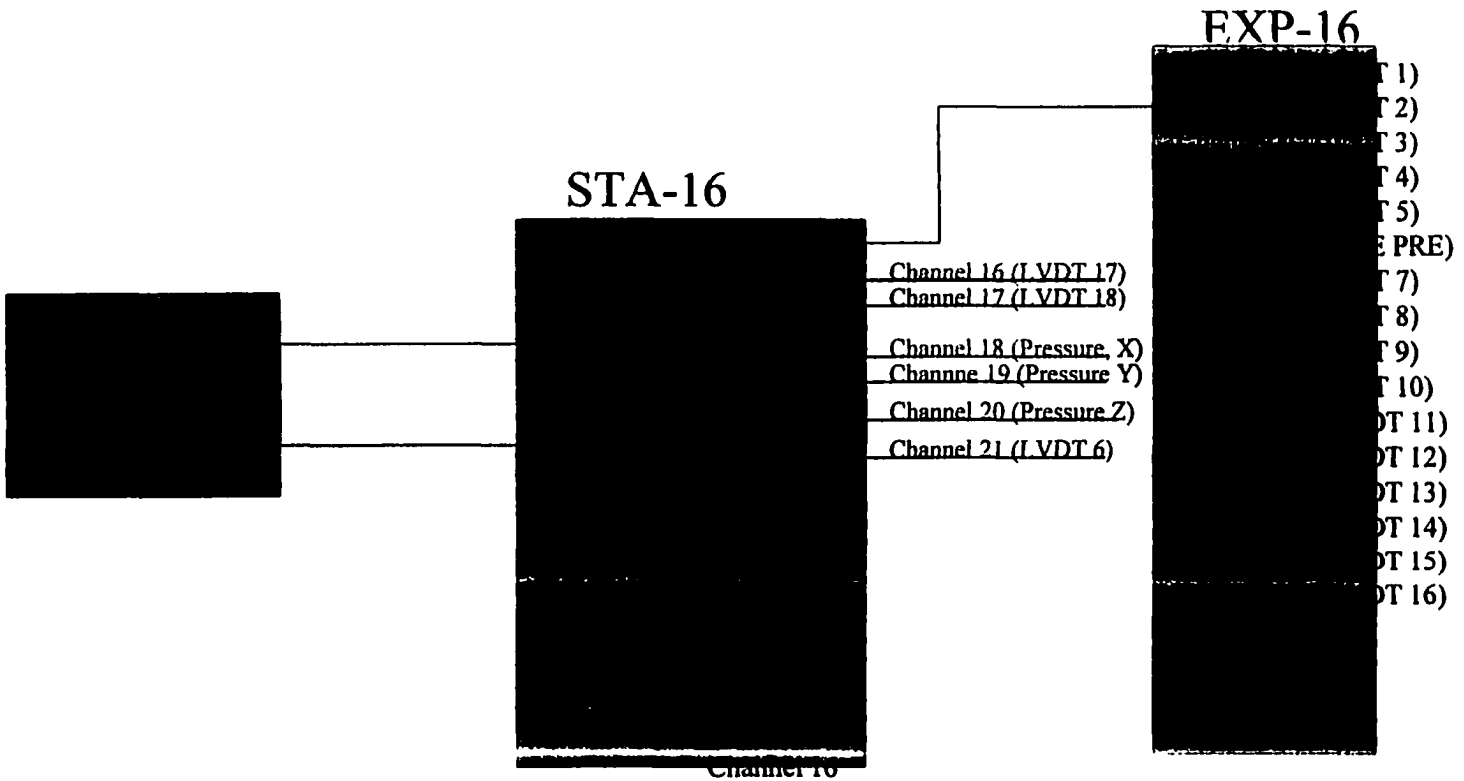

Figure 3.19 Diagram of the Detailed Connection of the Channels

3.2.5 STA-8 AO Screw Terminal Accessory

STA-8 AO (Figure 3.20) is a screw terminal accessory used for connection from the relay output accessory to the PDISO-8, which is slotted in the PC 486 (Figure 3.5, top cable connected to the rear part of computer). The detailed connection is shown in the bottom part of Figure 3.20. The STA-8 AO is connected to the PDISO-8, through the 37-pin D-type male connector by using C-1800 cable (Figure 3.5). The command is received from the PDISO-8 by program controlled and the selenoid valves are closed and open as program control. The voltage required to operate the solid state relay is 5V and is connected to the STA-8 AO (Figure 3.6). The black wire is used for connection and connected to the common as shown in Figure 3.11 and 3.12.

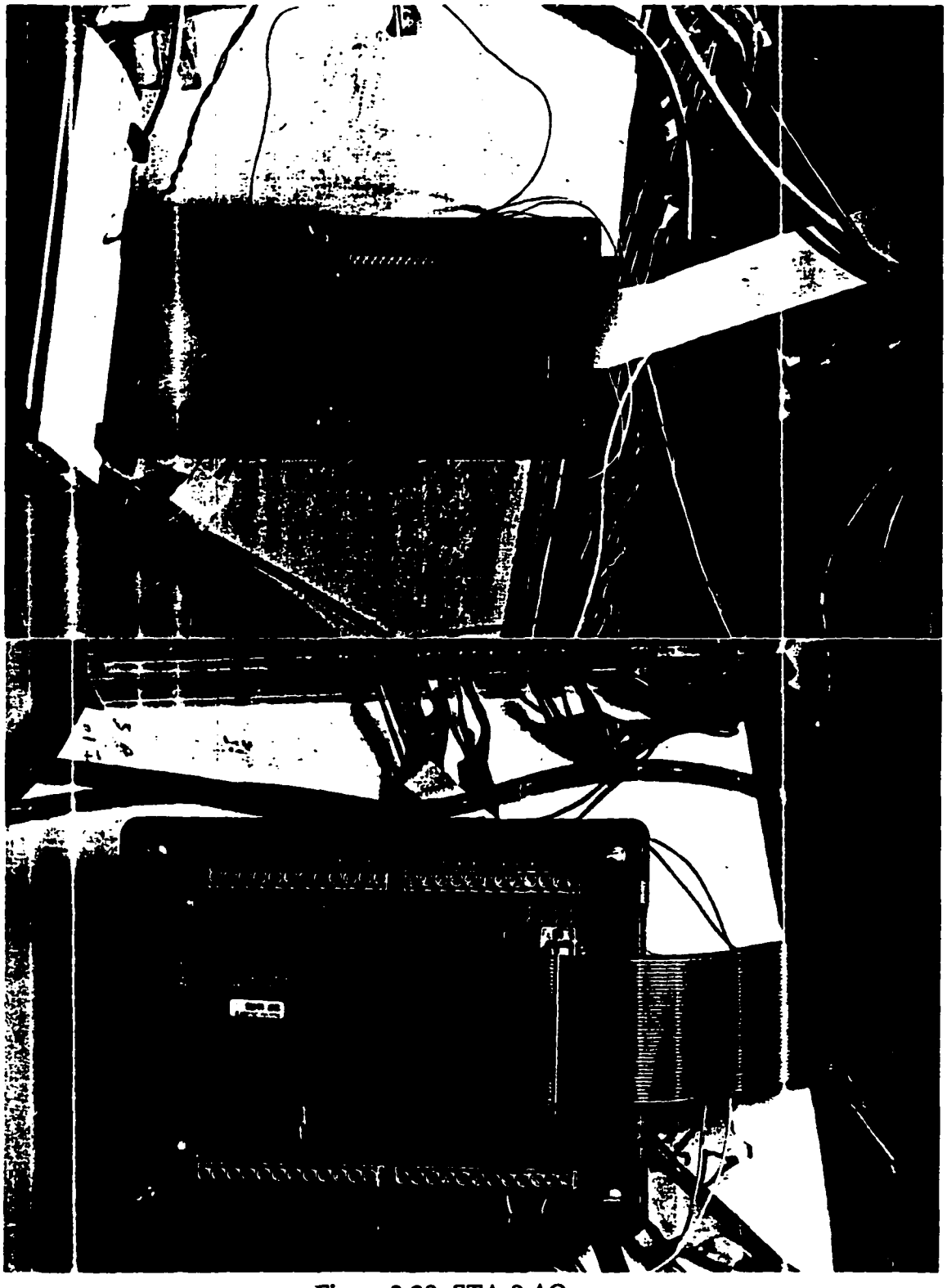

Figure 3.20 STA-8 AO

3.3Control Board and Servo-controlled Pressure System

Figure 3.21 shows the view of the servo-controlled laod or pressure system.

3.3.1 Spangler Two-way selenoid valve

The Spangler 2-way solenoid valves, 90 series , normally open and normally closed, from the company, TOMCO is used for control the air pressure (Figure 3.22). Figure 3.23 shows the function of the valves. As shown in the figure 3.23, the normally closed valve is closed in normal position, and open when energized through the solid-state relay from the PDISO-8 which is installed in the computer by program control. The normally open valve is open in normal position and closed when energized.

The pressure loading and unloading are controlled by the selenoid valves by the program control. Figure 3.24 presents the detailed setting of solenoid valves and solid state relay.

3.3.2 DP15 Variable Reluctance Differential Pressure Transducer

The pressure in the air line is measured by DP15 variable reluctance pressuer transducer, from Valedine Engineering Corp. The DP15 is installed between the normally closed and normally open selenoid valve (Figure 3.21, 3.22, 3.24, 3.25). According to the manufacturer, the accureacy of the DP-15 is + 0.25 to -0.25 %. The transducer can measure in the continuous range from 0.08 psi to 3200 psi. The transducer contains equal pressure inlet volumes and field interchangeable sensing diaphragms can

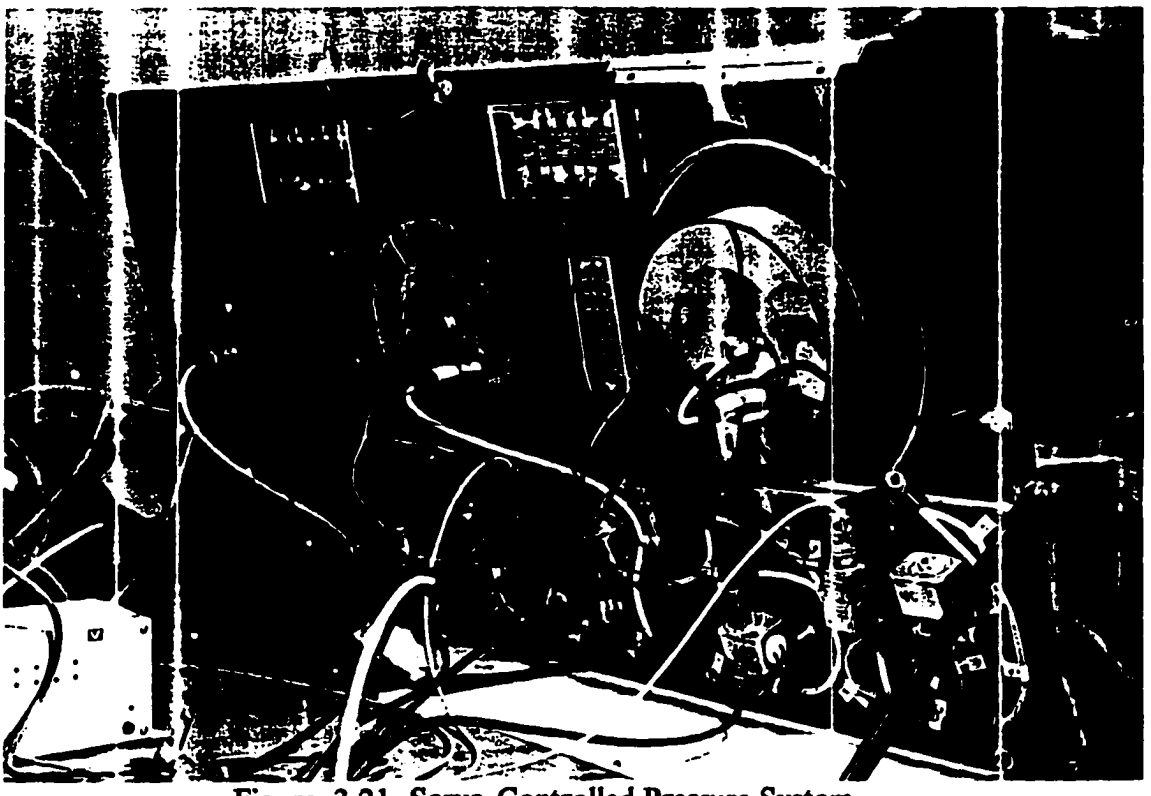

Figure 3.21 Servo-Controlled Pressure System

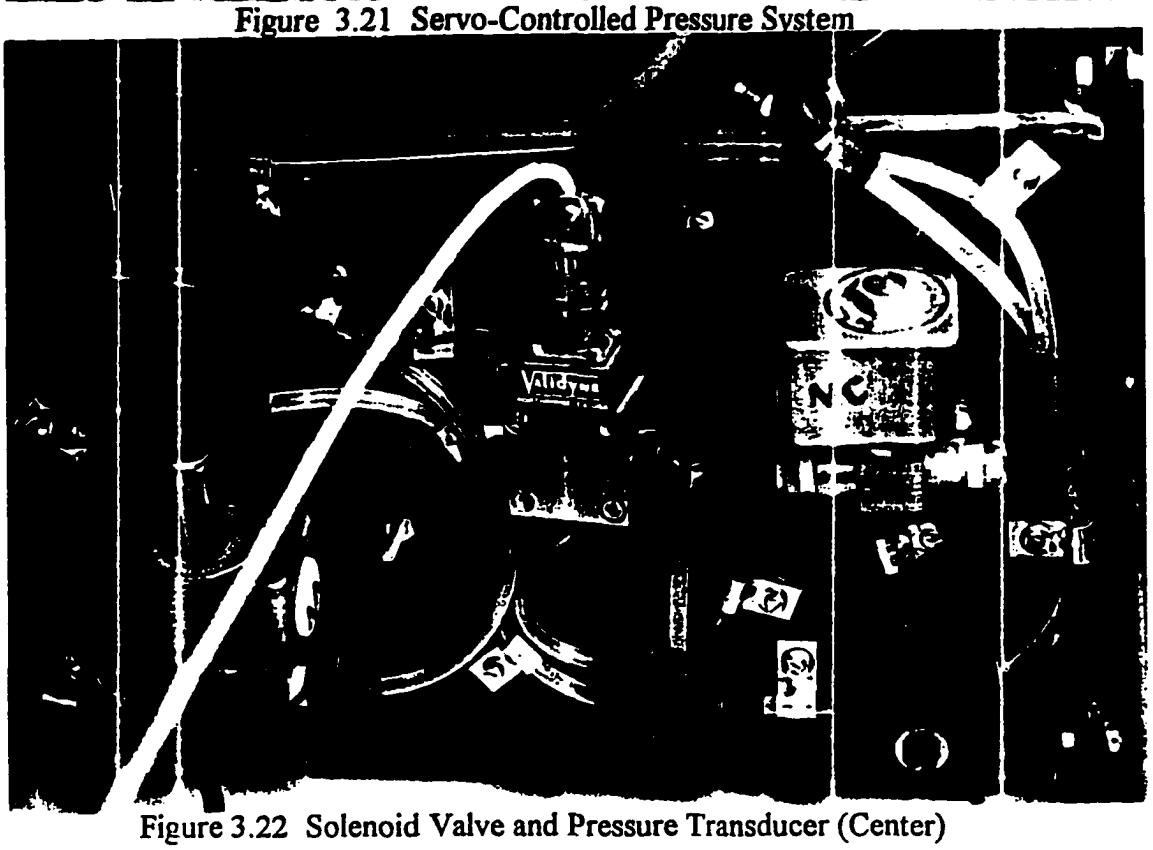

Figure 3.22 Solenoid Valve and Pressure Transducer (Center)

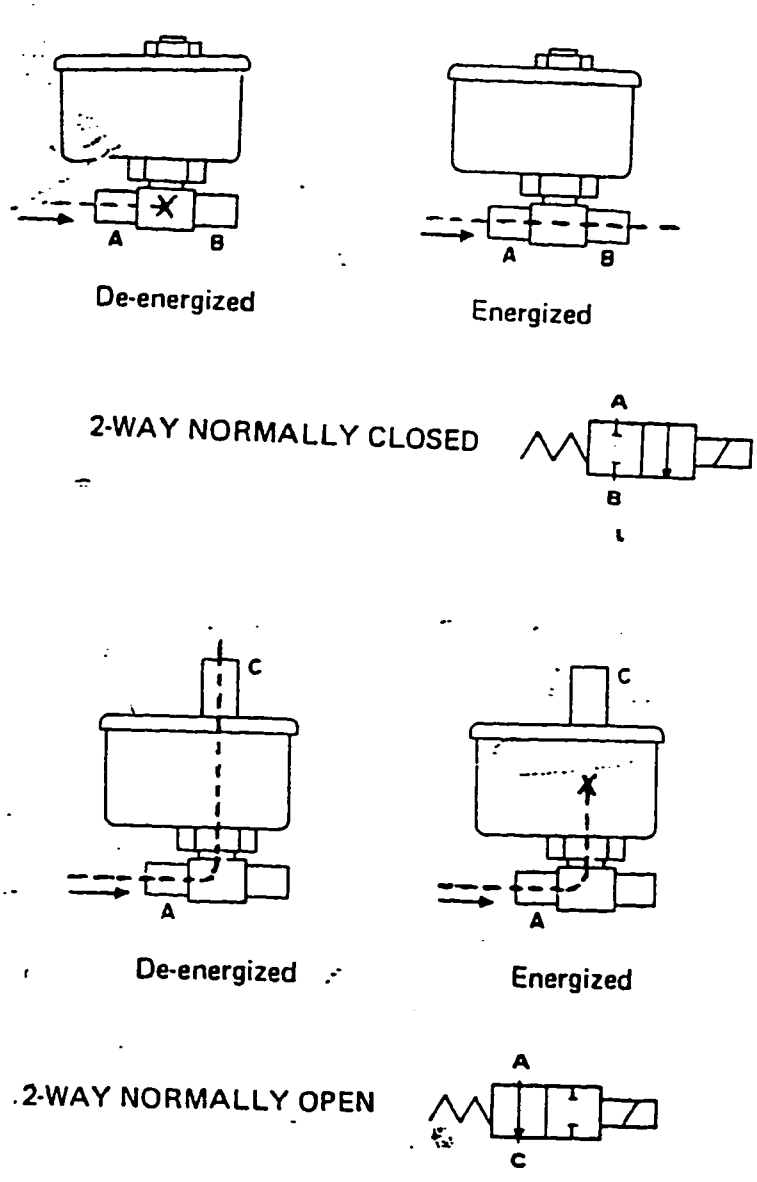

Figure 3.23 Function and Construction of the 2-way Normally Open and Normally Closed Valves

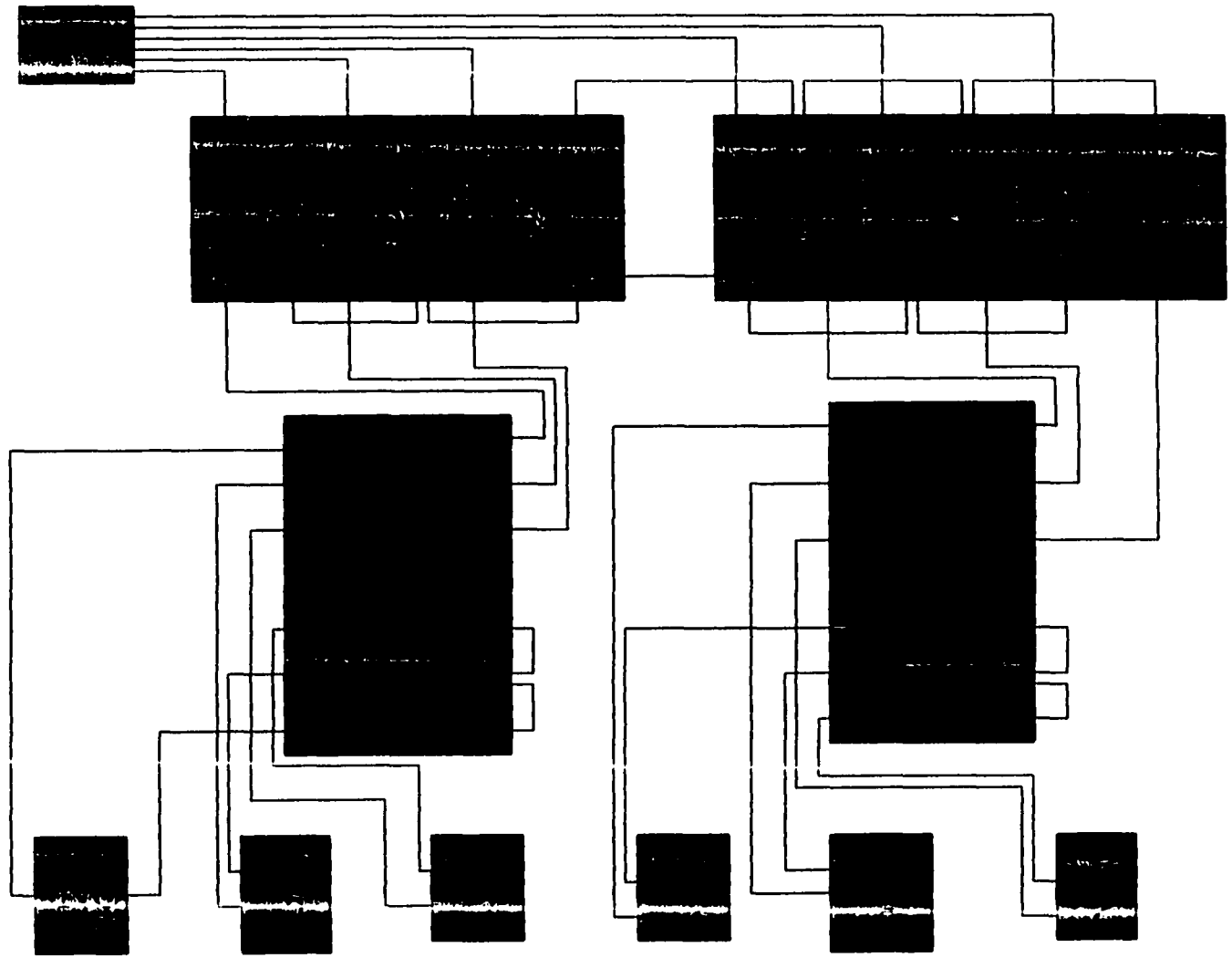

Figure 3.24 Detailed Configuration of Selenoid and Solid State Relay

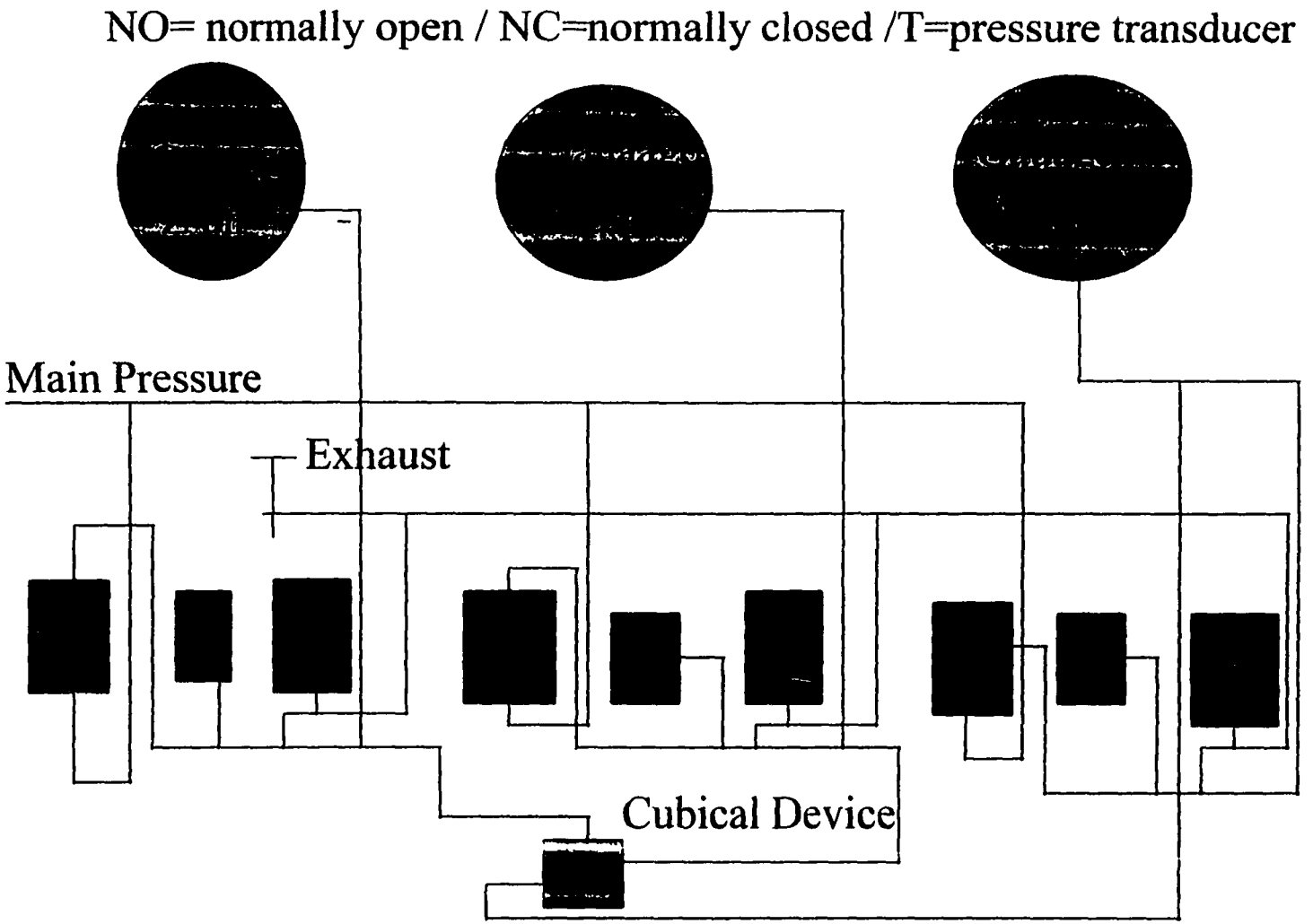

Figure 3.25 Servo-conrolled Pressure System

withstand extreme pressure overload. This type of transducer can be used both for corrosive liquids and gas.

The CD280 modular multichannel unit is used for excitation and signal conditioning.

3.3.3 CD280 Multichannel Demodular for Pressure Transducer

The CD280 (Figure 3.21, Left, white box) is a modular multichannel unit for excitation and signal conditioning of variable reluctance or linear variable differential transformer types of transducer. The CD280 contains four channels and each channel will convert full scale AC carrier signals as low at 17 mV/V to an output of +10 to -10 Vdc, with individual Zero and Span adjustment.

The three channels of the CD280 are connected to the three DP15 differential pressure transducers to measure the air pressure in the line which is connected to the cubical device. The output voltage of the CD280 is adjusted to 0-5 V.

3.3.4 Solid State Relay

The command received from the computer is activated by the aid of solid state relay installed on the servo controlled pressure board (Figure 3.21 and 3.26).The command comes from the PDISO-8 Solid State Relay Board, and the program control is received by the soild state relay through the STA-8 AO Screw treminal Accessory. The power reqired for the solid state relay is 5V DC. The six number of solid state relay is

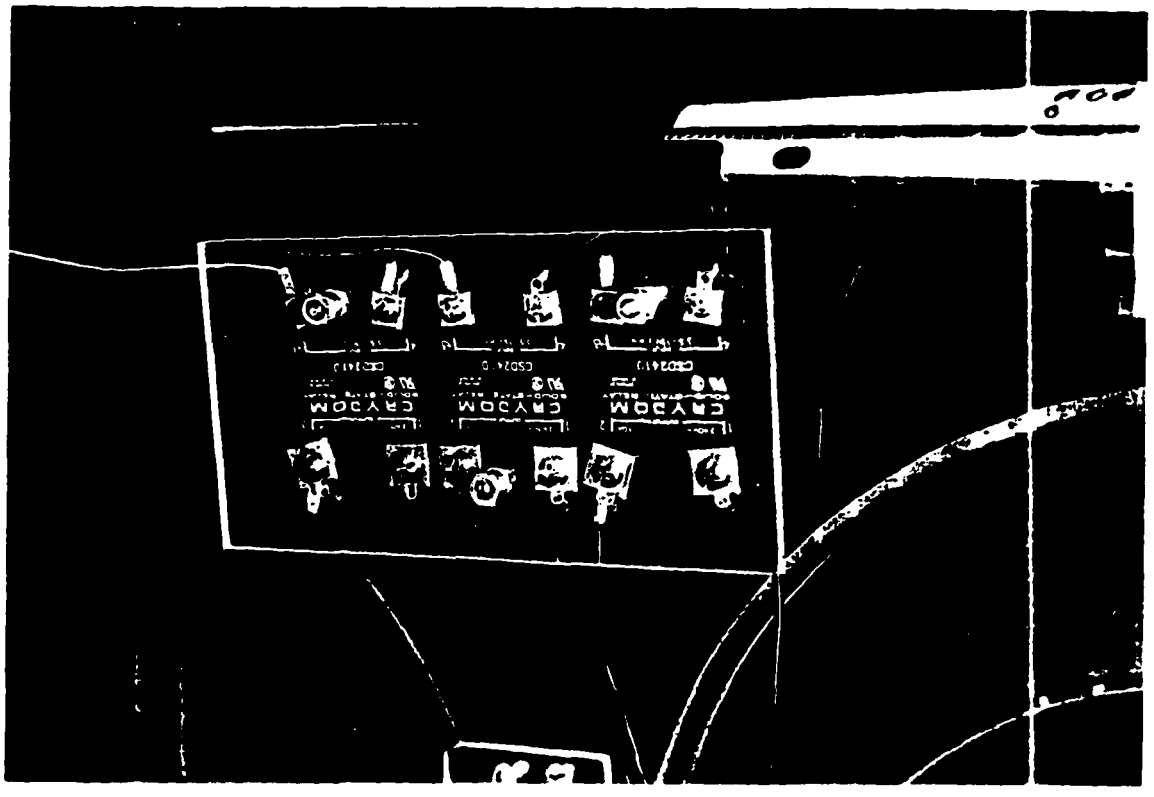

Figure 3.26 Solid State Relay

installed on top of the pressure control board and each of the solid state relay is connected to the selenoid valve (Figure 3.24) through the screw terminal. The selenoid valve is energized by the function of solid state relay.

3.3.5 Saturation, Pore-Pressure Measurement and Drainage Board

Figure 3.27 presents the saturation, pore pressure measurement and drainage board. The pore-pressure line from the cubical device is connected to the Pore-pressure and Drainage board. The pore-pressure is measured by the pore pressure transducer (Figure 3.28) which is connected to the digital pore-pressure meter and then connected to the channel 5 of the EXP-16.

The pore-pressure is recorded by the computer as a voltage at the same time with the LVDT and pressure transducer, and then it is changed to pressure based on the calibration factor. Table 3.4 presents the calibration for the LVDTs, pressure transducers and pore-water pressure transducer.

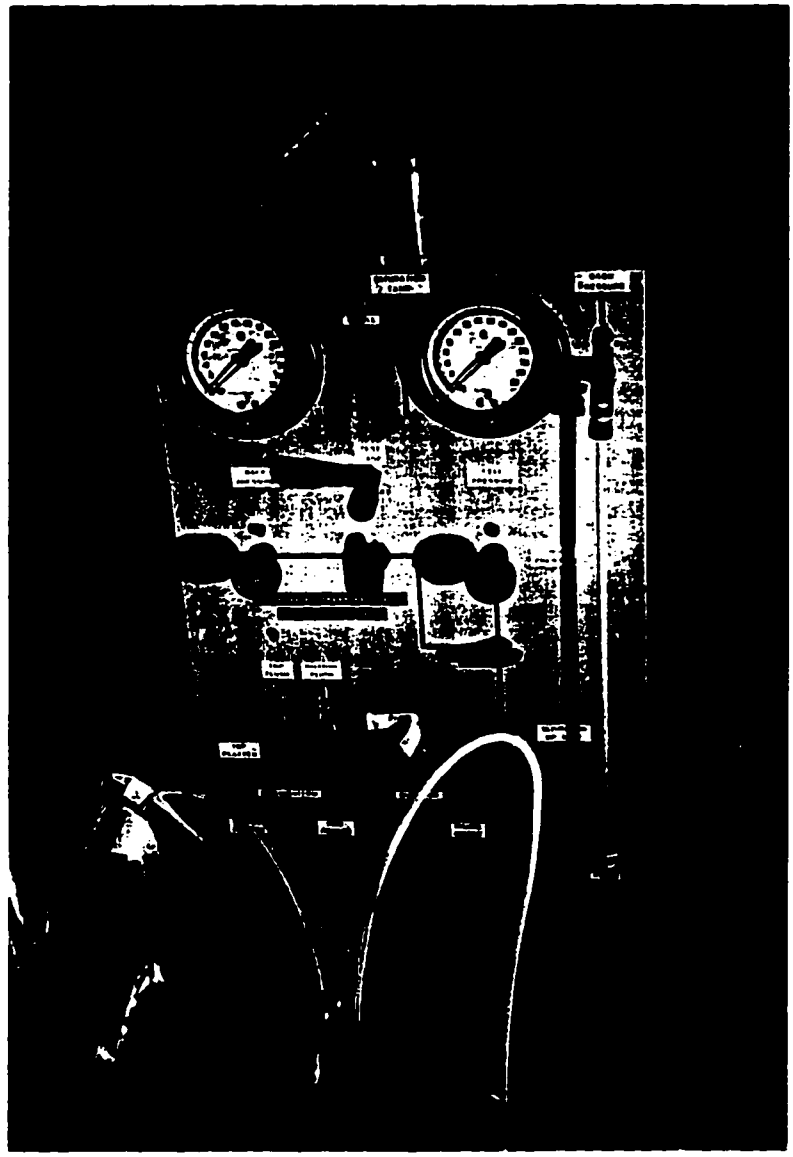

Figure 3.27 Pore-pressure Control Board

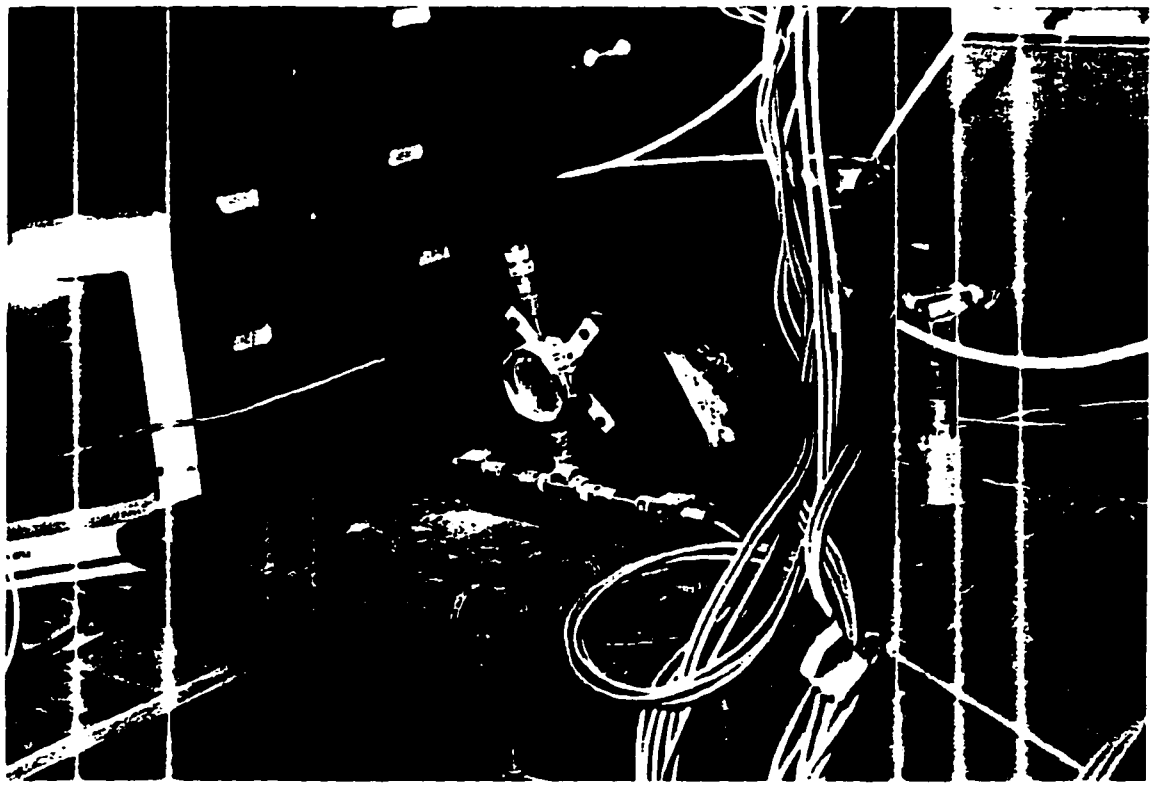

Figure 3.28 Pore-pressure Transducer

Table 3.4 Calibratin of the Channels

Channel Name	Type of Channel	Calibration
0	LVDT 1	Displ.= 0.000165 + 0.02917 * Volt
1	LVDT 2	Displ.= 0.00010 + 0.02700 * Volt
2	LVDT 3	Displ.= -0.00011 + 0.026312 * Volt
3	LVDT 4	Displ.= -0.000096 + 0.026763 * Volt
4	LVDT 5	Displ.= -0.00033 + 0.027636 * Volt
5	Pore Pressure	Pore Pressure = -0.33123 + 12.94886 * Volt
6	LVDT 7	Displ.= -0.0004 + 0.02782 * Volt
7	LVDT 8	Displ.= -0.00014 + 0.02727 * Volt
8	LVDT 9	Displ.= 0.000179 + 0.023599 * Volt
9	LVDT 10	Displ.= -0.00014 + 0.026748 * Volt
10	LVDT 11	Displ.= 0.000179 + 0.023599 * Volt
11	LVDT 12	Displ.= 0.000398 + 0.031525 * Volt
12	LVDT 13	Displ.= -0.00078 + 0.027371 * Volt
13	LVDT 14	Displ.= 0.000177 + 0.027371 * Volt
14	LVDT 15	Displ.= 0.000083 + 0.03053 * Volt
15	LVDT 16	Displ.= 0.00012 + 0.028086 * Volt
16	LVDT 17	Displ.= -0.000089 + 0.02831 * Volt
17	LVDT 18	Displ.= -0.00032 + 0.029626 * Volt
18	Transducer X	Pressure (psi) = 1.1445 + 19.89938 * Volt
19	Transducer Y	Pressure (psi) = -0.1400 + 19.81251 * Volt
20	Transducer Z	Pressure (psi) = 0.813889 + 19.87223 * Volt
21	LVDT 6	Displ. = -0.00014 + 0.027636 * Volt

Chapter 4

TEST MATERIALS, SAMPLE PREPARATION AND TEST PROCEDURES

4.1 Test Materials

Ottawa sand, a commercially available silica sand, was selected as the test material for this study. It is a uniform subrounded sand having grain size distribution as shown in Figure 4.1. The maximum and minimum densities of the sand are determined as per the American Society for Testing and Materials (ASTM Standard 4049). The index properties are shown below:

specific gravity	: 2.64
maximum void ratio	: 0.77
minimum void ratio	: 0.46

4.2 Sample Preparation

The sample preparation and procedures for cyclic testing of saturated sands can be found in numerous published papers.There are three kinds of sample preparation procedures which are widely used for the sand for laboratory testing (Ishihara, 1995). The basic requirements for these methods are firstly to obtain homogeneous samples with uniform distribution of void ratio, and secondly to be able to prepare samples of lowest

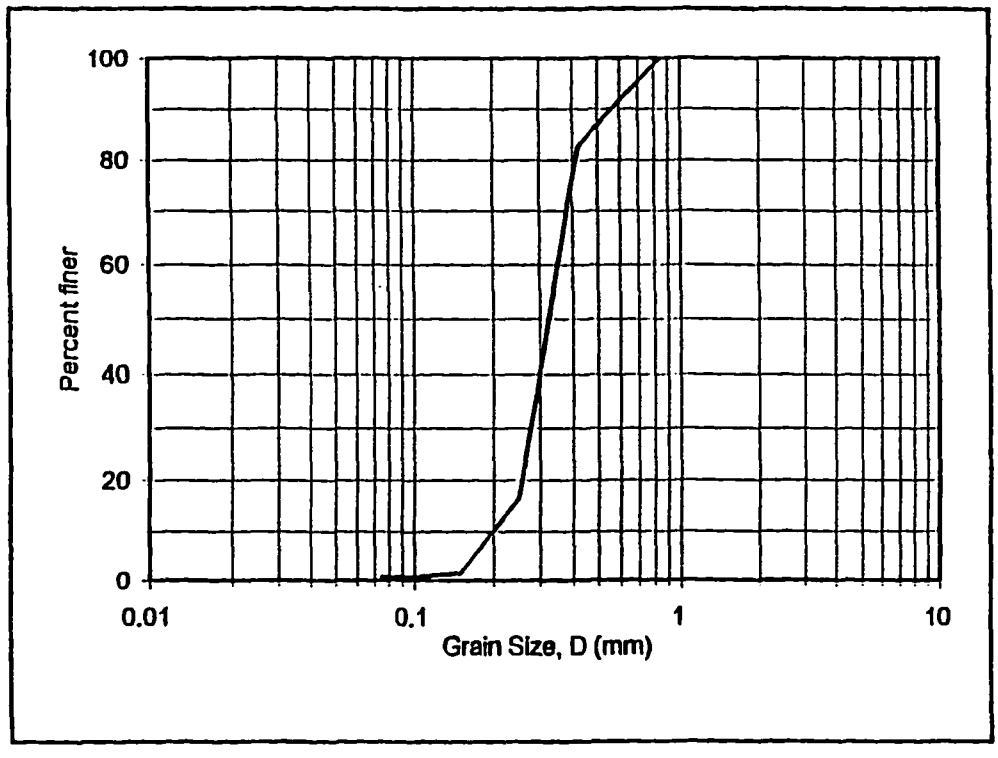

Figure 4.1 Grain Size Distribution of Ottawa Sands

possible density, to cover a wide range of density in samples reconstituted by an identical method. These three methods are:

(1) Moist placement method (wet tamping)

(2) Dry deposition method and,

(3) Water sedimentation method.

Figure 4.2 shows the three methods of sample preparation. In this study water sedimentation method is used for the sample preparation. In this method the sand is mixed with de-aired water and put in a funnel with a plastic tube attached to the end. The mixture of sand and water is poured through the plastic tube, in four layers, into the sample forming mold at zero height of fall at a constant speed, so that the surface of water is always coincident with that of sand sediment. If a denser sample is to be prepared, compaction energy is used by using the small vibrator (Figure 4.3).

4.2.1 Materials Required for Sample Preparation

Figure 4.3 shows the tools required for the sample preparation. Detailed description of the sample preparation can be found in the User's Manual (1996).

Sample Mold and Rubber Latex Membrane

Figure 4.4shows the sample mold and latex membrane used in sample preparation. The 12.7 cm (5 inch) diameter 0.03048 cm thick and 35.56 cm long (0.012 inch thick and 14 inch long) latex rubber membrane is used for the test. First the membrane is cut into two pieces at the center and one part is used for membrane put into the mold and

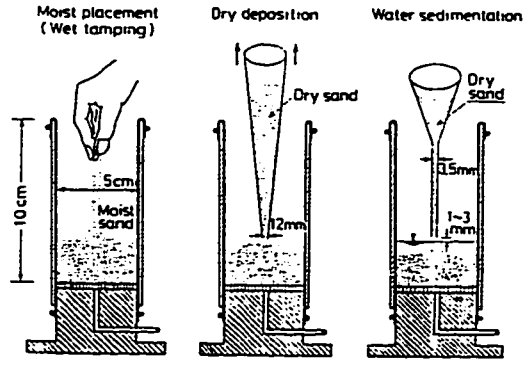

Figure 4.2 Three Methods of Sample Preparation (Ishihara, 1995)

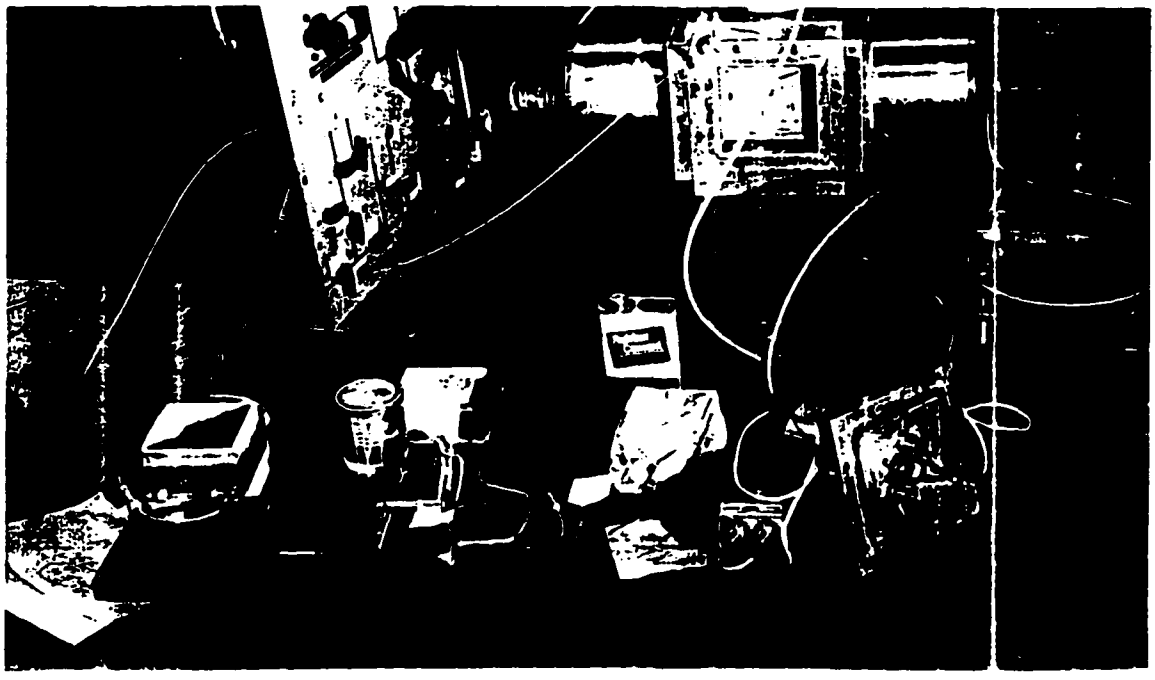

Figure 4.3 Tools Required For Sample Preparation

Figure 4.4 Sample Mold and Top Cover of Latex Rubber Membrane

remaining part is again cut into another two pieces and used as the covers from the top and bottom (Figure 4.4). Detailed steps are given in the User Manual (1996).

Rubber cement

Rubber cement is applied for all the area of the latex membrane except the center of the top and bottom cover. The rubber cement is applied on the folding part of the latex membrane put inside the mod (Figure 4.4). When cement is dry, the cover latex membrane is pasted on the membrane which is put in the mold. To obtain the good bonding, it is necessary to apply a pressure on the surface of the membrane and then wait for few minutes to make sure the bonding is complete. Then the mold is turn into the another side and filled with the sand mixed with water to obtain the required density. A small vibrator is used to obtain higher densities (Figure 4.3).

Pore-pressure Line

The thin plastic tube with inner diameter of 0.13208 cm (0.052 inch) and outer diameter of 0.19304 cm (0.076 inch) is used for the pore-pressure line, which is wrapped on the one side with the sponge to against the drainage of very fine materials, and then covered with the filter paper (Figure 4.6). The sponge is used instead of porous stone. The pore-pressure line is installed on top of the sample. Then the top latex membrane is covered and pasted. Then the sample is brought to the cubical device.

Vacuum

The pore-pressure line is connected to the vacuum line and then apply a vacuum of pressure of about 14 to 21 kPa (2 to 3 psi) is applied. Then the cover of the mold is removed and the sample is placed on a thin and long plate (Figure 4.3, second to the left). If the sample is not sufficiently strong to handle, increase the vacuum pressure to obtain a strong sample. If there are leaks, they need to be sealed.

Sample Insertion into the Cubical Device

Before sample is inserted into the cubical device the three directions of the cubical device (Y+ , X- and Z+ directions) are open and the remaining three directions are closed. The directions are shown in Figure 3.2. Then insert the sample into the cubical device from the one side (Y + direction) by slowly sliding it on the thin and long plate by the help of the small wood handle (Figure 4.5). Then the plate is slowly taken out and it is ensured that sample is at the center of the cubical cavity. Now, the sample together with the pore-water pressure line which is connected to the vacuum line are inside the cavity of the cubical device.

Then silicone rubber membrane is coverd on the X+ and Y+ direction to maintain the sample location. Then the pore-pressure line is disconnected from the vacuum line and put into the cubical device, from the Y+ direction . Then pore-pressure line is inserted into the small hole which is installed in the center of the frame of the cubical device, and then connected to the vacuum line. Make sure that sample is in good condition, and then cover it by the silicone membrane on the Z+ direction. The silicone membranes can

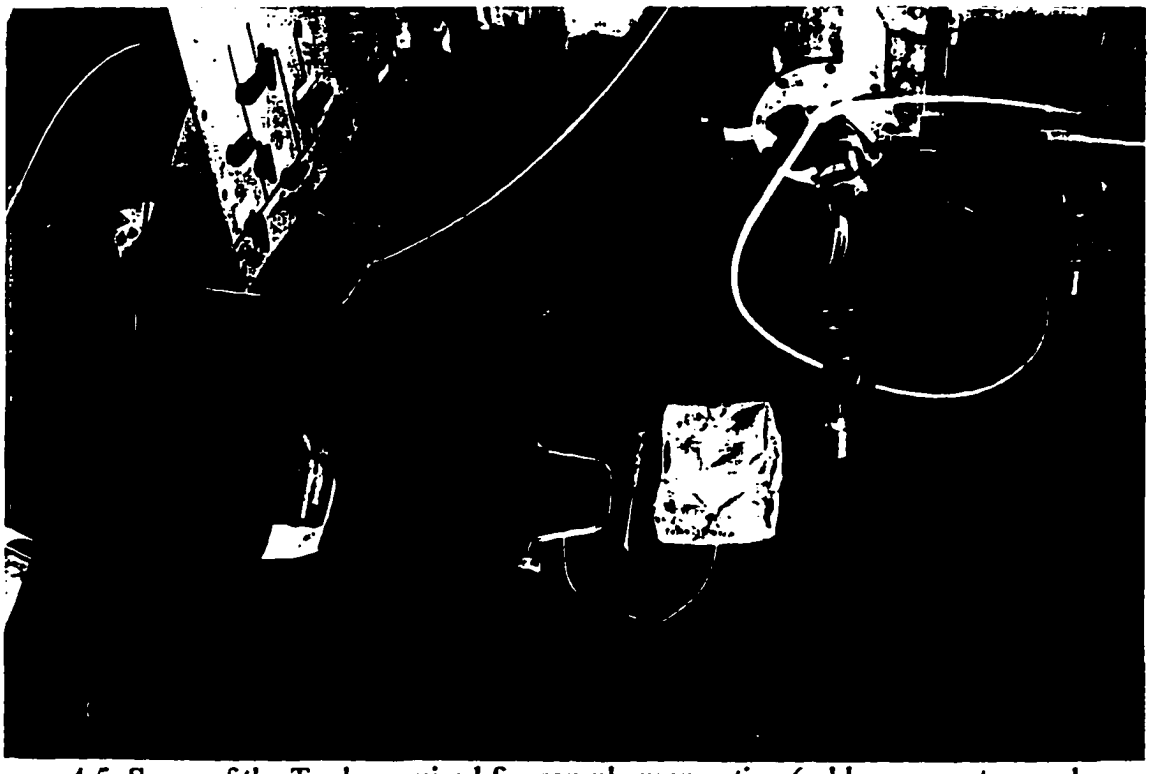

Figure 4.5 Some of the Tools required for sample preparation (rubber cement, wooden plunger, long wrench, shot wrench and sample covered with latex rubber membrane and connected with thin nylon tube)

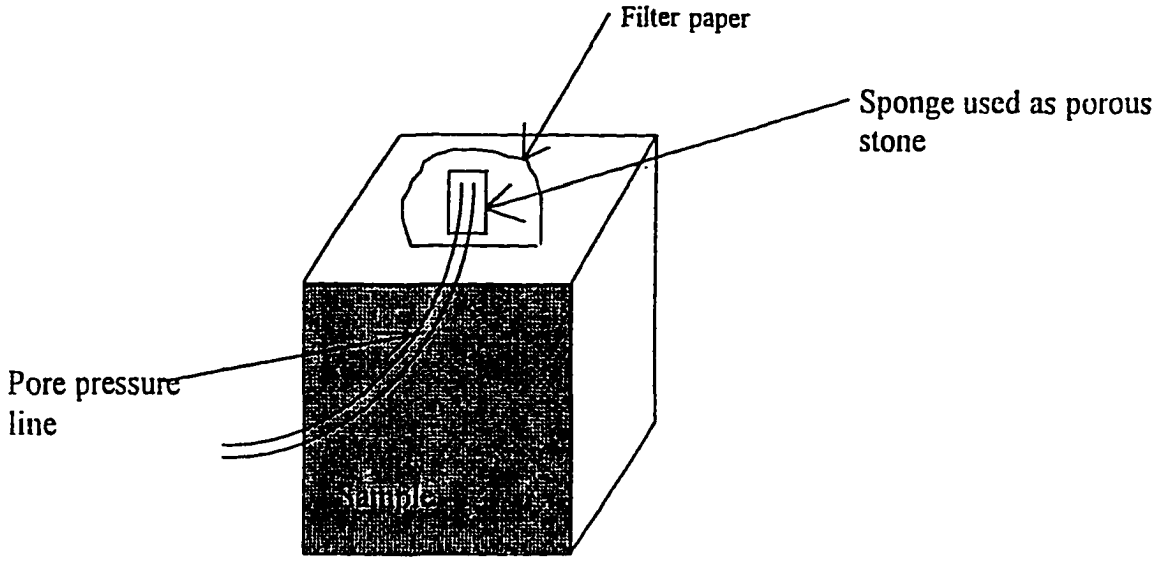

Figure 4.6 Diagram of the Attachment of Pore-water pressure Line with Sponge

temporarily hold the sample to maintain the good shape. The LVDT detecting cylinders are put on the silicone membranes, and the bolts are screwed by using the long wrench as shown in the Figure 4.5. The top plate (Z+ direction) can be tightened by the short wrench (Figure 4.5). An air pressure 14 to 21 kPa (2 to 4 psi) is applied in all the directions of the cubical device, while the vacuum pressure is released slowly. Next, the pore-pressure line is disconnected from the vacuum line, and connected to the pore-pressure to the saturation, drainage and pore-pressure board.

4.3 Test Procedures

Saturation

The de-aired water of the order of small amount is introduced into the specimen at a small differential head 3.5 kPa (0.5 psi). Thereafter a small back pressure of about 70 kPa (10 psi) is applied, while the cell pressure is increased. Then check the Skemption's B value is checked. The test is performed only when the B value is equal to or larger than about 0.96. Then the required inside cell pressure is applied.

Consolidation

The specimen is consolidated for at least one hour at the required confining pressure. In this study the three different confining pressures are used , 70, 140 and 210 kPa (10, 20 and 30 psi). Then the required axial stress is applied.

Testing

The cyclic axial load is applied to the specimen with the loading frequency of 0.10 Hz. The pressures, displacements in the x, y and z directions are automatically recorded and stored in the data file by the program control. The detailed steps to operate the programs are given in the User Manual. The program B9UTNDM.EXE is written in Pascal Language and can be used for CTC, RTE and HC tests.

Program B9UTNDM.PAS

This program is based on the program strain19.pas, written by Janos Toth for the testing of ceramic by using MTS machine for the measurement of signal from the single channel. The program will ask the data file name, type of the test (HC or CTC or Cyclic or RTE etc), pressure increment, maximum pressure for the loading step, minimum pressure for the unloading step, and increment pressure of each step etc. The detailed steps can be found in the User's Manual.

List of the Tests Performed

Table 4.1 shows the total tests performed. Unfortunately the tests performed in the beginning are not so good. The test results will be discussed mainly for the sand (Dr = 60 %) because the major purpose of the research is to study the behavior of sand (Dr = 60%). The other results are shown in Appendix. The chapter 5 presents the test results and discussion of the results.

Some Precautions for the Test

There are some difficulties in the test. The sample can bedisturbed very easily during the sample handling and insertion into the cubical chamber. Especially the loose sample, can disturbed very easily.

Initially leaking is a problem but the proper applying the rubber cement and membrane can protect from the leaking.

The sample should be centered during the insertion to obtain better results.

The sample should be handled very carefully, especially for the low confining pressure. The high confining pressure can maintain the sample in better shape than the low confining pressure.

The silicone membrane can not stand very high pressure and sometimes can break very easily in 394 to 690 kPa(60 to 100 psi). In the CTC test, due to the difference in the lateral and vertical pressure, the silicone membrane from the vertical direction (Z direction) can break very easily.

The pore-pressure line can be folded and sometimes the line can be totally closed.

Table 4.1 The Number of Tests Used in the Text

No.	Condition	Lateral Confining Pressure (kPa)	Type
1	Saturated, Dr=60%	69	CTC
2	Saturated, Dr=60%	138	CTC
3	Saturated, Dr=60%	207	CTC
4	Saturated, Dr=60%	69	CYCLIC
5	Saturated, Dr=60%	138	CYCLIC
6	Saturated, Dr=60%	207	CYCLIC
7	Saturated, Dr=60%	69	POSTCYCLIC
8	Saturated, Dr=60%	138	POSTCYCLIC
9	Saturated, Dr=60%	207	POSTCYCLIC

Chapter 5

RESULTS OF EXPERIMENTAL INVESTIGATION AND INTERPRETATION

5.1 Previous Investigation on the Liquefaction, Static, Cyclic and Postcyclic Behaviors of Saturated Sand

The previous investigations were presented in this section.

Various Views on Indication of Liquefaction

Cyclic triaxial tests have been used for seismic liquefaction evaluation of saturated sand since the pioneering work of Seed and Lee (1966) on isotropically consolidated specimens. The same authors later tested anisotropically consolidated specimens to simulate in situ static shear stresses, and they concluded that static shear due to anisotropic consolidation always increases the liquefaction resistance (Lee and Seed 1967; Lee et al. 1975; Seed and Lee 1966; Seed, et al. 1968; Seed et al. 1975; and Seed 1983).

Castro(1969, 1975), Casagrande (1976), Castro and Polus (1977) Castro, et al. (1982) studied the behavior of saturated sands under monotonic undrained loading and

developed the steady-state concept; they also performed cyclic triaxial tests on anisotropically consolidated sands.

The steady state concepts and **state diagram** are the pioneering work of Castro (1969) and are being increasingly used to analyze the stability of granular soil structures subject to monotonic or cyclic undrained loading. The key assumption in such analyses is that the sand has a unique steady state line in void ratio-effective confining stress space (state diagram). This line is determined by performing undrained triaxial compression test. The steady state line represents the locus of states in which a soil can flow at constant void ratio, constant effective minor principal stress (σ_3') (Castro, 1977). The void ratio at the steady state line is the same as the critical void ratio as defined by Casagrande (Castro, 1977). If the initial void ratio is smaller than the critical void ratio, negative pore-water pressure will be developed and if the initial void ratio is larger than the critical void ratio, positive pore-water pressure will developed and liquefaction can occur. The critical void ratio is not a unique property of the soil and depends on the confining pressure. The liquefaction is the result of undrained failure of a fully saturated highly contractive (loose) sample (Castro, 1977).

In the state diagram, for contractive soils (loose), the void ratio will move from the starting point toward the steady state line, horizontally and ending on the steady state line. During undrained conditions, the soil remains at that point in the state diagram (Castro, 1977). The state diagram is shown and explained in Figures 2.30 and 2.31.

A major difference between the work of Castro (1969, 1975) and Seed (1983) is in their respective definitions of liquefaction failure. Seed defines *failure as the development of a specified value of accumulated axial strain after a certain number of cycles* of uniform cyclic deviator stress. Castro (1975) defines failures as a *sudden loss of strength, which causes the specimen to flow and to develop unlimited strains* under steady-state condition; this steady state concept developed first for monotonic loading, is found to apply also to cyclic loading (Youd, 1973).

Recent studies (Castro et al. 1982; Dorby et al. 1985; Mohamad and Dorby 1986; Sladen et al. 1985; Sumes et al. 1984; Vaid and Chern 1985) have made significant contributions in delineating the relationships that exist between monotonic and cyclic undraind behavior of sand. But Alarcon-Guzman et al. (1988) stated that several aspects of this behavior remain unclarified , such as the state conditions marking the initiation of strain softening behavior for both monotonic and cyclic loading conditions. They pointed out that the previous investigators do not mark the strain softening region and strain hardening region (Alarcon-Guzman et al. 1988).

Vaid and Thomas (1995) reported that under *static loading* the term *liquefaction is associated with a strain softening type of undrained response, resulting in either unlimited or limited flow deformation* (Figure 2.5). This type of behavior is similar to the work of Castro (1969) and they termed this feature as *contractive*. On the otherhand, if strain softening does not occur the sand is called *dilative* (see Figure 2.5).

Line of Phase Transformation

The line of phase transformation is the same as steady state line and is a boundary between the areas of large strains and small strains. Figure 5.1 (after Ishihara et al , 1978) shows the typical undrained stress paths for the Fuji river sand. When a saturated sand sample is subjected to a shear stress in the triaxial compression in undraind conditions, the general pattern of the stress path in the p' -q stress space during shear has an appearance of a curve ABC as Figure 5.1. The straight line from the origin passing through the point B is called the "*line of phase transformation (PT Line)*" . This is called as phase transformation line because, the sample does not develop large strains and behaves in the manner of a solid plastic material between this line. If stress goes across these lines, the samples tend to develop considerably large strains and behaves in the manner of viscous fluid (Ishihara et al., 1978).

Previous Investigation of Behavior of Saturated Sand in Static Loading

Vaid and Chern (1985) showed the **three different modes** (steady state, contractive and dilative) of the effective stress paths and stress-strain relationships for the general behavior of sand (Figure 5.2). In this figure, curves for A and B correspond to **contractive** and **partly contractive behavior** respectively, while curve C corresponds to **dilative behavior.** Only curve A terminates at the steady state (shown as S_{SS} on the Figure 5.2a) and exhibits completely contractive behavior. Curve B exhibits softening behavior after reaching a peak stress until the phase transformation point (shown as S_{PT}

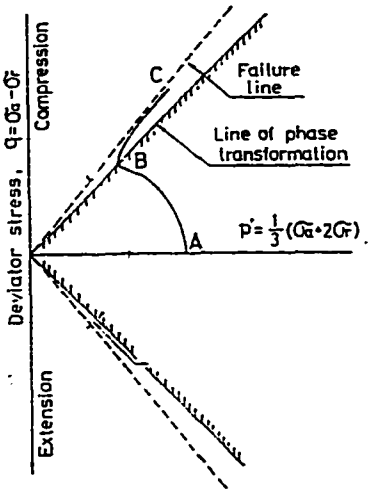

Figure 5.1 Line of Phase Transformation Shown in the p'-q stress space (After Ishihara and Okada, 1978)

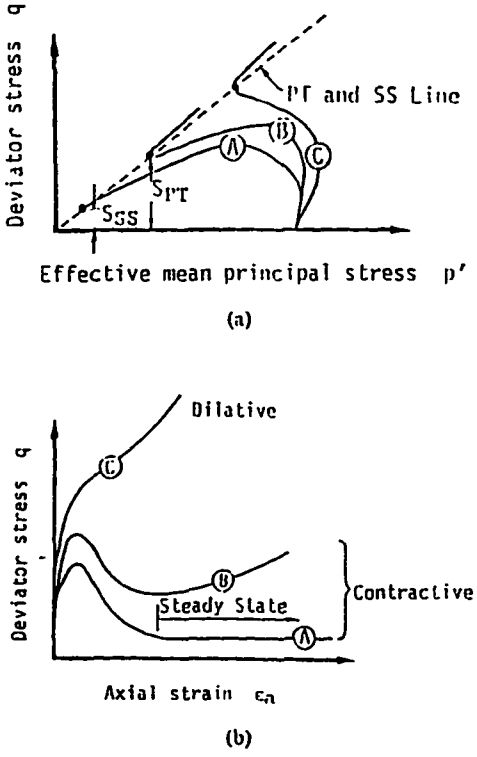

Figure 5.2 Schematic Diagram of Contractive, and Dilative Behavior of Sand in Monotonic Test (Vaid and Chern, 1985)

on the Figure 5.2a) and after that it behaves in a hardening manner. The Phase Transformation point is indicated as C on the dilative line (Figure 5.2b). In their work the phase transformation line (PT Line) and steady state line (SS Line) are shown as same line. The points of PT Line for these two lines in a same direction (Figure 5.2a).

Figure 5.3 presents the type of **contractive deformation** (Vaid et al., 1990). They reported that the steady state (SS) for a contractive sand corresponds to a state of **residual undrained strength** (following peak) that is sustained with continued deformation (Figure 5.2a). The term **liquefaction** is used for this type of response (Castro, 1969). They stated that the state of transient minimum strength associated with contractive response of the limited liquefaction type corresponds to the phase transformation (PT) state (Figure 5.1) of Ishihara (1978). Vaid et al. (1990) mentioned that this state signifies the start of dilation or decrease in pore pressure and increase in deviator stress with futher undrained shearing.

Figure 5.4 presents typical results of stress controlled monotonic loading undrained tests performed on loose and medium dense sand (Vaid and Chern, 1983). For the test S-1 and S-2 the deviator stress and pore-water pressure increased progressively with very small strain development and the effective stress path moved towards the failure envelope. A sudden decrease in deviatoric stress occurred accompained by sharp increase in pore-water pressure and axial strain in a very short period of time. They called this behavior as flow deformation , which was also observed in the cyclic loading tests, was stopped by dilation once the sample developed sufficient strain. The sample S-3 dilated and approached the failure envelope progressively.

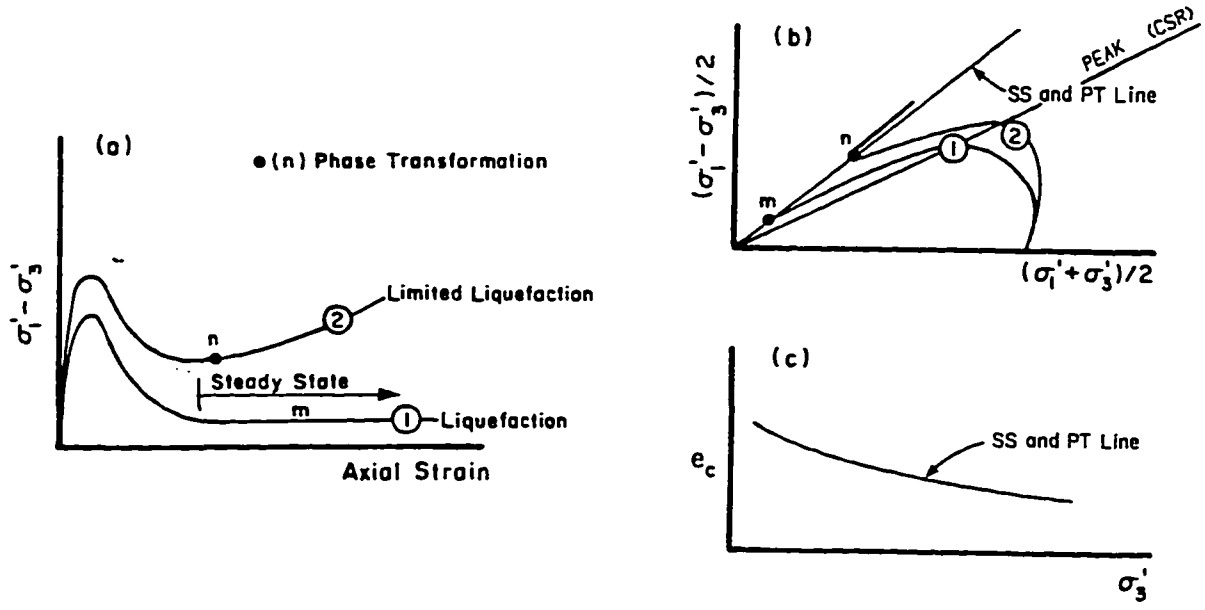

Figure 5.3 Type of Contractive Deformation (Vaid et al., 1990)

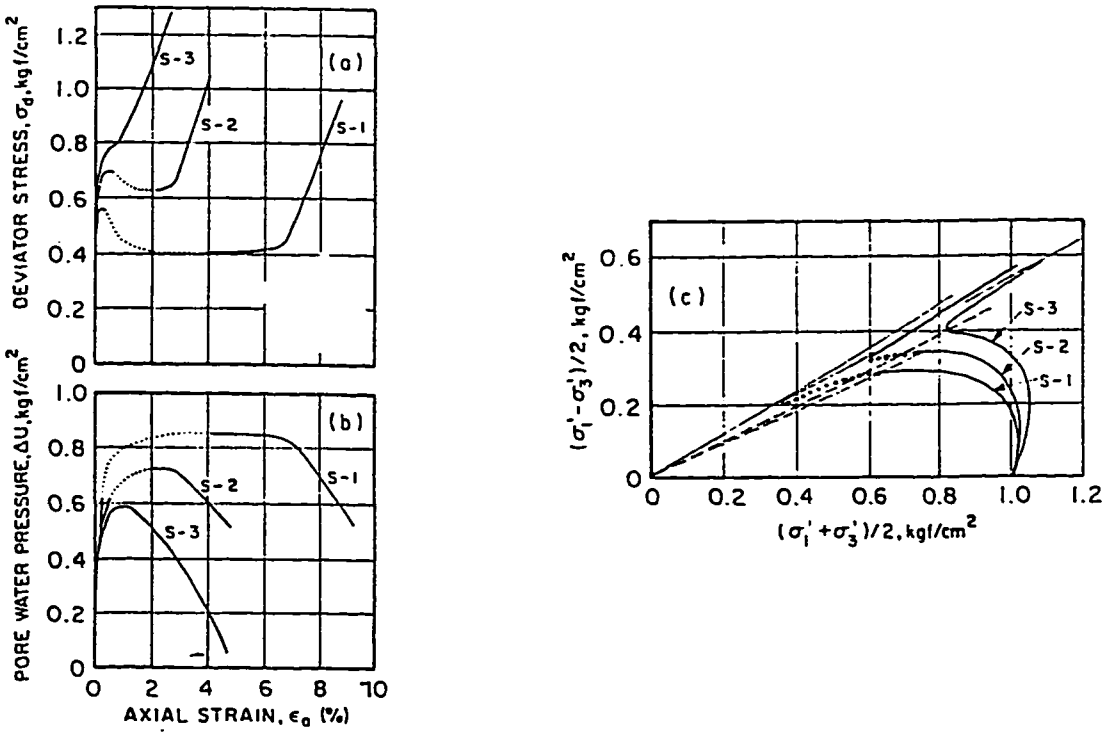

Figure 5.4 Stress-Strain, Pore-water Pressure and Effective Stress Path of Ottawa Sand (Vaid and Chern, 1983)

Figure 5.5 presents the stress-strain response of Banding Sand in consolidated undrained test (Castro, 1969). In test 1 (Figure 5.5a), the applied shear stress, first increased and then dropped rapidly to a constant, steady state or residual strength value (S_{us}). The test 2 indicates the partially-contractive specimen (Castro, 1969 and Mohamad and Dobry, 1986). They noted that for the effective stress path for a partially-contractive response invariably exhibits an **elbow,** i.e., a point where the effective stress path bends sharply upwards and to the right. They noted that this sample experienced **limited liquefaction.**

Discussion of the Static Loading and Unloading Results

As shown in the Figure 5.6a and 5.6b, the undrained behavior of the sand can be characterized by three regions (strain softening, transition and strain hardening region) in the state diagram for the monotonic loading as described by the Alarcon-Guzman et al. ;1988, Ishihara ;1985, Ishihara and Okada ; 1978, Vaid and Chern ; 1985, and Mohamad and Dorby ; 1986.

First, there is a region in the state diagram (Figure 5.6a) within which a sand exhibits marked strain softening behavior, i.e., after the peak point of the stress-strain curve, which occurs at a small strain, there is a marked reduction in strength until the stress is stabilized at an ultimate or residual strength. This is referred to as "*flow deformation*" and the residual strength is called as "*steady-state strength.*" The steady-state strength of sands exhibiting strain softening behavior is said to depend mainly on the grain characteristic and the void ratio of the sand (Casagrande 1976; Castro 1969; Castro 1975; Castro and Polus 1977; Polus 1981) such that the state conditions during

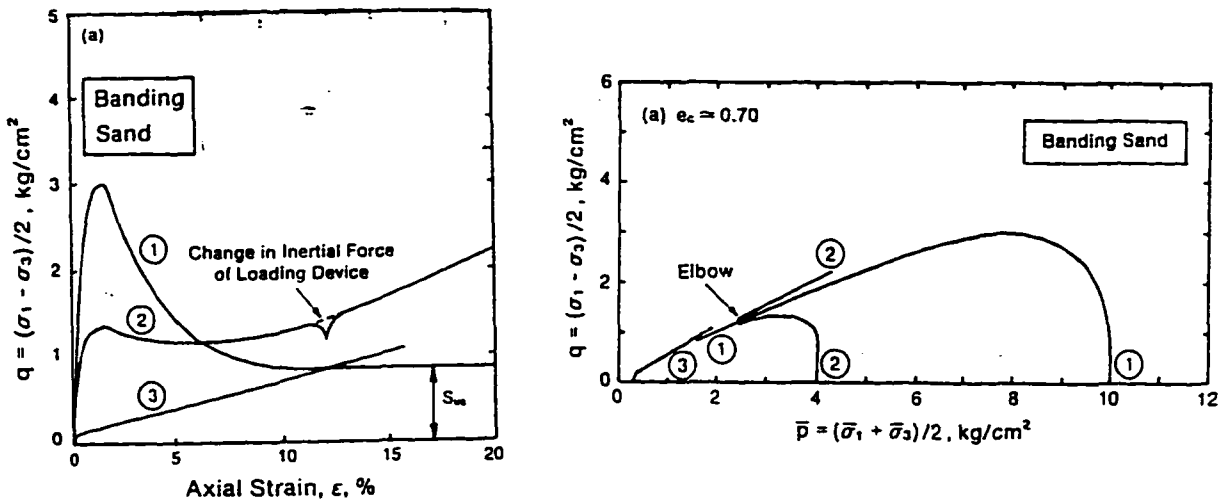

Figure 5.5 Stress-Strain Response of Banding Sand (Castro, 1969)

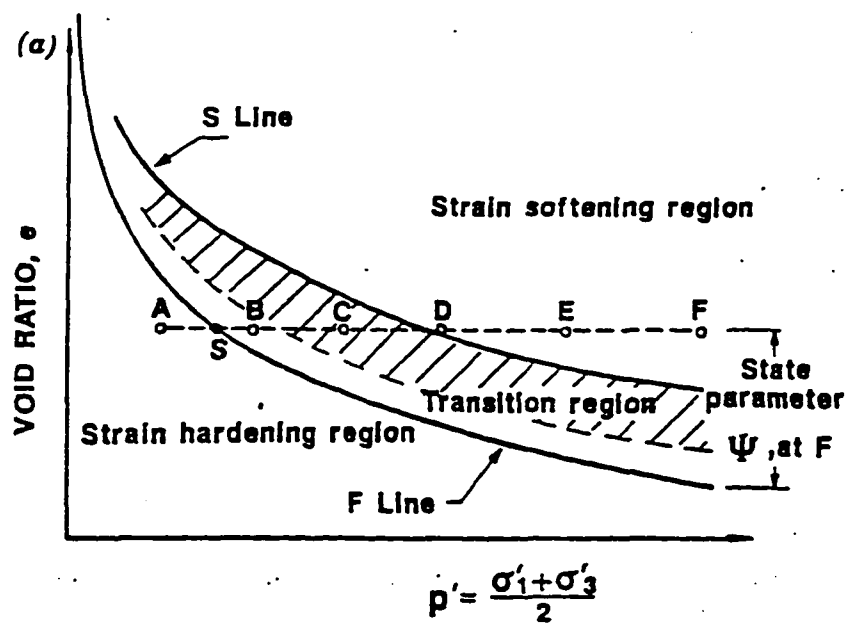

Figure 5.6a State Diagram (Alarcon-Guzman et al, 1988)

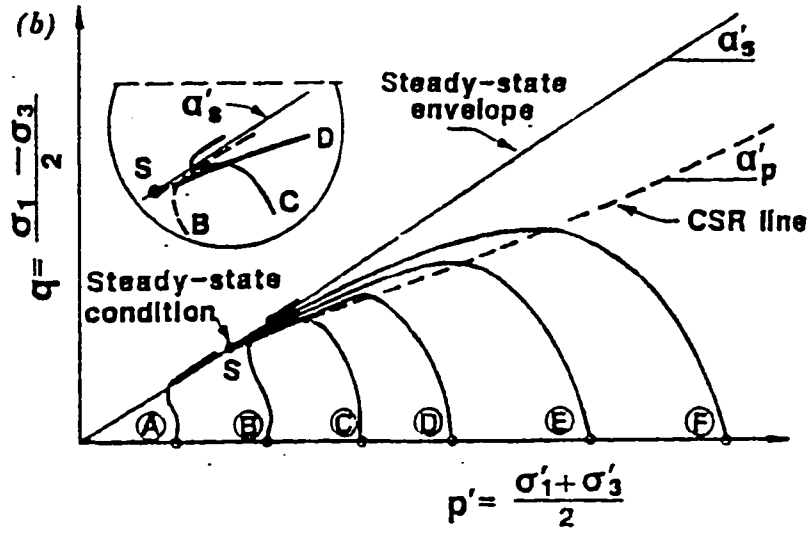

Figure 5.6b Stress Path Plot for Monotonic Undrained Loading (Alarcon-Guzman et al, 1988)

steady-state deformation defines a unique line in the state diagram (F line in Figure 5.6a, Alarcon-Guzman et al 1988) and called the "*steady-state line*". In the p′-q stress space, F line is defined as a straight line and called as "*steady-state (large strain) failure envelope*" (Figure 5.6b)

The *transition region* in the state diagram (Figure 5.6a) is a region in which the strength decreases to a residual value over a limited range of shear strains, but the specimen gains strength (strain harden), as further straining causes dilation and consequent reduction in pore-water pressure. In this region, the stress path shows an "elbow" after which it moves back along the failure envelope (F line).

The *strain hardening region* of a state diagram is a region in which a sand exhibits solely strain hardening behavior. After the initial tendency to contract, dilation occurs due to the results of the decrease in the pore-water pressure.

Previous Investigation of Behavior of Saturated Sand in Cyclic Loading

Figure 5.7 shows the schematic diagram of undrained cyclic behavior of sand by Alarcon-Guzman (1989). They indicates that this is the schematic diagram for the condition that the cyclic deviatoric stress is smaller than the static stress. As shown in figures 5.7, when the effective principal stress ratio reaches a critical value, dilation will prevail; the stress path, corresponding to the cycle in which this occurs, shows a *turnaround or elbows* and moves back along the failure line in a manner similar to that observed during monotonic loading within the strain hardening region of the state diagram (Alacorn-Guzman et al., 1988).

The transition from contractive to dilative behavior on loading, which occurs at a threshold value of the principal stress ratio, causes a drastic change in particle arrangement, which may include the formation of metastable holes (Nemat-Nasser and Takahashi 1984; Youd 1977).

As shown in the Figure 5.7 upon reversal in the direction of shear straining (point R in Figure 5.7), the number of contact points between neighboring grains is drastically reduced. Accordingly, the sand structure tends to collapse, producing a correspondingly (large) increase in pore-water pressure, as reflected by the effective stress path moving towards the origin of the stress space diagram [point O in Fig. 5.7].

The value of ϕ' that corresponds to the threshold principal ratios at which dilation occurs on loading within the strain hardening region of the state diagram define the so-called "*phase transformation lines*" (Ishihara 1985, Ishihara et al. 1975). Reversal in the direction of shearing from stress states beyond such lines eventually results in the

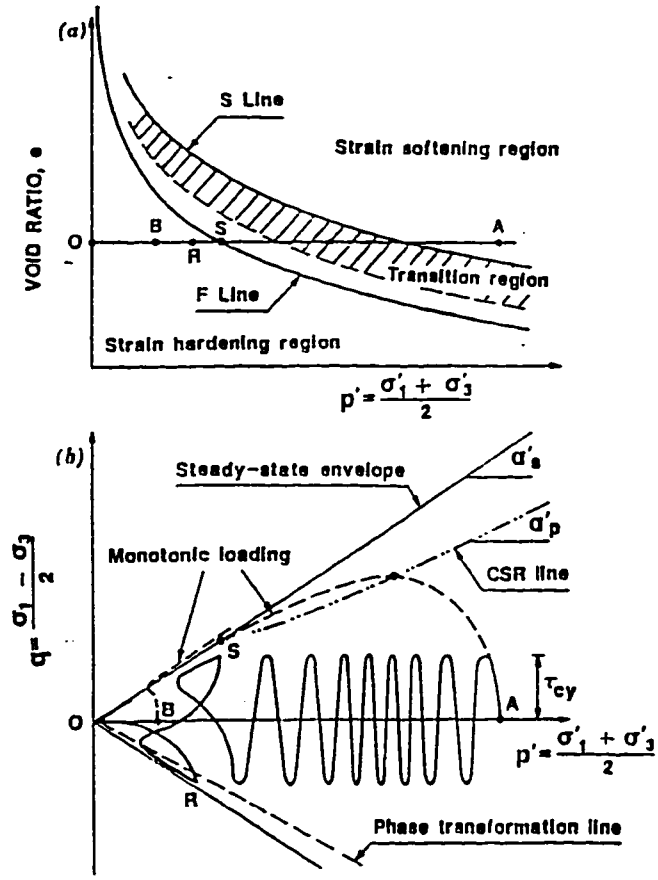

Figure 5.7 Stress Path Plot (After Alarcon-Guzman et al., 1988)

occurrence of a zero effective stress state at the instant the stress cycle passes through the hydrostatic stress state. This condition has been referred to as a "***initial liquefaction***" (Seed 1979, Seed and Lee 1966).

The location of the phase transformation lines in the stress space depends on the relative density and the type of sand. For initially contractive specimens, the angle of phase transformation is slightly smaller than shear resistance (Vaid and Chern 1985). In this case, initial liquefaction is likely to develop during the first few unloading stages after the stress path crosses the phase transformation line. As the relative density of the sand increases, the lines of phase transformation move away from the failure line, since dilation would prevail at much lower stress ratio (Ishihara, 1985).

Accordingly, in a dense sand, many cycles of loading and unloading may be required to reach a condition of zero effective stress after crossing the phase transformation line. Once initial liquefaction develops, a certain amount of shear strain is required to mobilize a given shearing resistance in the opposite direction, which is a function of the relative density of the sand (Seed and Lee 1966; Selig and Chang 1981; Youd 1977).

5.2 Present Investigation of Static, Cyclic and Postcyclic Behaviors of Saturated Ottawa sand

This section presents the present study on the static, cyclic and postcyclic behaviors of saturated Ottawa sand.

5.2.1 Static Loading Behavior of Saturated Ottawa Sand

Figures 5.8 to 5.10 show the present results for the Ottawa sand (Dr = 60%) in consolidated undrained test (CTC) with the confining pressure of 69, 138 and 207 kPa, respectively. Deviator stress is defined as $(\sigma_1 - \sigma_3)$. Figure 5.11 plots the peak values of $(\sigma_1 - \sigma_3)$ from Figure 5.8 to 5.10. Figure 5.12a shows the corrosponding effective stress paths for the confining pressure of 69, 138 and 207 kPa.

As shown in the Figure 5.12a (Phase Transformation Point is mark as filled cycle), the behavior of the present result is similar to the ***dilative*** sample of Figure 5.2 (marked as B) . The location of PT point (marked as filled cycle) for σ_3' = 207 kPa is similar to the Figure 5.2 (B sample) and Figure 2.5a (dilative sample). As shown in the Figure 5.8 and 5.9, the axial strains increased to 9 to 10 % and after that a dilative tendency took over.

This behavior is similar to the one mentioned in the report of Vaid and Thomas (1995). They reported that on unloading, the specimen liquefied, i.e., it shows σ_3' is equal to zero. As can be seen in the Figure 5.8, the pore-water pressure increases to the 69 kPa (pressure same as the confining pressure) when unloading from 35.5 kPa (5 psi). In Figure 5.9 , the pore-water pressure increased to the 138 kPa (20 psi) when unloading

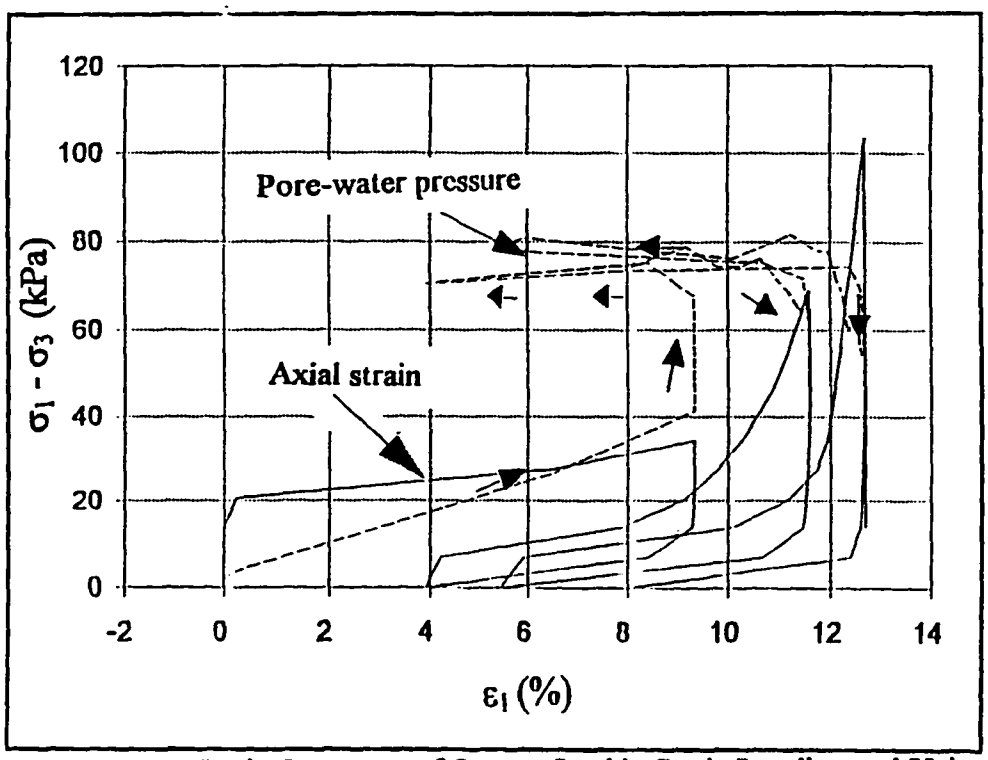

Figure 5.8 Stress-Strain Response of Ottawa Sand in Static Loading and Unloading ($\sigma_3' = 69$ kPa)

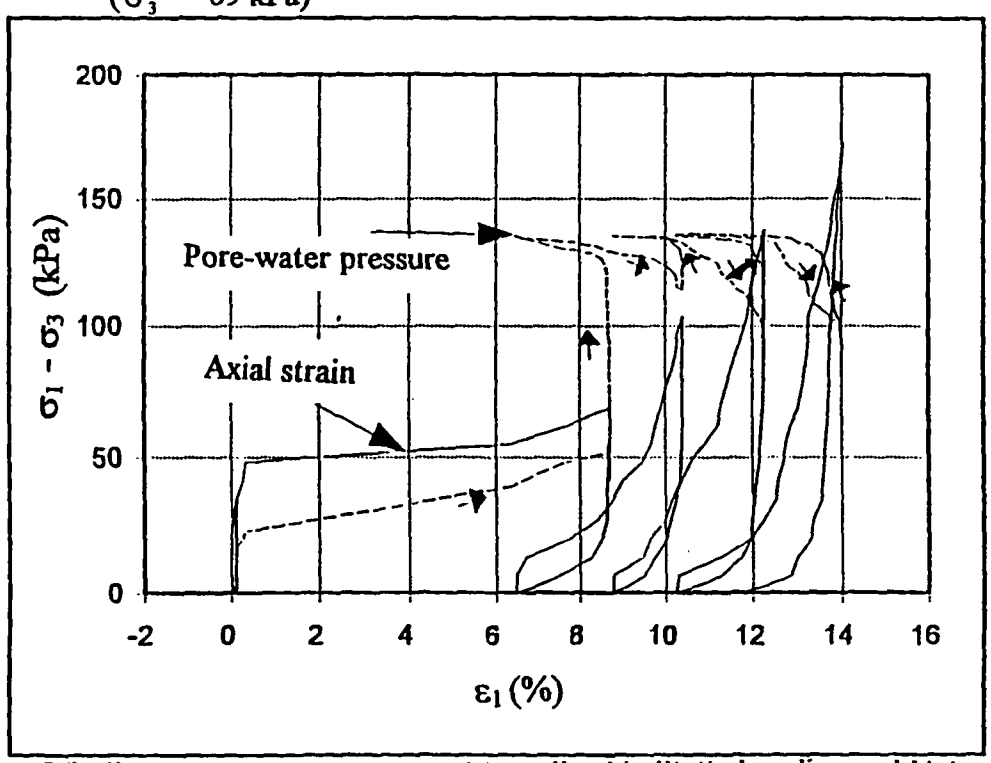

Figure 5.9 Stress-Strain Response of Ottawa Sand in Static Loading and Unloading ($\sigma_3' = 138$ kPa)

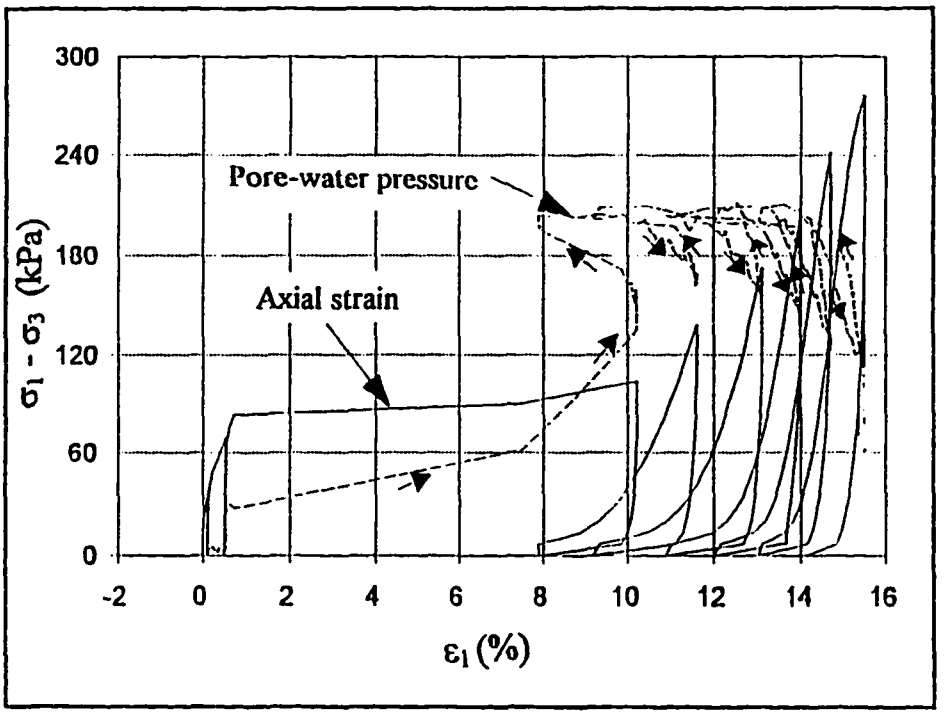

Figure 5.10 Stress-Strain Response of Ottawa Sand in Static Loading and Unloadin ($\sigma_3' = 207$ kPa)

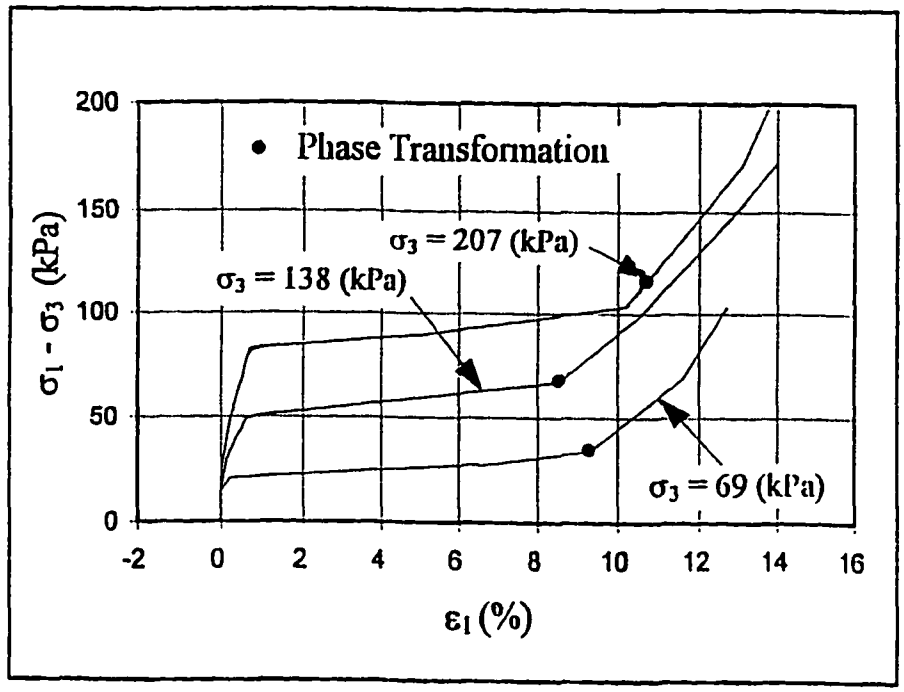

Figure 5.11 Stress-Strain Response of Ottawa Sand in Static Loading and Unloading (σ_3' = 69, 138 and 207 kPa)

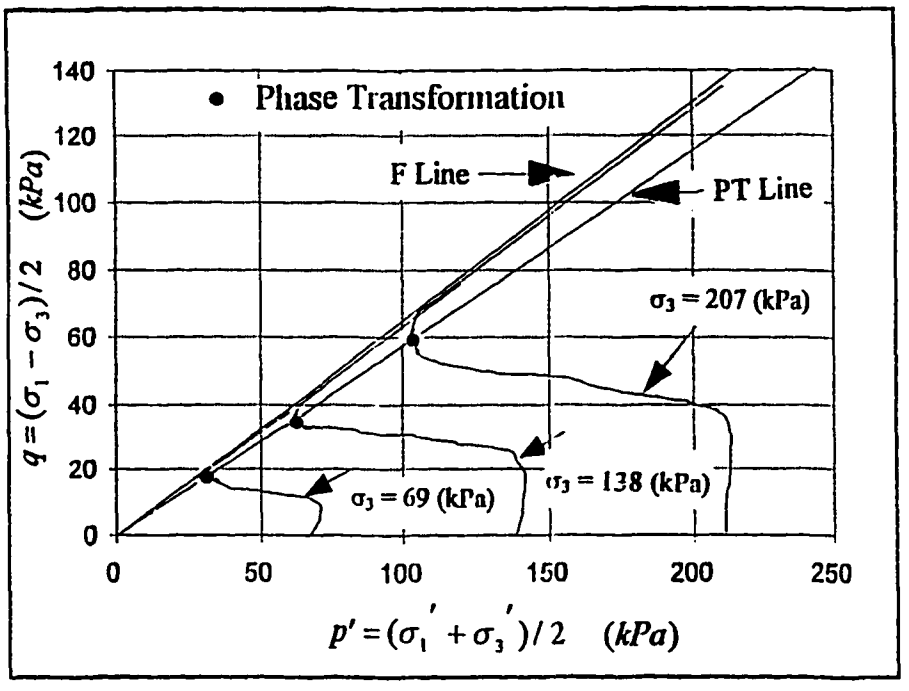

Figure 5.12a Effective Stress Path for the Ottawa Sand in Static Loading and Unloading Test (Plots the loading part only)

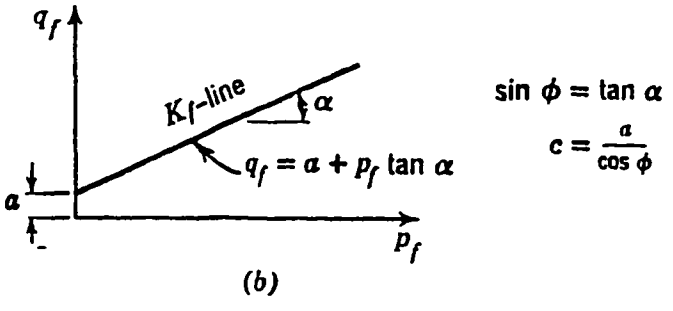

Figure 5.12b Relation of p'-q diagram to Mohr-Coulomb envelope

from 69 kPa (10 psi). In Figure 5.10, the pore-water pressure increased to the 207 kPa (30 psi) when unloading from 103.5 (15 psi). This type of behavior is referred as *liquefaction* induced by static loading and unloading cycles as liquefaction induced by cyclic loading (Vaid and Thomas 1995).

In preset tests, the strains reached to about 9 to10% before the sample reached the phase transformation state so get the enough straining and the zero effective stress state is realized on unloading.

Effective Stress Path, Phase Transformation (PT) Line of the Present Test

The effective stress path of the samples tested indicate a type contractive response and invariably exhibits an '***elbow***' i.e., a point where the effective stress path bends sharply upwards and to the right as shown in Figure 5.12a. The effective stress path slightly increased to PT point (Figure 5.12a).

The Phase Transformation Line (PT Line) and Failure (F Line) Lines are drawn in the Figure 5.12a, are similar to those in the Figure 5.1 (Ishihara, 1978). The angle of the failure line is about 33 degrees. The friction angle at the steady state and PT (phase transformation) states is 30 degrees.

Strength Parameter

The effective angle of shearing resistance, ϕ' is calculated from effective stress path (Figure 5.12b). As shown in the Figure 5.12b, the curve drawn through the failure point is called the K_f-line and the relationship between the slope of the K_f-line (α) and angle of shearing resistance (ϕ')can be found in the follwing equation.

$$\sin \phi' = \tan \alpha \qquad (1)$$

$$c = a / \cos\phi$$

$$\phi' = \sin^{-1}(\tan\alpha) \qquad (2)$$

As shown in Figure 5.12, the slope of the K_f-line (α) is 33° and $a = 0$. So,

$\phi' = \sin^{-1}(\tan 33^\circ) = 40^\circ$.

5.2.2 Cyclic Undrained Behavior of Saturated Ottawa Sand

As mentioned in the Chapter 4, the results for the cyclic behavior at Dr = 60 % are given below. The other tests (for Dr = 80% and Dr = 20%) are not shown in the present thesis and will be used in future. The frequency of loading is 0.1 Hz.

Stress-Strain , Pore-water pressure, Axial strain-Time Relationships

Figures 5.13 to 5.15 present deviatoric stress, axial strain and excess pore-water pressure vs time for the confining pressure of 69, 138 and 207 kPa. Stress-strain relationships during cyclic loading with different confining pressure are presented in Figure 5.16 to 5.18.

As shown in Figures 5.16 to 5.18, the samples shows small strain in the first few cycles. After 5 to 9 cycles, the samples show much greater deformations (strain hardening behavior) and liquefaction ensues. As shown in the Figure 5.13 to 5.15, the excess pore-water pressure increases gradually, and after 5 to 9 cycles, it reached the value equal to the effective confining pressure. This condition has been referred to as a "***initial liquefaction***" (Seed 1979, Seed and Lee 1966).

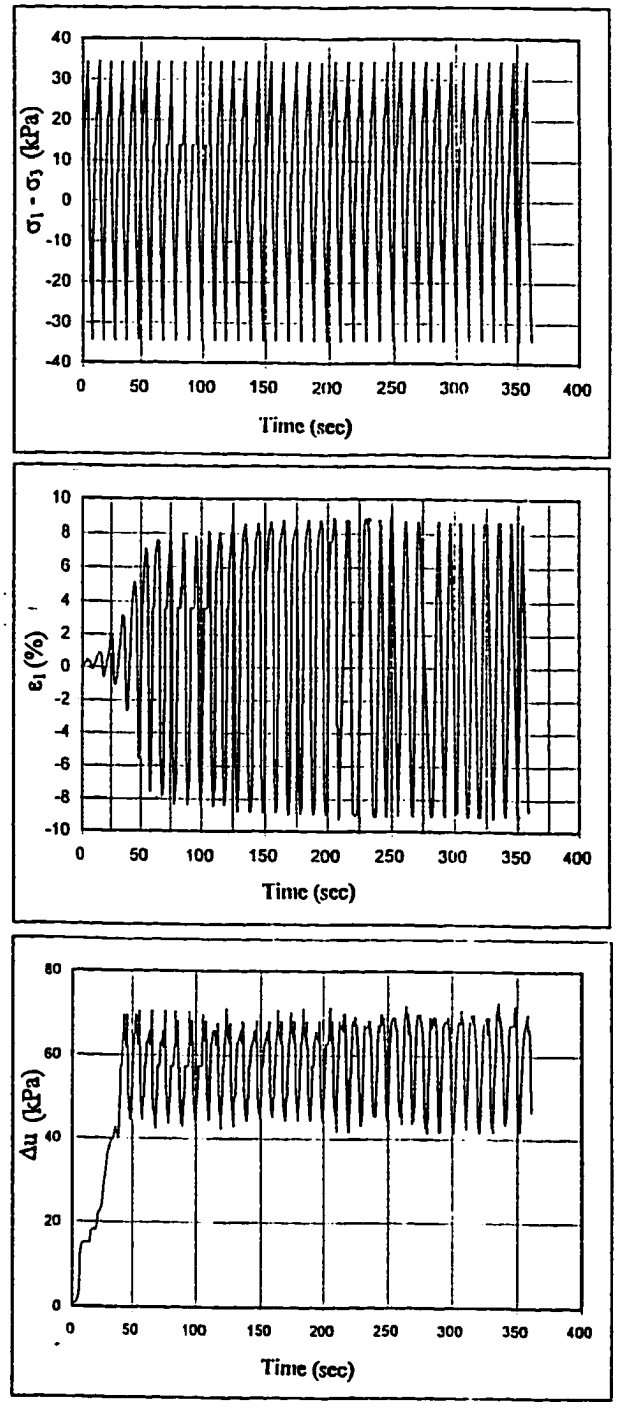

Figure 5.13 Result of the Consolidated Undrained Cyclic Test (σ_3' = 69 kPa), Time Vs Deviatoric Stress, Axial Strain and Excess Pore-water Pressure Plot

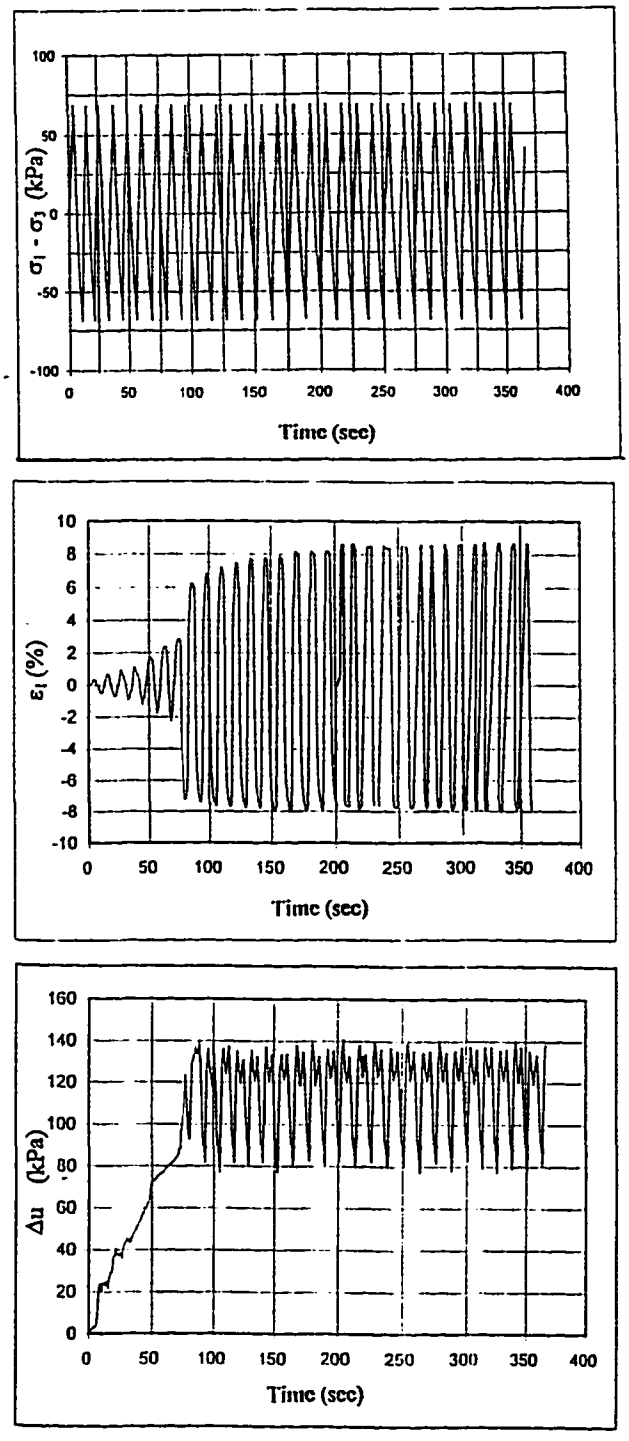

Figure 5.14 Result of the Consolidated Undrained Cyclic Test,(σ_3' = 138 kPa),Time Vs Deviatoric Stress, Axial Strain and Excess Pore-wate Pressure Plot

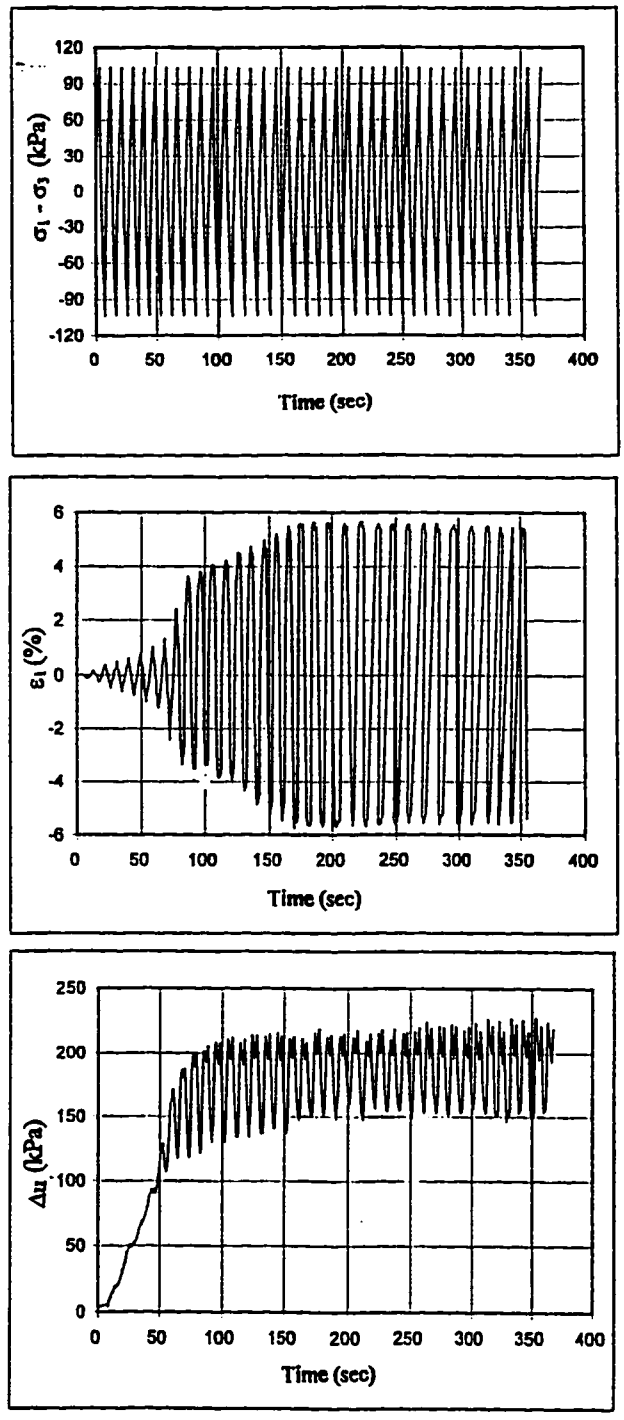

Figure 5.15 Result of the Consolidated Undrained Cyclic Test (σ_3' = 207 kPa),Time Vs Deviatoric Stress, Axial Strain and Excess Pore-water Pressure Plot

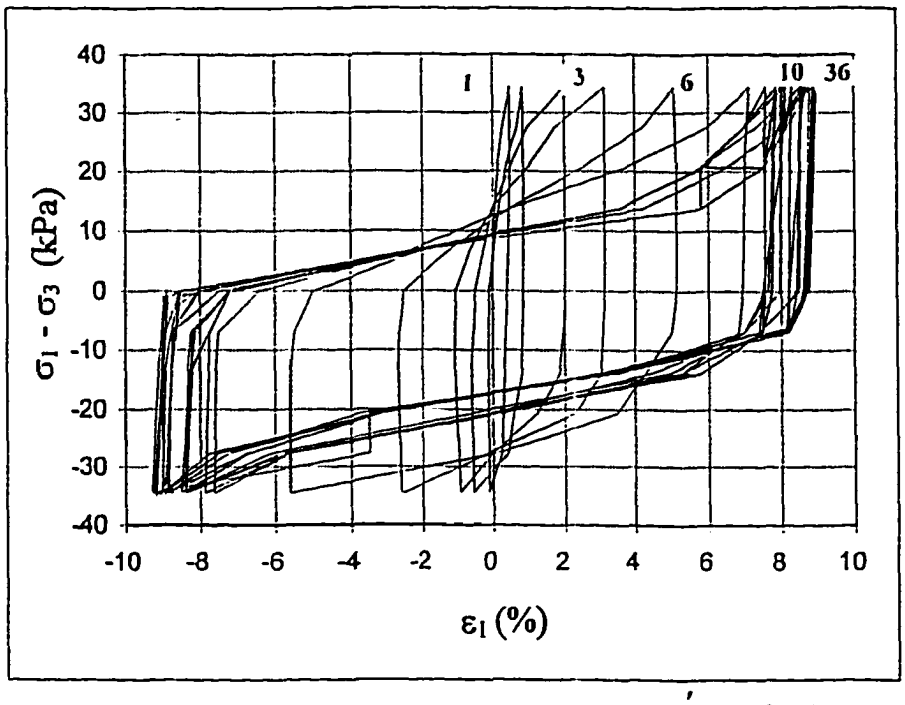

Figure 5.16 Stress-Strain Plot of Cyclic Test (σ_3' = 69 kPa)

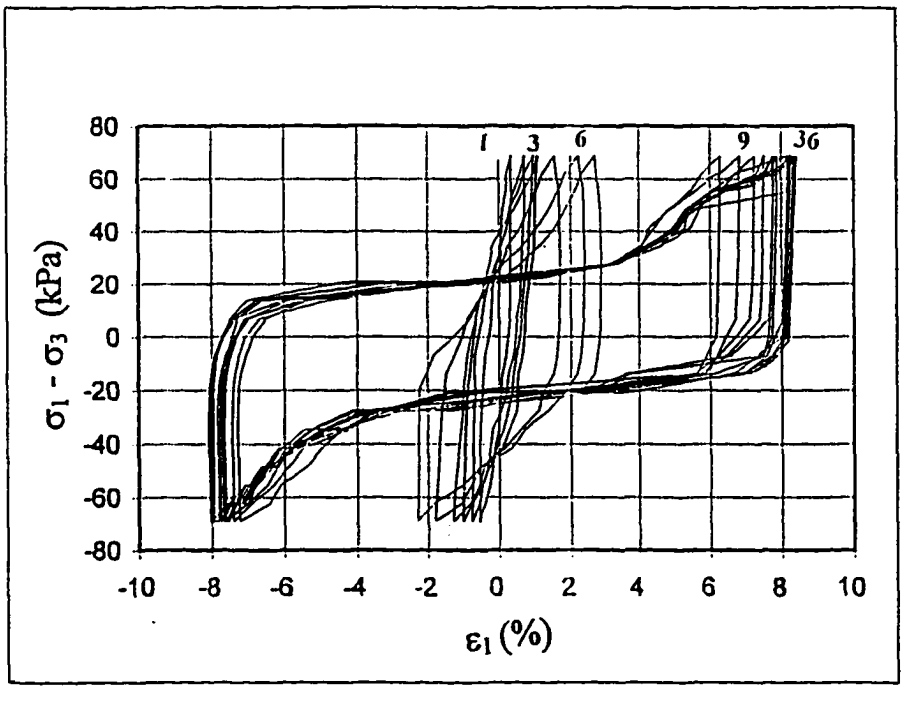

Figure 5.17 Stress-Strain Plot of Cyclic Test (σ_3' =138 kPa)

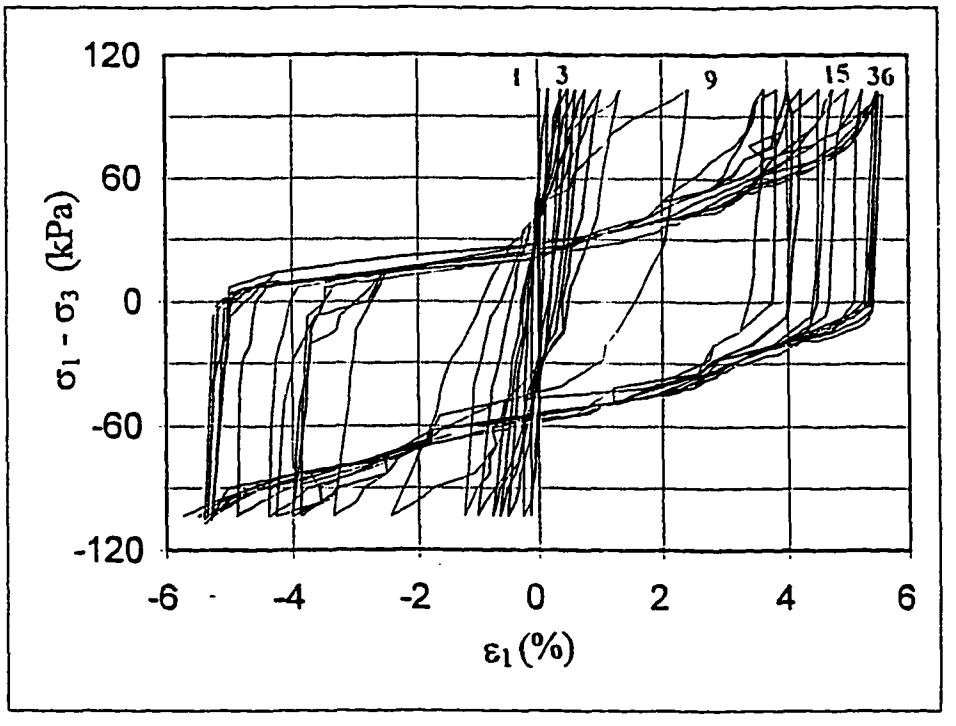

Figure 5.18 Stress-Strain Plot of the Cyclic Test ($\sigma_3' = 207$ kPa)

Cyclic Stress Ratio Vs Numbers of Cycles

Figure 5.19 shows the **cyclic stress ratio** ($\sigma_d / 2\sigma_0'$) vs number of cycles to liquefaction. The **cyclic stress ratio** (SR) is the ratio of half of the deviatoric stress to the effective confining pressure.

The stress ratio (SR) is same for all the three tests. For the same confining pressure, if a higher deviatoric stress is applied, the cyclic stress ratio will be higher and the sample will be liquefied in very few cycles. On the other hand, if a smaller deviatoric stress is applied, the stress ratio will be lower and the sample will be liquefied after the many cycles.

$p' - q$ Diagram

Figure 5.20 to 5.22 presents the $p' - q$ diagram of the cyclic tests of Ottawa sand for the effective confining pressure of 69, 138 and 207 kPa.

As shown in the figures 5.20 to 5.22, when the effective principal stress ratio reaches a critical value, dilation will prevail; the stress path, corresponding to the cycle in which this occur, shows a *turnaround or elbows* and moves back along the failure line in a manner similar to that observed during monotonic loading within the strain hardening region of the state diagram (Alarcon-Guzman (1988).

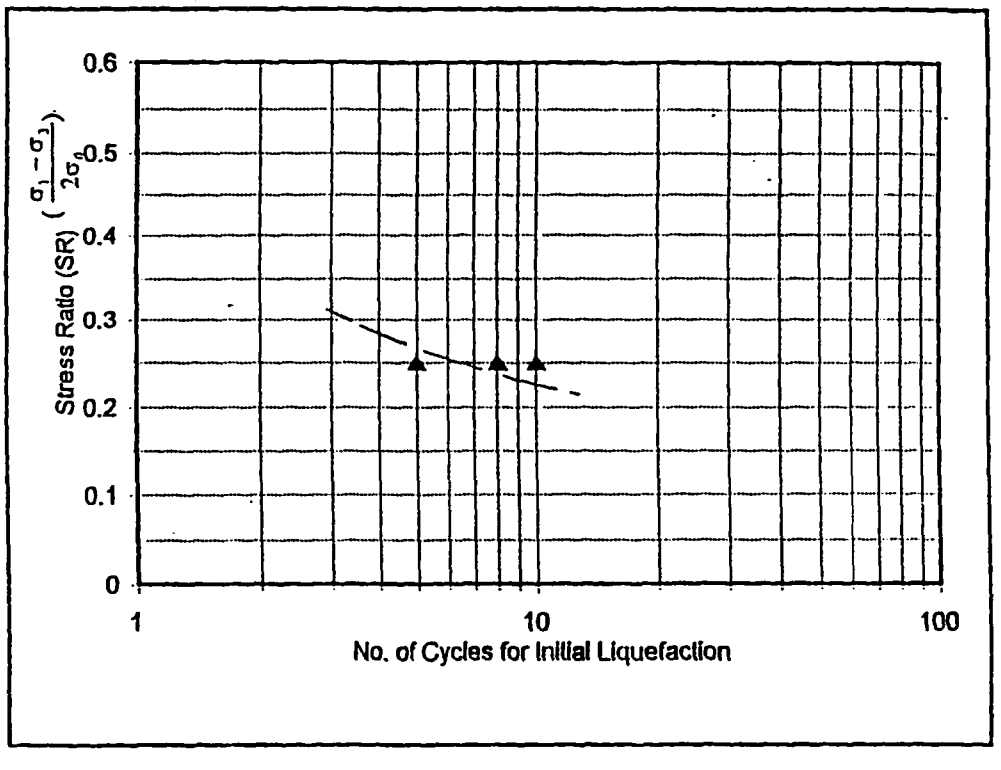

Figure 5.20 Cyclic Stress Ratio Vs Nos. Of Cycles

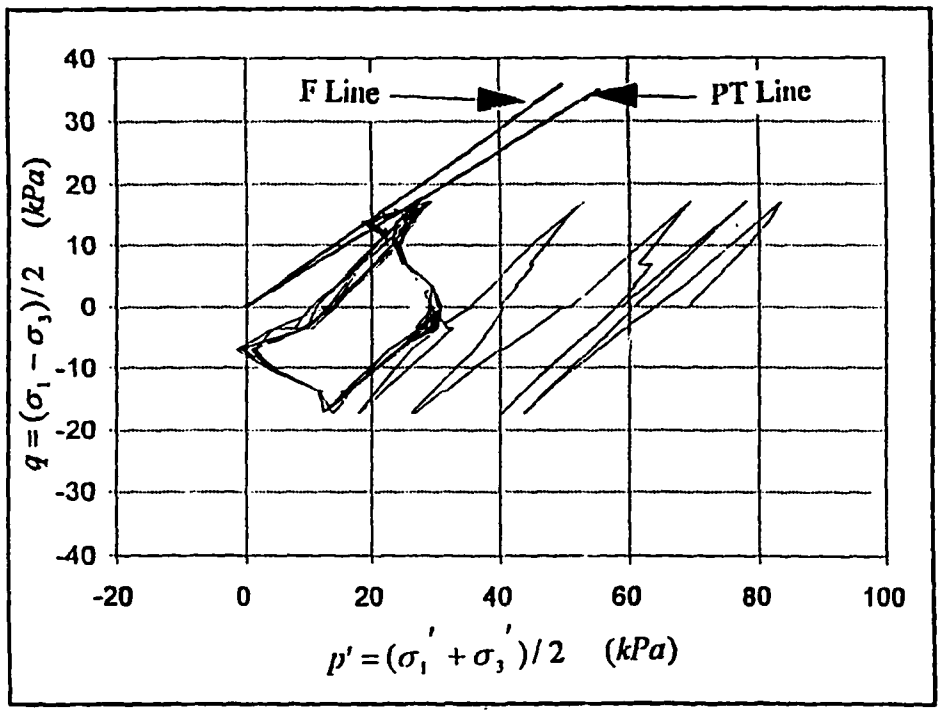

Figure 5.20 Stress Path For σ_3 = 69 kPa

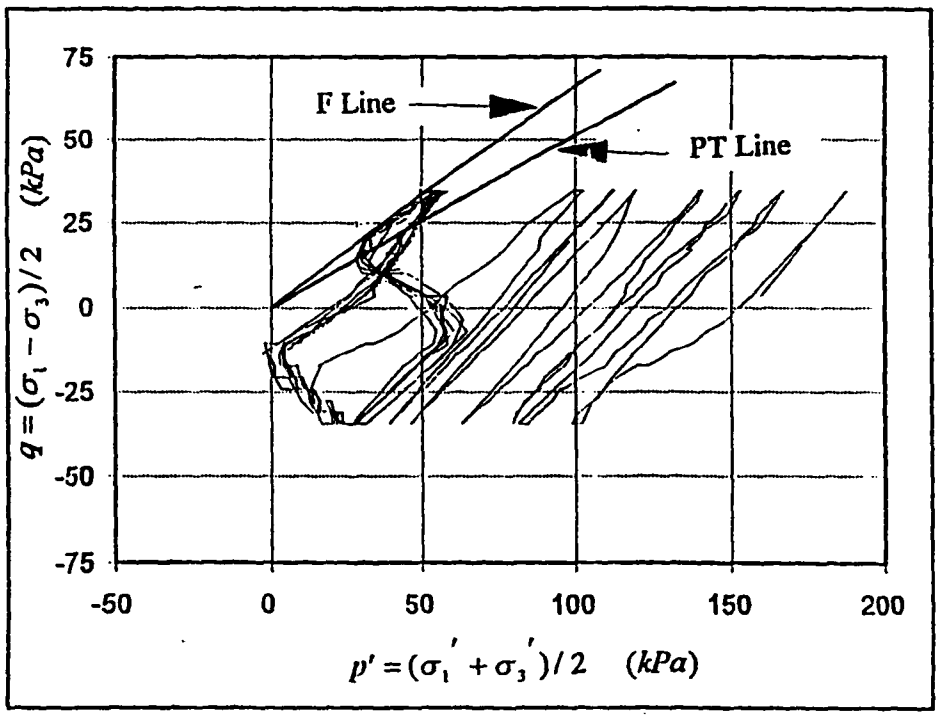

Figure 5.21 Stress Path for σ_3' =138 kPa

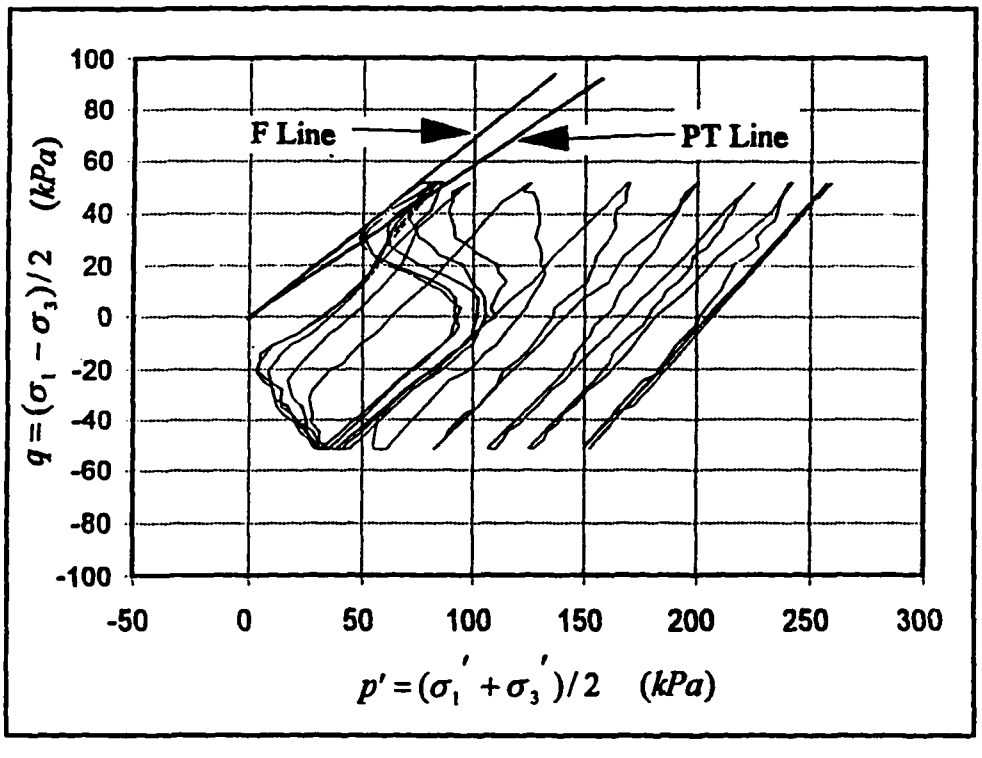

Figure 5.22 Stress Path for σ_3' = 207 kPa

As reported by (Alarcon-Guzman (1983) upon reversal in the direction of shear straining, the number of contact points between neighboring grains is drastically reduced. Accordingly, the sand structure tends to collapse, producing a correspondingly (large) increase in pore-water pressure, as reflected by the effective stress path moving towards the origin of the stress space diagram.

The Phase Transformation Line (PT Line) and Failure (F Line)Line s are drawn in the Figure 5.20 to 5.22 based on Figure 5.1 (Ishihara et al., 1978). The present results indicate the higher pore-water pressure response in the extension part and this is due to the higher development of pore-water pressure in the extension part. Miura and Toki (1982) indicates that a fairly higher pore-water pressure develops in extension test than in the compression test. The another difference is that the size of the sample tested in this study is very much bigger than the sample tested in the other laboratories.

Mohr-Coloumb Diagrams

Figure 5.23a to 5.23c show the Mohr-Coloumb Diagram of the Ottawa Sand from the ***consolidated undrained cyclic test*** for the effective stress. As shown in the figures the effective stress decreases and moves to the left due to the slowly development of pore-water pressure. The friction angle of the Ottawa sand is about 40 degree for the effective stress.

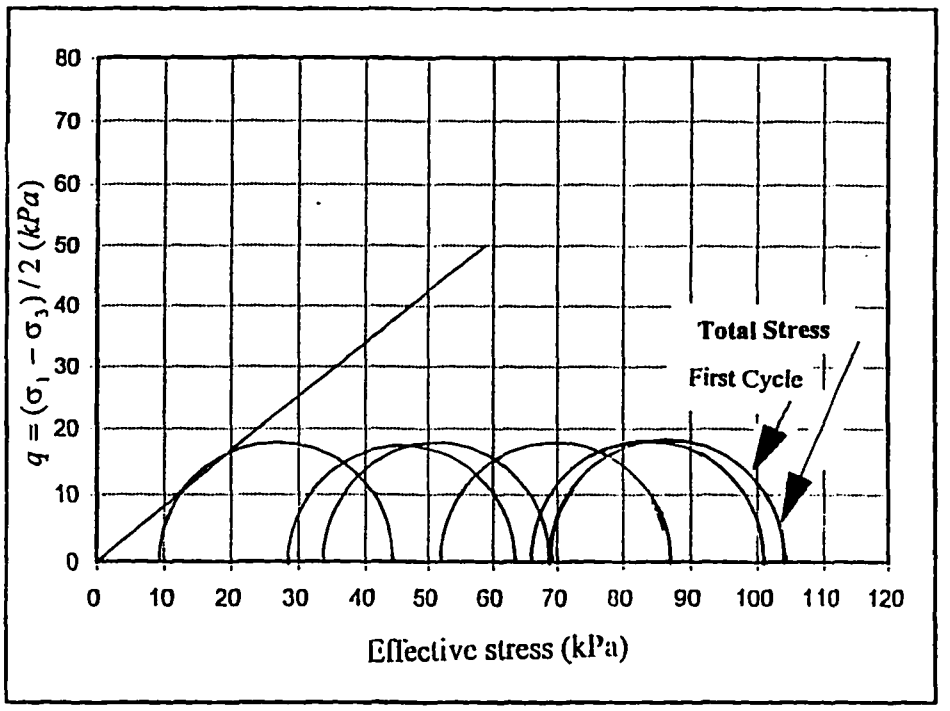

Figure 5.23a Mohr-Coloumb Envelope for the Cyclic Test (σ_3' = 69 kPa)

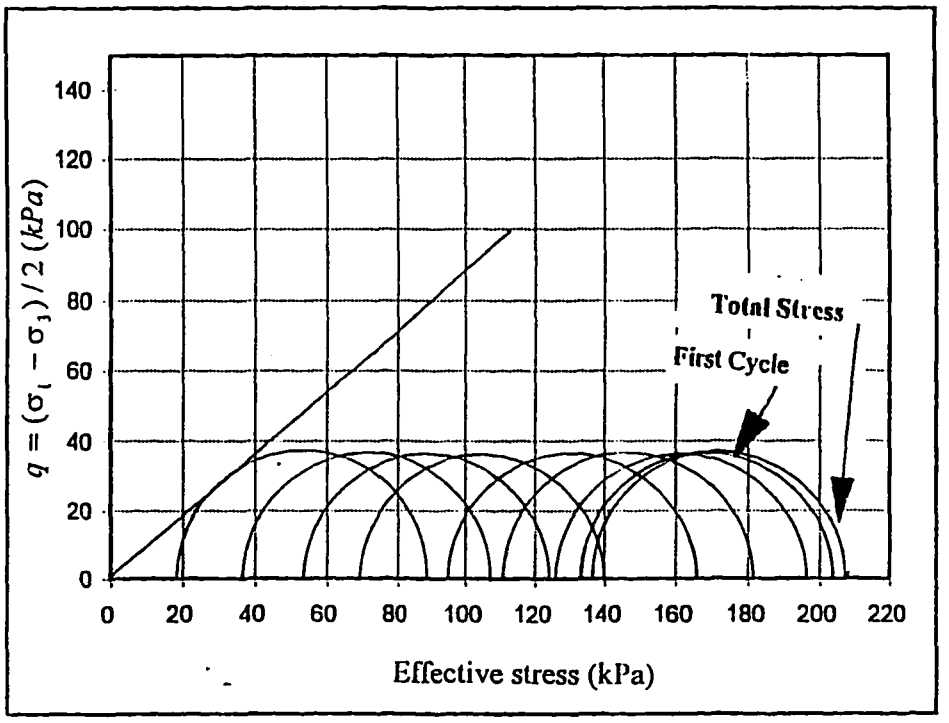

Figure 5.23b Mohr-Coloumb Envelope for the Cyclic Test (σ_3' = 138 kPa)

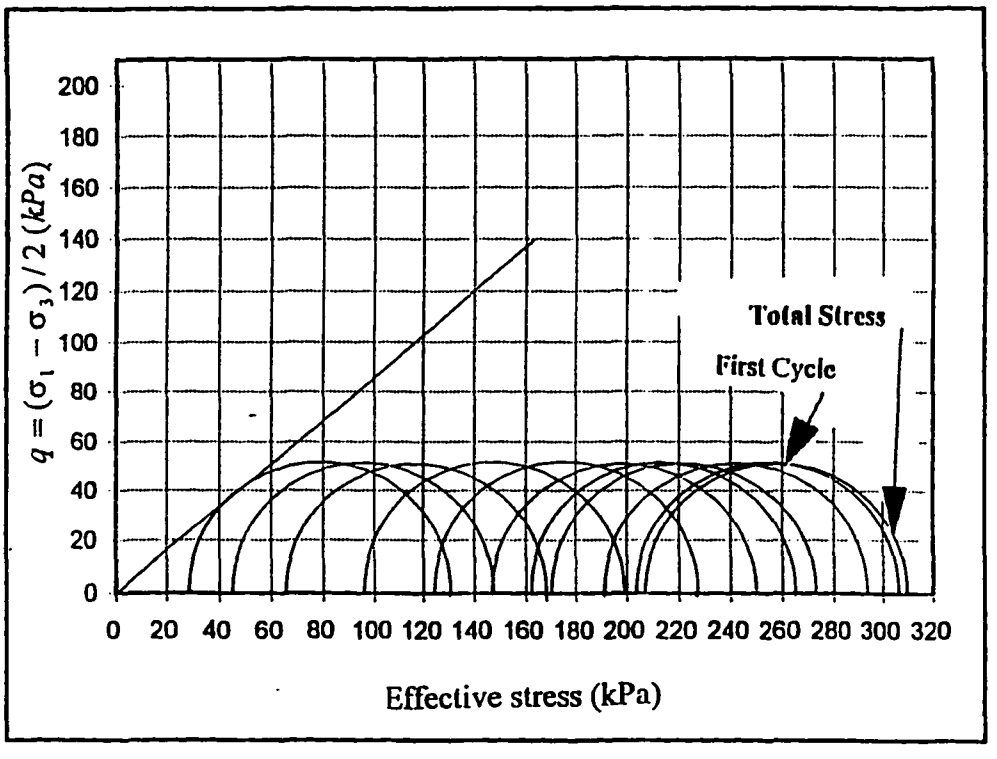

Figure 5.23c Mohr-Coloumb Envelope for the Cyclic Test (σ_3' = 207 kPa)

5.2.3 Post Cyclic Behavior of Saturated Ottawa Sand

Figure 5.24a to 5.24c shows the static undrained loading and unloading results of Ottawa sand after the cyclic test. When the cyclic loading is stopped the pore-water pressure in the sample was equal to the applied confining pressure. At this stage sample was subjected to the static loading . Initially, the sample deformed considerably without mobilizing significant resistance to deformation and without change in the pore-water pressure. Later the sample developed a tendency to dilate, the pore-water pressure decreased, and the resulting increase in effective stress led to the development of an appreciable resistance to deformation.

Vaid and Thomas (1995) noted that in their postliquefaction undrained compression loading, the sand deformed at virtually zero stiffness over a large range of axial strain. With further straining, the stiffness increased with an increase in strain. They also pointed out that this type of stress-strain response, in which the modulus increases with an increase in axial strain is opposite to the usual response of soil in which the modulus moduelus decreases with an increase in strain. They also concluded that this unusual result is due to the dilation of soil during shearing, which will cause the effective stress to increase.

As shown in the Figures 5.24a to 5.24c, the postcyclic stress-strain behavior is always ***dilative*** (strain hardening), the stiffness is small during the initial loading, but with an increase in the strain level stiffness increases.

The postliquefaciton undrained stress-strain curve can be divided into at least three parts as reported in Vaid and Thomas (1995). The first part is a very small region,

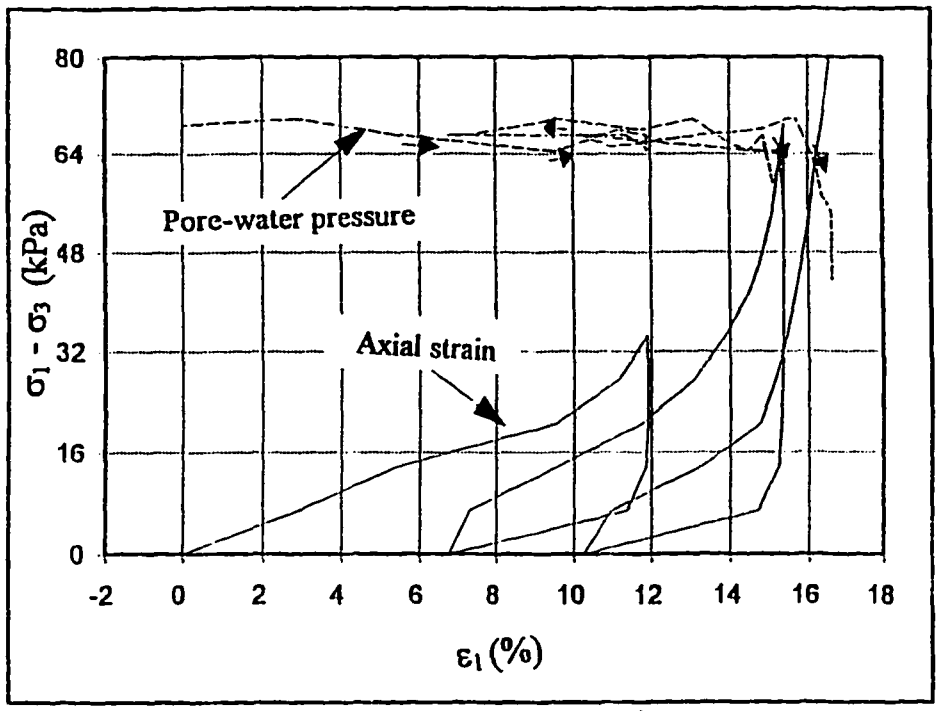

Figure 5.24a Post-Cyclic Behavior (σ_3' = 69 kPa)

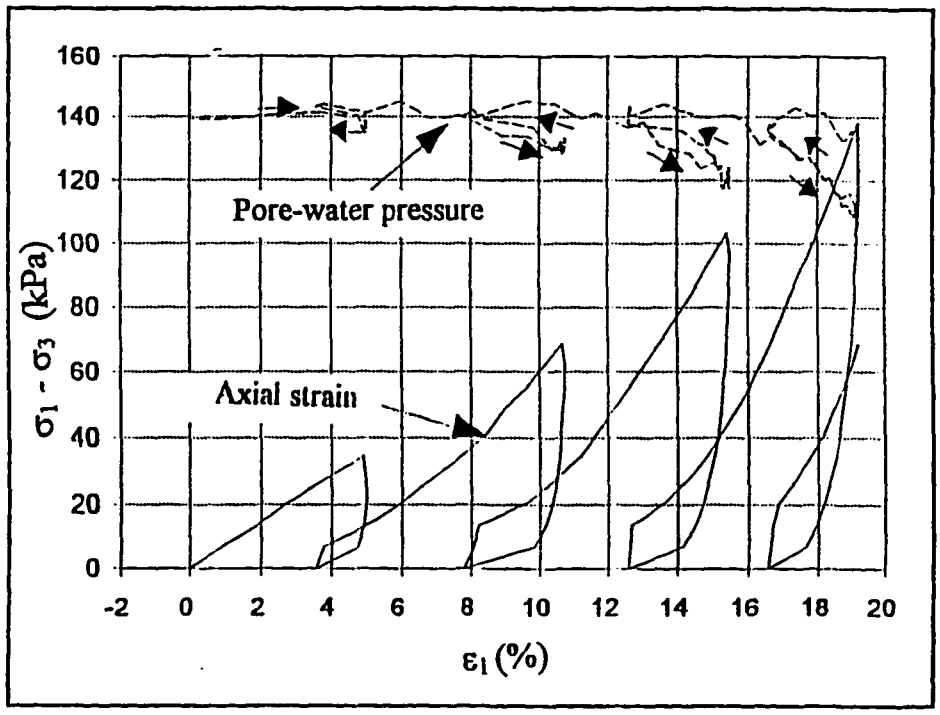

Figure 5.24b Post-Cyclic Behavior (σ_3' = 138kPa)

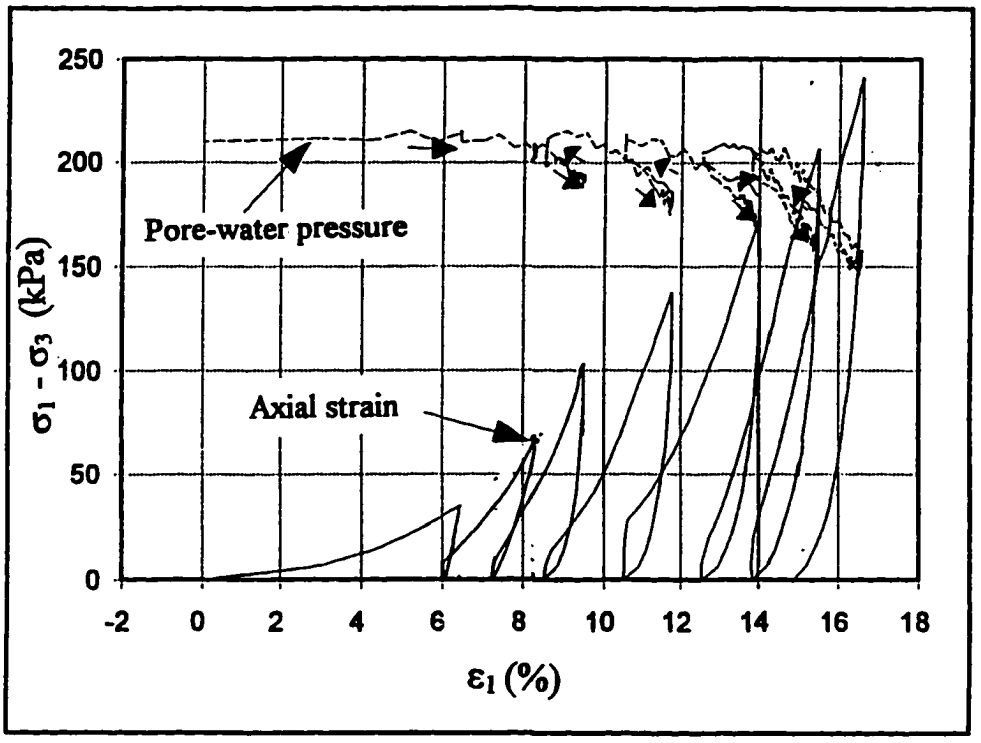

Figure 5.24c Post-Cyclic Behavior (σ_3' = 207kPa)

starting from the end of cyclic loading to the measurable deviatoric stress and the stiffness is very small in this part. The second part is a parabolic type curve representing the continuous increase the stiffness with the axial strain. The third part is a more or less linear curve and representing the constant ***modulus***.

Vaid and Thomas (1995) noted that the undrained stress-strain behavior of sand does not correspond to the situation where the modulus continually degrades with strain as assumed by most researchers during the effective stress analysis of the earthquake problem (Finn et al. 1986; Prevost 1981). They noted that depending on the residual effective stress state, the modulus in the postcyclic loading does decrease initially, but starts increasing once dilation commences.

5.3 Comparison of the Present Results with Others

Present investigaion indicates that the static and cyclic loading results are similar to the previous investiogaion.

Static Loading Test

The present results can be compared with the recent investigation by Vaid and Thomas (1995). As shown in the Figure 2.5 and 2.15 (Chapter 2) , the static triaxial compression behavior of insotropically consolidated sand up to confining pressure of 800 kPa is ***dilative behavior*** (strain hardening). For the consolidation stress of 1200 kPa, the sample shows slightly contractive response. Present investigaion indicates that the static loading behavior in compression is ***dilative behavior*** (see Figure 5.8 to 5.11).

Accoring to the Vaid and Thomas (1995), the specimen liquefied on the ***unloading part*** and they noted this behavior as ***liquefaction*** induced by a static load and unload cycle. Present investigation also shows a similar result and the sample liquefied on the unloading part (Figure 5.8 to 5.10).

According to Vaid and Thomas (1995), a static loading/unloading cycle did not always result in the state $\sigma_3' = 0$, upon unloading, for dense sand consolidated to 400 kPa and higher in the compression mode of loading, and was apparently due to an insufficient level of strain prior to unloading. They noted that straining on static loading must surpass a minimum level beyond the PT (phase transformation state) before a state of zero effective stress state is realized on unloading.

In the $p' - q$ ***diagram***, the present investigaion shows the ***elbow*** shape, the

effective stress path bends sharply upwards and then turn to the right (Figure 5.12a). This behavior is similar to the sample B of Figure 5.2 and S-3 of Figure 5.4c(Vaid and Chern, 1983). The effective stress path slightly increased to PT point (Figure 5.12).
The point of phase transformation is similar to the one given in Figure 5.2 (Vaid and Chern, 1983).

Cyclic Loading Test

Present investigation shows that during the cyclic l tests, the ***initial liquefaciton*** (excess pore-water pressure equal to the effective confining pressure) reached at about 5 to 9 cycles. Figure 5.25 and 5.26 show the cyclic stress ratio vs number of cycles to liquefaction by co-operative tests in U. S. A. (Silver et al. 1976) and Japan (Mura et al 1994). According to Ishihara (1993), small size of specimens show slightly different (greater) resistance to cyclic strength than the larger samples. The sample 10.2x 10.2x10.2 cm (4 x 4 x 4 in) is larger than the samples tested in the figure 5.25 and 5.26, so present result is slightly different from their results. But as shwon in the Figure 5.26, the sample liquefied in 5 to 10 cycles for the stress rastio (SR) of 0.25 and therefore the present test result can be considered compare well with the result of coperative test program of Japan (1994). **The stress ratio (SR)** (the ratio of deviatoric stress to effective confining pressure) of the present investigation is 0.25 for all the tests. The mean grain size (D_{50}) of the Ottawa sand of the present investigation is 0.4mm. Seed and Peacock (1971) reported :hat the stress ratio (SR) required to cause liquefaction in 10 cycles for the sand with (D_{50}) = 0.4mm is 0.26 (Figure 2.12, Chapter 2). So present results are similar to the results investigated by the Seed and Peacock (1971).

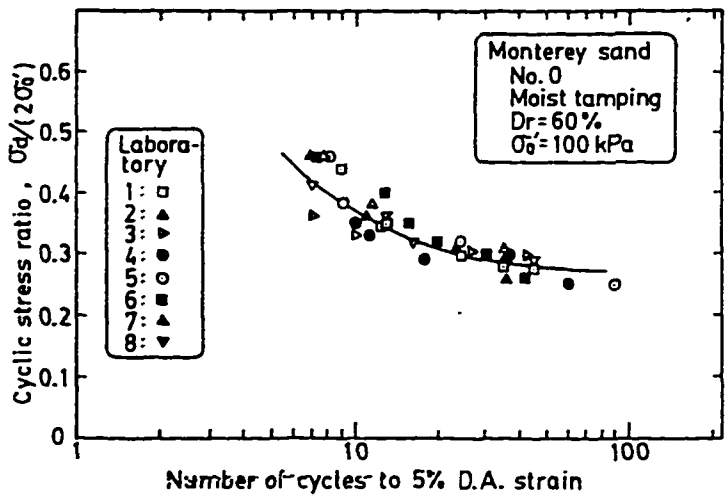

Figure 5.25 Results of the Co-operative Tests in the U. S. A on the Cyclic Strength of Sand (Silver et al., 1976)

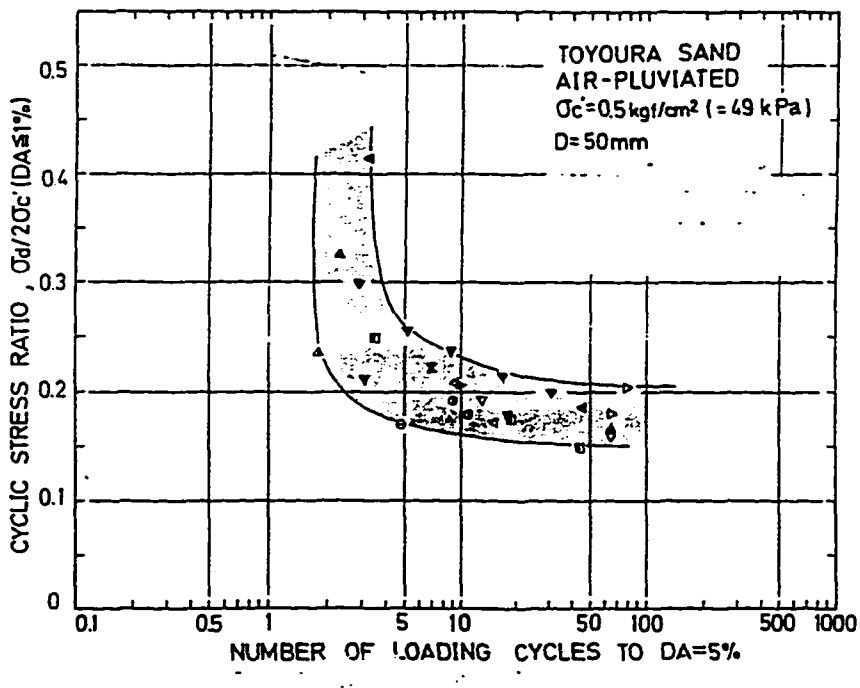

Figure 5.26 Results of the Co-operative Tests in Japan on Cyclic Strength of Sand (Mura et al. 1994)

The stress strain curves (Figure 5.16 to 5.18) of the present investigation are similar to the results reported by Seed and Lee (1966) (Figure 5.19). Figure 5.27 presents the test result from Seed and Lee (1966).

Postcyclic Behavior

There are few publications on the postcyclic behavior of sand. Present results indicate that the postcyclic stress-strain behavior is ***dilative*** (Figure 5.24a to 5.24c) and is similar to the results of Vaid and Thomas (1995) (Figure 2.16 to 2.18).

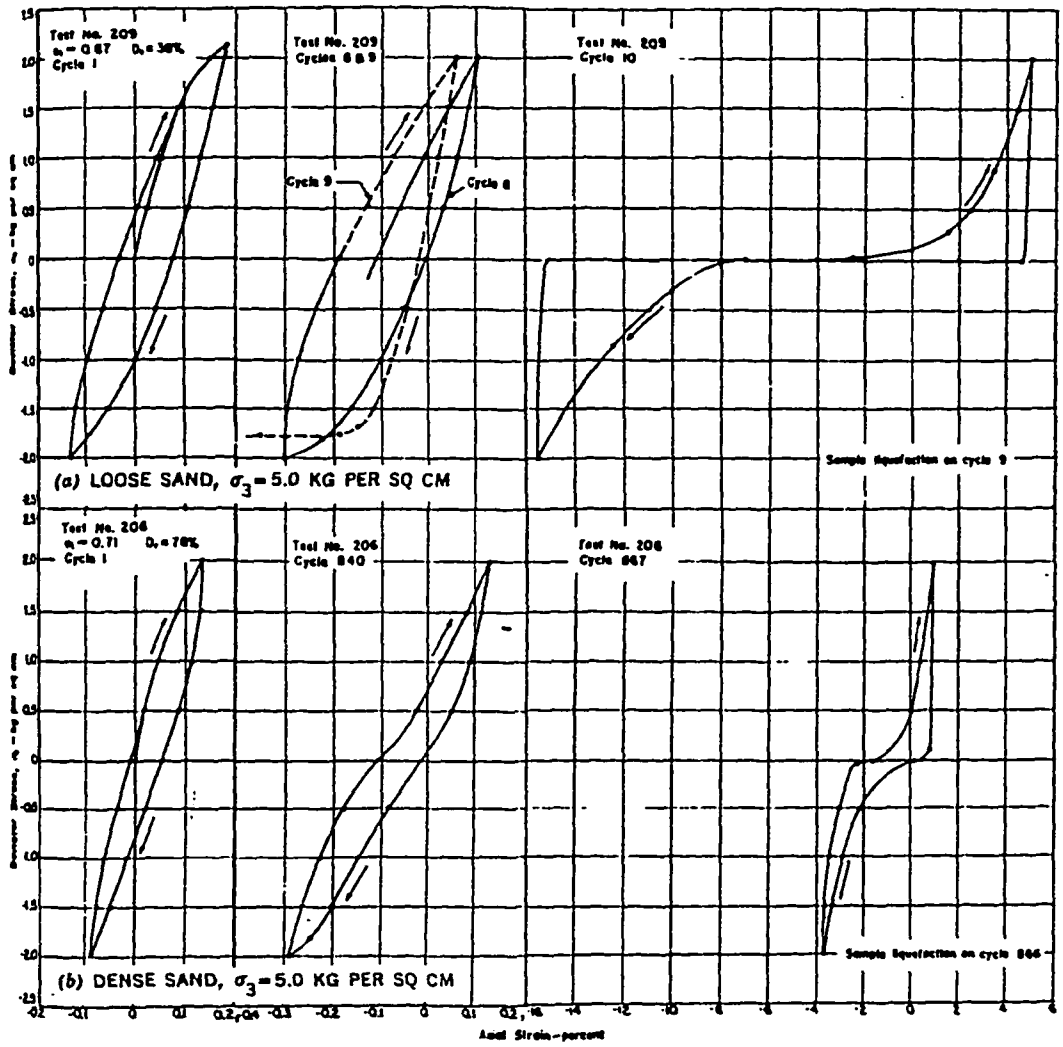

Figure 5.27 Hysteresis Curves For Cyclic Loading Test on Sacramento River Sand (Seed and Lee, 1966)

5.4 Analysis of the Cyclic Behavior and Liquefaction Potential

Based on the test results, the cyclic behavior is analysed and the liquefaction potential of the Ottawa sand is presented in this section.

Stress-Strain Behavior

The term liquefaction and liquefaction failure encompasses all phenomena involving excessive deformation of saturated cohesionless soils (National Research Council, 1985) . As shown in Figures 5.16 to 5.18, during the first few cycles of loading, the samples had somewhat similar stress-strain relationships. The sample with the smaller confining pressure developing slightly higher deformation. After four to nine stress cycles, the samples began to show large deformations, and liquefacion developed during the five to ten cycles.

Figures 5.16 to 5.18 also indicate that the sample was able to mobilize resistance to the applied cyclic deviatoric stress after undergoing the large strains (4 to 8%). The figures also show that the sand had virtually no resistance to deformtion over a strain range of 2 to 6%.

The present test indicates that higher the confining pressure, the greater was the number of cycles required to introduce liquefaction.

p – q' Diagram

The effective stress paths during cyclic loading for Ottawa sand (relative density = 60%) with different confining pressure (69, 138 and 207 kPa) are shown in Figures 5.23

to 5.25. Irrespective of effective confining pressure, the effective stress paths moved toward the failure envelope progressively with cycles of loading.

However, at low confining pressure (69 kPa) (Figure 5.23), the stress path suddenly reached the failure envelope while for confining pressure 138 kPa, the stress path moved progressively toward the failure envelope. For confining pressure of 207 kPa, the development of pore-water pressure and axial strain are at a slower rate than that for lower confining pressure (69 and 138 kPa).

Shear Modulus (G) vs Number of Cycles

Figure 5.28 presents the variation of shear modulus vs number of cycles of Ottawa sand for different confining pressures (69, 138 and 207 kPa). The decay of the shear modulus (G) is noted for all the tests. As expected, the shear modulus is higher at the higher confining pressure. The higher the confining pressure of the sample, the slower the drop in the shear modulus. Finally, the modulus approximately reaches the same low value in all cases after large number of cycles. This behavior is similar to the previous investigation by Figueroa et al. (1994).

Here, G can be defined as follow:

$$G = \frac{E}{2(1+\mu)} \qquad (3)$$

$$E = \frac{(\sigma_1 - \sigma_3)_{max}}{\varepsilon_1} \qquad (4)$$

where μ = Poisson ratio, E = Secant Modulus and E can be calculated based on the data from Figure 5.16 to 5.18.

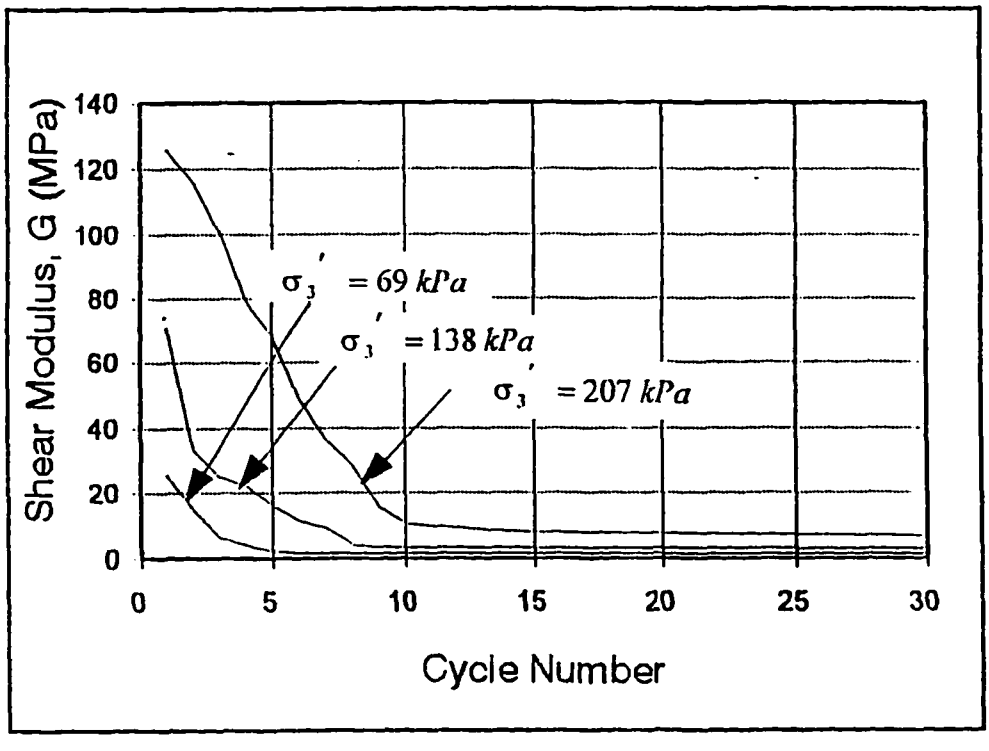

Figure 5.28 Variation of Shear Modulus vs Number of Cycles

Liquefaction Potential

Various procedures for predicting the liquefaction potentialof saturated soil deposits have been developed in the past.

The methods presently being used for evaluating the liquefaction potential of a soil deposit may be classified into the following three categories (Valera and Donovan, 1977):

(1) Method where both the cyclic shear stresses induced within a soil deposit and the significant number of stress cycles and their distribution with time are computed using simplified procedures;

(2) methods where the cyclic stresses induced within a soil deposit are computed by means of ground response analysis; and

(3) empirical methods based on the comparison of sites where liquefaciton has or has not occurred during past earthquakes.

The methods one and two are based on laboratory test data on the ***cyclic stresses*** required to develop liquefaction or significant cyclic strains on representative samples of the in-situ soils. The **ratio of applied cyclic shear stress to the effective overburden pressure versus the number of stress cycles required to develop liquefaction** or significant cyclic strains are used in the analysis. A comparison of the cyclic stresses induced in the field with the cyclic stresses required to develop liquefaction or significant cyclic strains in the laboratory are made, and then a factor of safety against the liquefaction is evaluated.

Method three usually involves the determination of some in-situ characteristics such as a mean when comparing the liquefaction potential of a proposed site with that of other sites where liquefaciton is known to have occurred in previous earthquake.

These mehtods hve been primarily developed by Seed and can be found in the paper of Seed and Idriss (1967, 1971) and they proposed a general method for evaluation of liquefaction potential involving the following steps:

1. Establish soil condition and design earthquake, determine the time history of shear stress induced by earthquake ground motions at different depths within the deposit.
2. By appropriate weighting of the **stress levels** involved in the various stress cycles through the earthquake, convert the stress history into an **equivalent uniform stress level** as a function of depth, as shown in Figure 5.29.
3. Based on the available field data or **laboratory soil tests** on the representative samples, conduct under various confining pressures, determine the **cyclic shear stresses** that would have to develop at various depths to cause liquefaction in the same number of stress cycles as that determined in step 2.
4. Then compare the **shear stresses** induced by the earthquake with those required to cause liquefaction.

As described in the paper (Seed and Idriss, 1971), the **ground response analysis** is performed to evaluate the stress history at various depths to determine how pore-water pressure dissipates during an earthquake and after earthquake motion. The **ground response analysis** consists of the following steps.

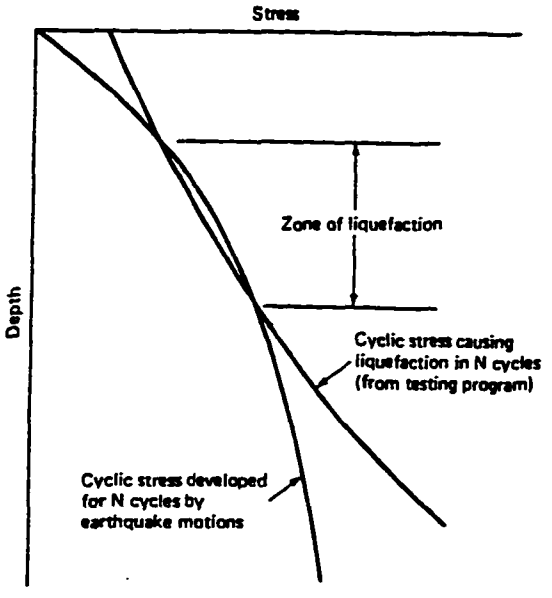

Figure 5.29 Method of Evaluating Liquefaction Potential (Seed and Idriss, 1967, 1971)

1. Computation of maximaum shear stress in deposit

At any point in a soil deposit, **shear stresses** due to upward propagation of **shear wave** can be calculated by following equation.

$$(\tau_{max})_r = \frac{\gamma h}{g} a_{max} \qquad (5)$$

where $(\tau_{max})_r$ = maximum shear stress,

a_{max} = maximum ground surface acceleration,

γ = total unit weight of the soil, and

h = depth.

The actual shear stress $(\tau_{max})_d$ will be less than the $(\tau_{max})_r$ and can be expressed by the following equation.

$$(\tau_{max})_d = r_d (\tau_{max})_r \qquad (6)$$

where r_d = a stress reduction factor less than 1.

The maximum shear stresses developed during earthquake can be calculated form the equation,

$$\tau_{max} = \frac{r h}{g} a_{max} r_d \qquad (7)$$

and the value of r_d can be taken from the Figure 5.30.

2. Determination of Equivalent Number of the Significant Stress Cycles, N_c

In this step the irregular form of actual time history of shear stress is changed to the equivalent shear stress by appropriately weighting individual stress cycles, based on

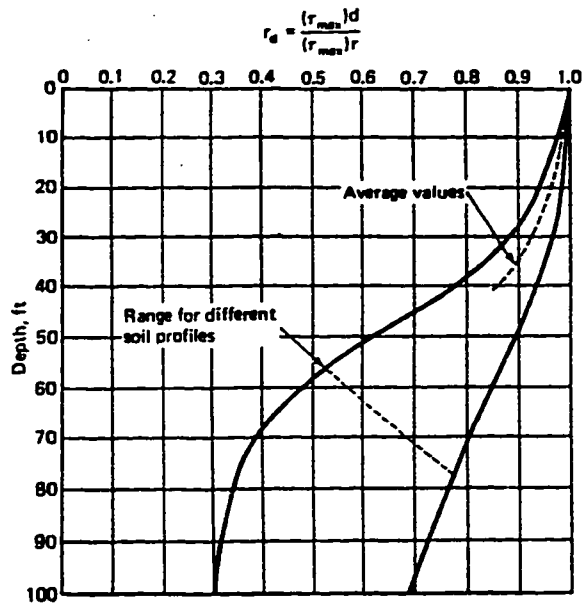

Figure 5.30 Range of Value of Rd for the Different Soil Profiles in Liquefaction Analysis (Seed and Idriss, 1971)

laboratory data. The average equivalent uniform shear stress is about 65 percent of the maximun shear stress and therefore,

$$\tau_{av} = 0.65 \frac{r\,h}{g} a_{max}\, r_d \qquad (8)$$

The equivalent uniform cycle was first presented by Seed and Idriss (1971) and have been updated by Lee and Chan (1972) and Seed et al. (1975). The number of cycles corresponding to an equivalemt uniform stress (usually 0.65 τ_{max}) has been plotted as a function of the earthquake magnitude (Seed et al., 1975).

3. Determination of Stress Causing Liquefaction

A cyclic triaxial or simple shear test result is used to determine stress that caused liquefaction within a given number of cycles, depending on the magnitude of the earthquake. The results of a number of triaxial tests with different grain sizes, represented by the mean grain size D_{50}, and at a relative density of 50 percent are summarized in Figure 2.12 (Seed and Peacock, 1971). In this figure, the stress ratio (the ratio of cyclic deviatoric stress to initial ambient pressure under which the sample was consolidated. The stresses required to cause liquefaction for sands at othe relative densities may be estimated from the fact that the shear stress required to cause initial liquefaction is approximately proportional to the relative density.

The value of the stress ratio $(\frac{\tau}{\sigma_0})$ causing liquefaction under field condition, estimated from the test value have shown that the field vaue of $(\frac{\tau}{\sigma_0})$ is less than the test

value of $(\frac{\sigma_d}{2\sigma_o})$ and the field and lab stress ratio can be correlated as the following equation.

$$(\frac{\tau}{\sigma_0}) = (\frac{\sigma_d}{2\sigma_0}) C_r \qquad (9)$$

The C_r is a correlation factor to be applied to laboratory triaxial test data to obtain the stress conditions causing liquefacton in the field. Thus the test data given in Figure 2.12 together with the values of C_r , give the stress conditions likely to cause liquefacton of different soil in the field. The **stress ratio** causing liquefaction in the field for a given soil at a relative density Dr can be estimated from the following equation.

$$\frac{\tau}{\sigma_0'} = \frac{\sigma_d}{2\sigma_0} C_r \frac{D_r}{50} \qquad (10)$$

Table 5.2 shows the values of C_r for the preliminay analysis.

Table 5.1 Value of C_r for the preliminay analysis

Relative Density, Dr	Correction Factor, C_r
0 to 50%	0.57
60	0.60
80	0.68

Analysis of Liquefaction Potential Based on the Present Results

Based on the Eq. 10 and Figure 2.12, the stress ratio causing liquefaction in 10 cycles for the Sand with Dr = 60% and mean grain size D_{50} is calculated as

$$(\frac{\tau}{\sigma_0})_r = 0.26 \times 0.6 \times 60/50$$

$$= 0.1872$$

The present tests for Ottawa sand (Dr = 60%, D_{50} = 0.4mm) for the different confining pressures (69, 138, 207 kPa) indicate that the stress ratio of 0.25 can cause liquefaction in 5 to 10 cycles. The test data show that eventhough the stress ratio is same the number of cycles for liquefaction is increased for the higher confining pressure.

According to the Figure 2.12 for the sand with D_{50} = 0.4mm, the stress ratio to cause liquefaction in 10 cycles is 0.26. So for the stress ratio of 0.25, the number of cycles to liquefaction could be slightly smaller than 10 cycles. The present test results indicate that liquefaction happens in 5 to 10 cycles with the stress ratio of 0.25. So the present test result is similar to the **liquefaction potential** proposed by Seed and Idriss (1971).

Zone of Liquefaction

Based on the present results and Seed and Idriss's method (1971), the zone of liquefaction in the field can be calculated as follows:

$$(\frac{\tau}{\sigma_0})_r = (\frac{\sigma_d}{2\sigma_0}) C_r$$

$$= 0.25 \times 0.6$$

$$= 0.15$$

Then $\tau \quad = 0.15 \times \sigma_0'$

For the different depths the shear stress can be calculated as follows.

Table 5.2 Shear Stress from the Present Investigation

Depth (m)	Eff. Overburden Pressure, kPa	Shear Stress, kPa
10	200	30
20	400	60
30	600	90
40	800	120
50	1000	150

The stress causing liquefaction can be calculted based on the Equation 3. Then the stress causing liquefaction and the shear stress shown in Table 5.2 can be plotted as shown in Figure 5.29. As shown in the Figure 5.28, the **zone of liquefaction** can be found if the the cyclic stress causing liquefaction is higher than the shear stress form Table 5.2.

Liquefaction Potential Based on Previous Performance During Earthquake

In this method the comparison of field conditions where liquefaction did or did not occur during previous earthquakes with the **actual site condition.**

The most recent correlation between field liquefaction behavior of sands for level ground conditions and corrected penetration resistance (SPT) based on the field data and large-scale laboratory test data are shown in the Figure 2.4b, Chapter 2. Values of the cyclic stress ratio known to be associated with liquefaction or no liquefaction in the field are plotted in the figure as a function of the corrected average peneration resistance of the sand deposit involved.

Chapter 6

SUMMARY AND CONCLUSIONS

6.1 Summary

The main purpose of this thesis is to modified the existing data acquisition systems of the multiaxial or cubical device and to study the behavior of Ottawa Sand. The main focus is on the behavior of saturated sand under cyclic loading. The high speed analog to digital data acquisition board , DAS-1600 to gether with EXP-16 is used to measure the signal from 22 channels, including 18 LVDT, 3 pressure transducers and 1 pore-water pressure transducer. The pressure system in the X-, Y- and Z-directions, is controlled by the open and closed solenoid valve for each direction, which is controlled by the PDISO-8, relay board installed in the computer, PC-486. From the test results, it can be concluded that the DAS-1600 board can obtain the data from the cyclic test, which was run currently at cyclic frequency of 0.1 Hz. The open and closed solenoid valves can control the pressure with good accureacy.

Chapter two presents the previous liquefaction studies. This chapter introduces the liquefaction, cyclic mobility, and factors controling the liquefaction potential and presents the example of various test results performed by the previous investigators.

The detailed features of the DAS-1600 and PDISO-8 boards are presented in this thesis. The channels used in this study is 22 channels, so additional multiplexer is required to obtain the data becauset he DAS-1600 board can handle the 16 channels and . The detailed description of multiplexer EXP-16 and detailed wire connection are presented in chapter three. The base address,and gain setting are presented.

The detalied steps of sample preparation, sample insertion and testing procedure, which is important in the cubical device, are presented in Chapter four. Additional operation manual is prepared for the future use . The water can easily leak from the sample across the latex rubber membrane, so the sample preparation is one of the important parts of the testing program.

A series of the laboratory tests was performed to understand the behavior of the Ottawa sand, especially the cyclic behavior. The tests include, consolidated undrained loading and unloading tests, consolidated undraind cyclic tests and postcyclic tests at the various confining pressure.

The laboratory tests indicate that the Ottawa Sand is liquified around 5 to 10 cycles of loading, with frequency of 0.1 Hz. The liquefaction is also can seen in the static test (consolidated undrained test). The postcyclic tests indicate that the postcyclic feature is strain hardening. It is found that the test data are comparable with the results of previous investigators.

The data obtaind in this study will be used to construct the DSC (disturbed state concept) model, in future. So in future, the DSC model can predict the liquefaction potential.

6.2 Conclusions

Based on the results, it can be conclude that DAS-1600 board can obtain the reasonable data from the multichannels. The selonoid valves can control the pressure with reasonable accureacy.

The laboratory tests indicate that the Ottawa Sand is liquified on the 5 to 10 cycles of cyclic loading, with frequency of 0.1 Hz. The liquefaction is also can seen in the static test (consolidated undrained test). The postcyclic tests indicate that the postcyclic feature is strain hardening. It is found that the test data are comparable with the results of previous investigators.

The data obtaind in this study will be used to construct the DSC (disturbed state concept) model, in future. So in future, the DSC model can predict the liquefaction potential.

6.3 Recommendation

1. Some improvements could be made to the computer, data acquisition system and pressure control system. The DAS-1600 board required large memory area in the computer. Therefore to read the data from the multi-channels the memory should be extended.

2. The additional pressure transducers should be installed for the pore-water pressure board. So the back pressure can be controlled and checked by the computer.

3. The additional pressure transducer should be installed for the main pressure regulator. So the computer can controlled the main pressure, before entering into the pressure control system, which is controlled by the open and closed solenoid valves.

REFERENCES

Alacon-Guzman, A., Leonards, G.A. and Chameau, J.L. (1988). " Undrained Monotonic and Cyclic Strength of Sand," *J. of the Geotech. Engrg.*, ASCE, Vol.114, N0.10, pp. 1089-1109.

Ambraseys, N. N., and Sarma, S.(1969). "Liquefaction of Soils Induced by Earthquakes," *Bulle., Seis. Soc. of America*, Vol. 59, No.2, pp.651-664.

Annaki, M. (1975)., "Liquefacition of Sand in Triaxial Tests using Uniform and Irregular Cyclic loading," Thesis Submitted to the University of California, at Los Angeles, Calif., in partial of the requirements for the degree of Doctor of Philosophy.

Annaki, M., and Lee, K. L.(1977)., "Equivalent Uniform Cycle Concept for Soil Dynamic," *J. of the Geotech. Engrg.*, ASCE, Vol.103. No.GT6, pp.549-564.

Casagrande, A. (1936)." Characteristics of Cohesionless Soils Affecting the Stability of Earth Fill," *J. of Boston Soc. of Civil Engrg.*.

Casagrande, A.(1975). "Liquefaction and Cyclic Deformation of Sands-A Critical Review," presented at the , *Fifth Pan american Conference on Soil Mechanics and Foundation Engineering*, held at Buenos Aires, Argentina.

Casagrande, A.(1975)"The Role of the Calculated Risk in Earthwork in Foundation Engineering," *J. of Soil Mech. and Found. Engrg.* ASCE, Vol. 91. No. SM.4, pp.1-40.

Castro, G.(1969). "Liquefaciton of Sands," *Havard Soil Mech. Ser. No.81*, Havard University, Cambridg, Mass.

Castro, G.(1975)." Liquefaction and Cyclic Mobility of Saturated Sand," *J. of Geotech. Engrg.*, ASCE, Vol.101. No.GT6, pp.551-569.

Castro, G. Et. al.,(1982)." Liquefaction Induced by Cyclic Loaing," Geotechnical Engineers, Inc., Report submitted to National Science Foundation, Mar.

Castro, G.and Poulos, S. J.(1977)."Factors Affecting Liquefaction and Cyclic Mobility," *J. of Geotech. Engrg.*, ASCE, Vol.103. No.GT6, 1977, pp.501-506.

Dealba, P., Seed, H. B., and Chan, C. K.(1976)."Sand Liquefaction in Large-Scale Simple Shear Tests," *J. of Geotech. Engrg.*, ASCE, Vol.102., No.GT9, pp.909-927.

Sture, S and Desai, C. S. (1979). "Fluid Cushion Truly Triaxial Test or Multiaxial Testing Device," *Geotech. Testing J.*, Vol. 2. No.1, pp.20-33.

Dorby, R. et al. (1982). "Prediction of Pore Water Pressure Buildup and Liquefaction of Sands during earthquakes by the cyclci strain method," National Bureau of Standards, Building Science Series 138, U. S. Dept. of Commerce.

Dixon, S. J., and Burke, J. W.(1973). "Liquefaction Case History," *J. of Soil Mech. and Found. Divisi.*, ASCE, Vol.99. No.SM11, Nov., 1973, pp.921-937.

Finn, W. D. L., Brandby, P. L., and Pickering, D. J.(1970). "Effect of Strain History on Liquefaction of Sand," *J. of Soil Mech. and Found. Divi.*, ASCE, Vol.96. No.SM6, , June., pp.1917-1934.

Finn, W. D. L., Lee, K. W., and Martin, G. R.(1977). "An Effectivd Stress Model for Liquefaction," *J. of the Geotech. Engrg.*, ASCE, Vol.103, No.GT6, pp.517-533.

Finn, W. D. L., Bransdby, P. L., and Pickering, D. J.(1971). "Sand Liquefaction in Triaxial and Simple Shear Test," *Journal of the Soil Mech. and Found. Divi.*, ASCE, Vol.97, No.SM4, , pp.639-659.

Figueroa, J. L., and Sadda, A. S.(1994)."Evaluation of Soil Liquefaction by Energy Principle," *J. of Geotech. Engrg.*, ASCE, Vol.120, No.9, pp.1554-1569.

Geuze, E. (1948)." Critical Density of Some Dutch Sand," *Proced. of Second Intern. Conf. on Soil Mech. and Found. Engrg.*, Vol. III, Rotterdam, The Netherlands, pp.125-130.

Gyi, M. M. and C. S. Desai (1996). "User Manual of the Servo-controlled Cubical Device with Automatic Data Acquisition System", Dept. of Civil Engrg. and Engrg. Mech., U of A.

Ho, R. W. and Wong, P. S.(1989), "The Effect of Wave-form and frequency n cyclic triaxial tests," *Engineering Geol. and Geotech. Engrg.*, Walter, Eds., Balkema, Rotterdam, pp.349-355.

Ishihara, K. and Yasuda (1972). "Sand Liquefaction and Due to Irregular Excitation," *Soil and Found.*, Vol. 12, No.4, pp. 65-77.

Ishihara, K. (1993). " Liquefaction and flow failure during Earthquake ," *Geotechnique*, Vol. 43, No.3, pp. 351-415.

Keithley MetraByte Co. (1994). "User Manual ".

Keithley MetraByte Co. (1994). "User Manual, Function Call Driver ".

Kishida, H.(1965). "Damage of Reinforced Concrete Buildings in Niigata City with Special Reference to Foundation Engineering," *Soil and Found.*, Vol. 6, No.1, pp.123-143.

Koppejan, A. W., and Wamelen, B. M. and Weingerg, L. J.(1948)."Coastal Flow Slides in the Dutch Provience of Seeland," *Proced. of Second Intern. Conf. on Soil Mech. and Found. Engrg.*, Vol. V, Rotterdam, The Netherlands, pp. 89-96.

Ladd, R. S.(1974)."Specimen Prepation and Liquefaction of Sand, "Technical Note, *J. of the Geotech. Engrg.*, ASCE, Vol.100, No.GT10, pp.1180-1184.

Ladd, R. S.(1977)"Specimen Prepation and Cyclic Stability of Sand, "*J. of Geotech. Engrg. Division*, ASCE, Vol.103, No.GT6, pp.535-547.

Lee, K. L., (1976). "Fundamental Considerations for Cyclic Triaxial Tests on Saturated Sands, " *Proced. Int. Con. on Behavior of Off-Shore Str.*, Trondheim, Norway.

Lee, K. L., and Albasia, A. (1974). "Earthquake Induced Settlements in Saturated Sands,"*J. of Geotech. Engrg.*, ASCE, Vol.100, No.GT4, pp. 387-406.

Lee, K. L., and Fitton, J. A.(1969). "Factors Affecting the Cyclic Loading Strength of Soils,"Vibration Effects of Earthq. on Soil and Found., ASTM, Spec. Pub. 450.

Lee, K. L., and Focht, J. A.(1975). "Liquefaction Potential of Ekofisk Tank in North Sea,"*J. of Geotech. Engrg.*, ASCE, Vol.100, No.GT1, pp.1-18.

Lee, K. L., and Seed, H. B.(1967). "Cyclic Stress Conditions Causing Liquefaction of Sand,"*J. of Soil Mech. and Found. Divi.*, ASCE, Vol.93, No.SM1,pp. 47-70.

Martin, G., R., Finn, W. D. L., and Seed, H. B.(1975). "Fundamentals of Liquefaction under Cyclic Loading," *J. of Geotech. Engrg.*, ASCE, Vol.101, No.GT5, pp. 423-483.

Miura, S. et al., (1994). "Cyclic Undrained Triaxial Behavior of Sand by a Cooperative Test Program in Japan," *Dynamic Geotechnical Testing II*, ASTM STP 1213, Ronald J. Ebelhar, Vincent P. Drnevich, and Bruce L. Kutter, Eds., American Society for Testing and Materials, Philadepha, pp.246-260.

Miura, S. and Toki, S. (1982). " A Sample Preparation Method and Its Effect on Static and Cyclic Deformation Strength Properties of Sand", *Soil and Found.*, Vol.22, No.1, 1982, pp.61-77.

Mulilis et. Al. (1977). " Effect of Sample Preparation on Sand Liquefaction", *J. of Geotech. Engrg. Divi.*, ASCE, Vol.103, No.GT1, pp. 91-108.

Mohamad, R. and Dobry, R. (1986). " Undrained Monotonic and Cyclic Triaxial Strength of Sand," *J. of Geotech. Engrg. Divi.*, ASCE, Vol. 112, No. GT 10, pp. 941-958.

National Research Council (NRC). (1985). " Liquefaction of Soils during Earthquake," *Rep. No.CETS-EE-001*, Nat. Acad. Press, Washington, D.C.

Peacock, W. H., and Seed, H. B.(1968). "Sand Liquefaction Under Cyclic Loading Simple Shear Condition," *J. of Soil Mech. and Found. Engrg.*, ASCE, Vol.94, No.SM3, pp. 689-708.

Poulos, S. J.(1971). "Stress Strain Curves for Soil," Geotechnical Engineers Inc., Winchester, Mass.

Prakash, S. (1980). " Soil Dynamic," McGraw- Hill Book Company.

Rahman, M. S., Seed, H. B., and Booker, J. R.(1977). "Pore Pressure Development Under Offshore Gravity Structure," *J. of Geotech. Engrg.*, ASCE, Vol.103, No.GT2, pp. 1419-1436.

Rocker, K., Jr.(1968). "The Liquefaction Behavior of Sands Subjected to Cyclic Loading," *Soils Publication*, No. 221, MIT, Cambridge, Mass,.

Seed, H. B. and Idriss, I. M.(1967). "Analysis of Soil Liquefaction: Niigata Earthquake," *J of Soil Mech. and Found. Engrg.*, ASCE, Vol.93, No.SM3, pp. 83-108.

Seed, H. B. and Idriss, I. M.(1971). "Simplified Procedure for Evaluating Soil Liquefaction Potential," *J. of Soil Mech. and Found. Engrg.*, ASCE, Vol.97, No.SM9, pp. 83-108.

Seed, H. B. (1979). "Soil Liquefaction and Cyclic Mobility Evaluation for Level Ground During Earthquake,"*J. of Soil Mech. and Found. Engrg.*, ASCE, Vol.105, pp. 201-255.

Seed, H. B. and Lee, K.L.(1966). "Liquefaction of Saturated Sands During Cyclic Loading," *J. of the Soil Mech. and Found. Engrg.*, ASCE, Vol.92, No.SM6, pp. 105-134.

Seed, H. B. and Arango, I., and Chan, C. K. (1975). "Evaluation of Soil Liquefaction Potential During Earthquake,"*Report No. EERC 75-28*, Earthquake Engineering Research Center, University of California, Berkeley.

Seed, H. B., Martin, P. P.and Lysmer, J.(1976). "Pore Pressure Changes During Liquefaction of Sand," *J. of Geotech. Engrg.*, ASCE, Vol.102, No.GT4, Apr., pp. 246-270.

Seed, H. B., and Peacock, W. H.(1971). "Test Procedures for Measuring Soil Liquefacitons Characteristic" *J. of Soil Mech. and Found. Engrg.*, ASCE, Vol.97, No.SM8, pp.1099-1119.

Seed, H. B., et al.(1975)."The Slides in the San Fernando Dams During the Earthquake of Feb. 7, 1971,"*J. of Geotch. Engrg., ASCE*, Vol. 101, pp.651-688.

Shibata, T.(1970). "Liquefaction of Saturated Sands During Cyclic Loading," *Proc. III Japan Earthq. Engrg. Sym.*, Tokyo, Japan.

Silver, M. L., et. al.(1976). " Cyclic Triaxial Strength of Standard Test Sand," *J. of Geotech.l Engrg.*, ASCE, Vol.102, No.GT5, pp. 511-523.

Sture, S. and Desai, C. S. (1989). "Fluid Cushion Truly Triaxial or Multiaxial Testing Device," *Getch. Test. J.* Vol. 2, No.1, pp.20-33.

Tanimoto, K., and Suga, Y.(1970). "On the Dynamic Strength of Saturated Sands," *Proced. III Japan Earthq. Engg. Sym.*, Tokyo, Japan.

Tanimoto, K., and Suga, Y.(1971). "Liquefying Procress of Saturated Sands Subjected to Dynamic Loading," *Proced. IV Asian Reg. Conf., Soil Mech. and Found. Engrg.*, Bangkok, Thailand.

Townsend, F. C. (1977). "Factors Affecting the Cyclic Triaxial Strength of Standard Sand," *Miscellaneous Paper, U. S. Army Corps of Enger*, Waterways Experiment Station, Vicksburg.

Toki, S. et al. (1986). "Cyclic Undrained Triaxial Strenth of Sand by a Cooperative Test Program", *Soil and Found.*, Vol. 26, No. 3, pp.117-128.

Vaid, Y.P., and Thomas, J.(1995). "Liquefaction and Postliquefaciton Behavior of Sand,"*J. of Geotech. Engrg.*, ASCE, Vol. 121. pp. 163-173.

Vaid, Y.P., and Chern, J. C. (1983). " Effect of Static Shear on Resistance to Liquefaction,"*Soil and Foundation*, Vol. 23. pp. 47-60.

Vaid, Y.P., Chern, J. C. and Kuerbis, R. H. (1990). " Stress Path and Steady State," J. *Can. Geotech. J.* Vol. 27. pp. 1-7.

Valera, J. E., and Donovan N. C. (1977). " Soil Liquefaction Procedures- A Review," *J. of Geotech. Engrg.*, ASCE, Vol.103, No GT6, pp.607-625.

Wong, R. T., Seed, H. B., and Chan, C. K.(1975)."Cyclic Loading Liquefaction of Gravally Soil, " *J. of Geotech. Engrg.*, ASCE, Vol.103, pp.571-583.

Yen, B. C.(1967). "Viscosity of Saturated Sand Near Liquefaction," *Proce. Int. Sym. on Wave Prop. and Dynm. Prop. of Earth Mat.*, Albuquerque, N. M.

Yokel, F. Y., et al. (1980). "Liquefaction of Sand during Earthquake, The Cyclic Strain Approach," *Intl. Sympo. on Soil Under Cyclic and Transient Loading*, Swansea,pp. 571-580.

Yoshimi, Y., and Kuwabara, F.(1973). "Effect of Subsurface Liquefaction on Strength of Surface Soil," *Soil and Foundations*, Vol.13, No.2, pp.67-81.

Youd, T. L. (1973). " Liquefaction, Flow and associated ground failure", Circular 688, USGS.